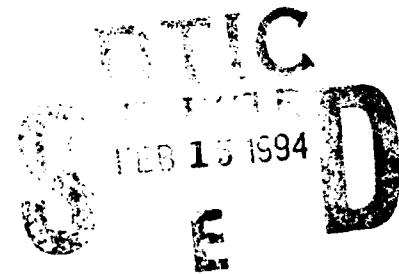




NPS-OC-93-007

NAVAL POSTGRADUATE SCHOOL

Monterey, California



THESIS

WATER MASSES AND THE THERMOHALINE
CIRCULATION AT THE ENTRANCE TO THE GULF OF
CALIFORNIA

by

Lt. Monty Graham Spearman
September 1993

Thesis Advisor:

Prof. Curt A. Collins

Approved for public release; distribution is unlimited.

Prepared for:
Dean of Research (Code 08)
Naval Postgraduate School
1 University Circle RM 141C
Monterey, CA 93943-5019

DTIC QUALITY INSPECTED 2

94-04995



233/88

94 2 14 036

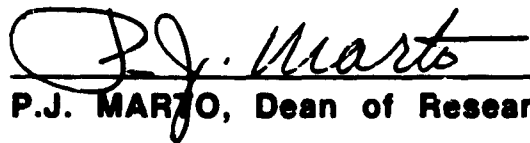
NAVAL POSTGRADUATE SCHOOL
Monterey, California 93943

Rear Admiral Thomas A. Mercer
Superintendent

This thesis was prepared in conjunction with research sponsored and funded by the Naval Postgraduate School.

Reproduction of all or part of this report is authorized.

Released by:


P.J. MARZO, Dean of Research

REPORT DOCUMENTATION PAGE			Form Approved OMB No. 0704-0188	
<small>Public reporting burden for this collection of information is estimated to average 1 hour per response, including the time for reviewing instructions, searching existing data sources, gathering and maintaining the data needed, and completing and reviewing the collection of information. Send comments regarding this burden estimate or any other aspect of the collection of information, including suggestions for reducing the burden to Washington Headquarters Services, Directorate for Information Operations and Reports, 1215 Jefferson Davis Highway, Suite 1204, Arlington, VA 22202-4302, and to the Office of Management and Budget, Paperwork Reduction Project (0704-0188), Washington, DC 20503.</small>				
1. AGENCY USE ONLY (Leave Blank)	2. REPORT DATE September 93	3. REPORT TYPE AND DATES COVERED Master's Thesis		
4. TITLE AND SUBTITLE WATER MASSES AND THE THERMOHALINE CIRCULATION AT THE ENTRANCE TO THE GULF OF CALIFORNIA		5. FUNDING NUMBERS		
6. AUTHOR(S) Monty Graham Spearman, Lieutenant, USN				
7. PERFORMING ORGANIZATION NAME(S) AND ADDRESS(ES) Naval Postgraduate School Monterey, CA 93940		8. PERFORMING ORGANIZATION REPORT NUMBER NPS-OC-93-007		
9. SPONSORING/MONITORING AGENCY NAME(S) AND ADDRESS(ES)		10. SPONSORING/MONITORING AGENCY REPORT NUMBER		
11. SUPPLEMENTARY NOTES The views expressed in this thesis are those of the author and do not reflect the official policy or position of the Department of Defense or the U.S. Government.				
12a. DISTRIBUTION/AVAILABILITY STATEMENT Approved for unlimited distribution		12b. DISTRIBUTION CODE		
13. ABSTRACT (Maximum 200 words) CTD data obtained during the period 28 December 1992 to 08 January 1993 are used to examine the hydrography and water mass distributions at the entrance to the Gulf of California. Data were collected for one across- and one along-gulf transection that intersected near the Gulf's mouth. The circulation at the Gulf's entrance was generally cyclonic. In the upper 200 m, a narrow, high-salinity core of strong baroclinic outflow (max speed 72 cm/sec) traversed the western sector of the region. The high-salinity ($S \geq 34.9$) component of the core correlates to Gulf Water that originates in the inner-Gulf. Partitioned at the mid-basin Alarcon Seamount, the mouth's eastern sector was characterized by numerous bands of reverse flow, including inflowing cores of fresher ($S \leq 34.6$) water from the Pacific. The estimated net transport across this section was a 1.9 Sv inflow, with the majority of the flow occurring below 500 m. Comparison with data from an April 1992 cruise along the same across-gulf transection revealed greater transport and the notable absence of Gulf Water. The April circulation may represent simple recirculation of waters resident across the region.				
14. SUBJECT TERMS Water Mass Distribution, Thermohaline Circulation, Geostrophy, Baroclinic Flow, Volume Transport			15. NUMBER OF PAGES 199	
			16. PRICE CODE	
17. SECURITY CLASSIFICATION OF REPORT Unclassified	18. SECURITY CLASSIFICATION OF THIS PAGE Unclassified	19. SECURITY CLASSIFICATION OF ABSTRACT Unclassified	20. LIMITATION OF ABSTRACT UL	

Approved for public release; distribution is unlimited.

**WATER MASSES AND THE THERMOHALINE CIRCULATION
AT THE ENTRANCE TO THE GULF OF CALIFORNIA**

by

Monty Graham Spearman

**Lieutenant, United States Navy
B.S., University of Tennessee, 1986**

**Submitted in partial fulfillment of the
requirements for the degree of**

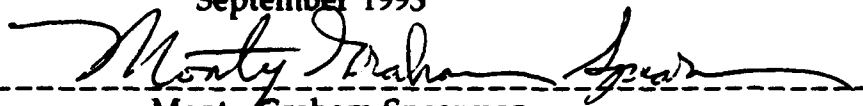
MASTER OF SCIENCE IN PHYSICAL OCEANOGRAPHY

from the

NAVAL POSTGRADUATE SCHOOL

September 1993

Author:

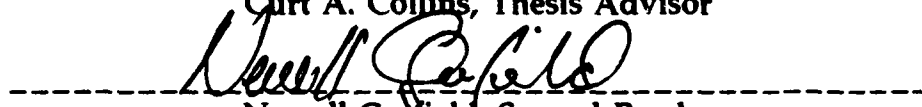


Monty Graham Spearman

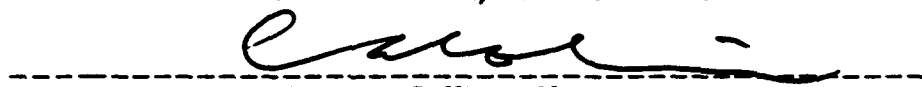
Approved by:



Curt A. Collins, Thesis Advisor



Newell Garfield, Second Reader



Curt A. Collins, Chairman,
Department of Oceanography

ABSTRACT

CTD data obtained during the period 28 December 1992 to 08 January 1993 are used to examine the hydrography and water mass distributions at the entrance to the Gulf of California. Data were collected for one across- and one along-gulf transection that intersected near the Gulf's mouth. The circulation at the Gulf's entrance was generally cyclonic. In the upper 200 m, a narrow, high-salinity core of strong baroclinic outflow (max speed 72 cm/sec) traversed the western sector of the region. The high-salinity ($S \geq 34.9$ psu) component of the core correlates to Gulf Water that originates in the inner-Gulf. Partitioned at the mid-basin Alarcon Seamount, the mouth's eastern sector was characterized by numerous bands of reversed flow, including inflowing cores of fresher ($S \leq 34.6$ psu) water from the Pacific. The estimated net transport across this

section was a 1.9 Sv inflow, with the majority of the flow occurring below 500 m. Comparison with data from an April 1992 cruise along the same across-gulf transection revealed greater transport and the notable absence of Gulf Water. The April circulation may represent simple recirculation of waters resident across the region.

Accession For	
NTIS CRA&I	<input checked="" type="checkbox"/>
DTIC TAB	<input type="checkbox"/>
Unannounced	<input type="checkbox"/>
Justification	
By	
Distribution /	
Availability Codes	
Dist	Avail and/or Special
A-1	

TABLE OF CONTENTS

I.	INTRODUCTION.....	1
	A. OCEAN CIRCULATION IN THE GULF OF CALIFORNIA	
	3
	B. BACKGROUND REVIEW.....	5
II.	METHODS.....	11
	A. CTD DATA COLLECTION.....	14
	B. CTD DATA PROCESSING.....	16
III.	RESULTS.....	20
	A. HYDROGRAPHIC CONDITIONS.....	20
	1. Temperature.....	20
	2. Salinity.....	23
	3. Density Anomaly (γ_θ).....	28
	4. Water Mass Analyses.....	32
	a. T-S Diagram.....	33
	b. γ_θ -S Diagram.....	35
	5. Summary.....	37
	B. BAROCLINIC FLOW.....	39

1. Geostrophy Using Deepest Common Depth	
.....	39
2. Geostrophy Using 1500 m Reference	
Level.....	41
3. Geostrophy Using Reid and Mantyla	42
4. Along-gulf Geostrophy.....	44
5. Volume Transport.....	45
6. Salt Budget.....	50
7. Summary.....	54
C. SATELLITE IMAGERY.....	57
IV. CTD DATA FROM APRIL 1992.....	80
A. APRIL-MAY 1992 RESULTS.....	80
B. DIFFERENCES BETWEEN APRIL AND DECEMBER	
1992.....	89
V. CONCLUSIONS.....	104
APPENDIX A: LITERATURE REVIEW.....	110
APPENDIX B: SPICINESS (π).....	139
APPENDIX C: CTD DATA PROCESSING AND LISTINGS..	149
REFERENCES.....	185
INITIAL DISTRIBUTION LIST.....	188

ACKNOWLEDGMENT

I would like to express my gratitude to my thesis advisor, Dr. Curtis A. Collins, and to my co-advisors, Dr. Antonio Sanchez-Devora and Dr. Newell Garfield, for their support and guidance. I also thank Paul Jessen, and extend a special thanks to Tarry Rago for his help and patience.

I. INTRODUCTION

At the mouth of the Gulf of California, two prominent flows of water are observed. Nearshore, off the eastern banks of Baja California, is warm, highly saline ($S \geq 34.90\%$), equatorward flowing "Gulf Water" (Roden, 1964) that formed from a water mass originating in the northern Gulf. Converging at the southern tip of the Baja California peninsula, offshore from Cabo San Lucas, are Eastern Tropical Pacific Water of intermediate salinity ($34.65 \leq S \leq 34.85\%$) and cool, fresh California Current Water from the North Pacific ($S \leq 34.60\%$) (Roden and Groves, 1959). These two elemental water masses combine to supply a poleward flow of cooler, fresher water into the Gulf (Wyrcki, 1967; Griffiths, 1968), and are generally found along the central and easternmost sections of the Gulf's entrance.

This region is regarded as a transition zone in which the three aforementioned water masses interact to produce a complex local circulation (Stevenson, 1970). The vertical structure of these flows has been most recently studied by Bray (1988a). She inferred a three-layered thermohaline circulation system, having: 1) a surface layer, which is approximately 50 m thick and reverses transport direction with the seasonally reversing large-scale wind field, flowing north in the summer and south in the winter, 2) baroclinic outflow flowing along the western shores of the Gulf between the surface layer and about 250 m depth, and 3) baroclinic inflow flowing predominantly in the central sector of the Gulf between 250 and 500 m depth.

This paper is an attempt to refine the description of the hydrography and circulation occurring at the Gulf of California's entrance using Conductivity-Temperature-Depth (CTD) soundings collected in late December 1992 and early January 1993. The

December across-gulf structure will also be compared with a similar section obtained in April 1992 aboard the *USNS DeSteiguer* (Rago, et al., 1992).

A. OCEAN CIRCULATION IN THE GULF OF CALIFORNIA

The thermohaline circulation occurring near the mouth of the Gulf of California is the result of a series of complex forcing conditions within the Gulf that make the entire system unique (see Appendix A). Historically, the principal driving mechanism behind the Gulf's thermohaline circulation was thought to be evaporation in the northern Gulf. But Bray (1988a) noted that air-sea heat fluxes and momentum fluxes are likewise important to the Gulf's thermohaline circulation. She stated that, "...it appears that the Gulf gains heat from the atmosphere on an annual average, unlike the Mediterranean and Red seas, which have comparable evaporative forcing." To offset this heat gain and the accompanying moisture loss, Bray (1988b) explained that an advective flux of cold, fresh inflow and warm, salty outflow occurred at the

Gulf's entrance. Bray (1988a) also added that the Mediterranean and Red seas are characterized by a stabilizing vertical salinity gradient (in which salinity increases with depth) and show a two-layer exchange in which the outflowing layer is denser and more saline than the inflowing. The Gulf of California differs in that it consistently has a destabilizing vertical salinity gradient over the upper 700 m of the water column (salinity decreases with depth). This condition is maintained with few exceptions, and indicates that the temperature-salinity relationship follows a like trend, i.e., temperature decreases, salinity decreases. Lastly, temperature dominates the density signal and predictably decreases with depth. It follows that the vertical structure of transport, on average, consists of surface outflow and subsurface inflow. This theory agreed with observed vertical gradients of temperature and salinity and with baroclinically determined circulation patterns.

B. BACKGROUND REVIEW

Using temperature charts constructed from ships' logs, Thorade (1909) first described the circulation of surface waters in the southern regions of the Gulf of California as cyclonic with net surface transport in the direction of seasonal winds (Alvarez-Borrego, 1983; Merrifield and Winant, 1989).

Sverdrup (1941), using hydrographic data from the *E.W. Scripps* cruise of 1939, described the water masses of the Gulf. Analyzing water samples collected from cross-gulf transects along the entire Gulf, he noted that deep water samples collected in the "outer portion of the Gulf" (near the entrance) matched water properties of samples collected from the equatorial regions of the Pacific Ocean (salinity minimum $\approx 34.5\%$; temperature $\approx 5.0^{\circ}\text{C}$). Sverdrup added that surface temperatures in the "outer portion of the Gulf" were higher than those in the northern sections. Below the surface, at depths of 200 or 300 m and below, temperature was very uniform and decreased

regularly towards the bottom. His examination of the distribution of salinity revealed similar features. He noted that the highest salinities were found near the surface; but, maximum values increased going north from the Gulf's entrance. A layer of salinity minimum was observed at depths between 500 and 1100 m in the Gulf's "outer portion." Sverdrup added that the lowest values, corresponding to the salinity minimum of slightly less than 34.55‰, were observed near the Gulf's mouth.

Griffiths (1968) was able to build upon Sverdrup's findings at the Gulf's entrance. Deploying Nansen bottles along similar cross-gulf transections at the entrance, he observed an **Intermediate Water** at about 800 m (marked by a salinity minimum of ~ 34.5‰) and a **Subtropical Subsurface Water** overlying the Intermediate water, and extending up to about 200 m depth (marked by a salinity maximum of 34.8‰). Griffiths defined two additional layers. He explained that the convergence of southward flowing,

high-salinity **Gulf Surface Water** ($S > 35\%$) with the less saline **California Current Surface Water** at the entrance formed a high-salinity layer atop a salinity minimum. This minimum, found at about 100 m depth and at the western entrance of the Gulf, marks the presence of the California Current Surface Water (marked by a shallow salinity minimum of $\approx 34.1\%$).

Roden (1964) made similar conclusions from a series of hydrographic surveys conducted in the Gulf (1956-1961). He too noted the existence of numerous salinity maxima and minima in the water column's upper layers, and added that the region was characterized by a significant thermocline throughout the year. He stated that during February and April the isotherms and isohalines were observed ascending toward the coast of the Mexican mainland, suggesting upwelling by northwesterly winds. Spring and winter months revealed both a 50 m deep high-salinity core off the southern Baja coast and a salinity minimum of less than 34.7‰ at 100 m depth in the central sector of the Gulf.

Roden contended that the high-salinity core represented southeasterly flow from the interior Gulf, and that the salinity minimum reflected northwesterly flow from more southerly latitudes.

Roden (1972) conducted the most thorough sampling of the thermohaline structure at the Gulf of California's entrance. In late November-early December 1969, a densely spaced (* every 9 km) 34-station salinity-temperature-depth (STD) sensor cross-gulf transection was carried out. Observations were limited to the upper 1500 dbar. Excellent vertical and horizontal resolution of the thermohaline structure and baroclinic flow field at the Gulf's entrance was obtained. Like Griffiths (1968), Roden concluded that four distinct layers comprised the salinity structure at the Gulf's entrance. The layers described by Roden support Griffiths' earlier analysis with the exception of slight variation in depth ranges.

Roden (1972) computed the baroclinic flow across the Gulf of California entrance from the STD

data (see Appendix A). The observed flows were referenced to the 1500 dbar surface (or bottom, if encountered first). Baroclinic outflow from the Gulf was observed as a narrow high-velocity core near the western shore. The width of the core was about 30 km and extended to more than 1000 m in depth. Observed velocity maxima within the core included 55 cm/sec at the surface and just over 40 cm/sec at 600 m depth. Roden stated that this outflowing current had its origin in the northern realm of the Gulf and could be traced there using its salinity maximum, which exceeded 35.2‰ (Roden, 1964).

Roden observed the baroclinic inflow to be broader than the outflow, with the inflow predominantly in the central sector of the Gulf's entrance. Two cores of inflow were delineated. The first was approximately 20 km wide, with a maximum velocity of 26 cm/sec and centered between 50 and 450 m depth. The other core was located more to the east and found to be slightly wider. The corresponding flow

was restricted to the surface and had a maximum velocity of 46 cm/sec.

Roden (1972) determined the baroclinic transport above 1500 dbar to have a net outflow of 2.0 Sv (Sverdrup). This value was computed as the difference between the southward transport (12 Sv) and northward transport (10 Sv).

II. METHODS

As part of a joint study with the Mexican Navy and the Universidad Autonoma de Baja California (UABC), the Naval Postgraduate School (NPS) conducted a two-part study of the currents and hydrographic conditions at the entrance to the Gulf of California. The cruise and hydrographic surveys occurred during two consecutive weeks aboard the R.V. *Pt Sur*. Beginning on 28 December 1992 and ending on 08 January 1993, temperature and salinity data were collected via Conductivity-Temperature-Depth (CTD) soundings. Two transections were occupied and are represented in Figure 1. The first ran across-gulf, with the first CTD cast (CTD cast #20) made off the southeastern tip of Baja California. The transection extended approximately 180 km east-northeast to the continental shelf off El Dorado, Sinaloa, with a total of 19 CTD casts and 12 Pegasus drops.

The second transection ran along-gulf, consisting of 12 CTD casts collected between 03 and 08 January 1993. The transection started at $23^{\circ} 11'N$, $108^{\circ} 25'W$ (CTD cast #37) and extended 210 km northwest into the Gulf, ending at $24^{\circ} 34'N$, $109^{\circ} 50'W$ (CTD cast #60). The transections intersect at $23^{\circ} 35'N$, $108^{\circ} 47'W$. These two transections allow examination of both along- and across-gulf structure and associated geostrophic circulation at the Gulf's entrance.

Merrifield and Winant (1989) state that the region where the above transections were deployed consists "...of a series of trough-shaped, deep basins (1000-3000 m) and in open communication with the Pacific Ocean to depths of 3000 m..." The bathymetry of the across-gulf transection characteristically deepens offshore from Baja California and is dominated by the Alarcon Seamount located to the east. This narrow pinnacle, centered just north of the position where the along- and across-gulf transections intersect, rises sharply to within 1500 m of the surface

(Figure 1). Along the across-gulf transection, the seamount divides the Pescadero Basin into two bathymetrical regimes. The western basin separates the seamount from Baja and deepens quickly (in excess of 2500 m) in the absence of any significant continental shelf. East of the seamount, the Pescadero Basin initially acquires great depth, but the broad, shallow shelf extending some 80 km from the shores of Sinaloa is more characteristic. North of the Alarcon Seamount the Pescadero Basin narrows and extends for approximately 200 km, with maximum depths exceeding 3000 m. This deep water section (depicted by hatching in Figure 1) runs parallel to, and has its westernmost edge at 1-30 km from, the track marking the along-gulf transection. Centered between the 1000 and 2000 m isobath curves and bordering the narrow banks of southern Baja is the northernmost extension of the along-gulf transection (casts 55-60). West of this line and the 1000 m isobath are the shallows of the Cerralvo Bank. This shallow region, formed along the

outlying Isla Cerralvo (adjacent to cast #58), projects southward along with the southern reaches of Baja's banks. Depth contours along these features uniformly decrease inshore.

A. CTD DATA COLLECTION

The hydrographic data were collected using a Neil Brown MK-IIIIB CTD. For each cast the CTD was lowered to near the bottom. CTD data were acquired during the downcast. With retrieval of the CTD, water samples were collected at the deepest depth of the cast, at intermediate depths, and at the surface. The water samples would later be used to calibrate CTD salinity. The CTD is considered accurate to within ± 0.005 psu (salinity), ± 0.005 °C (temperature), and ± 3.2 dbar (pressure) when properly calibrated and operated. Salinity, temperature, and pressure are resolved to 0.001 psu, 0.0005 °C, and 0.05 dbar, respectively. Tables C1 and C2 of Appendix C provide the date/time (GMT), geographic position, and bottom depth (m) for

each cast of the transections examined. Table C3 lists the data of those casts.

The CTD temperature and pressure sensors were calibrated at the Naval Postgraduate School calibration laboratory just prior to departure for the cruise. The pre-cruise calibrations were applied to the data during *in situ* data collection processes. The CTD pressure transducer was calibrated against a known standard, deadweight tester (DWT). Indicated pressures from the DWT and the CTD sensor were recorded across several equally spaced pressure intervals between 0 to 6200 dbar, at room temperature. Regressions fitting the CTD pressures to those of the standard yielded a CTD pressure correction of: $P = 1.00015 * (\text{CTD } P) - 14.25718$. Similarly, indicated temperatures from a known standard and the CTD temperature sensor were recorded over a range of equally spaced temperatures from 0 °C to 25 °C. Subsequent regression analysis yielded a CTD temperature correction of: $T = 0.99989 * (\text{CTD } T) - 0.00031$.

Post-cruise calibration was performed on the CTD sensors upon return to the Naval Postgraduate School. Post-calibration checks instrument performance while assuring the accuracy of the data collected. Post-cruise calibration methods were similar to those of the pre-cruise. For this cruise, differences between the results of the two calibration sets were negligible.

B. CTD DATA PROCESSING

CTD data were recorded at a rate of 32 Hz. These data were first processed using standard software that allows the user to scan the raw data and then to eliminate and interpolate across obviously bad data points (EG & G Marine Instruments). The program is dynamic and allows for the application of the time response constants for the conductivity, temperature and pressure sensors. The data were then bin averaged over 2 dbar intervals. Conductivity derived salinities were calibrated against salinity values determined from salinometer analyses of upcast bottle samples

(Table C4 of Appendix C). Following the procedure described in Rago et al. (1992), data points greater than two standard deviations from the mean of the differences between the compared salinity sets were discarded. A regression analysis on the remaining data points provided final correction to the CTD salinity data. Final correction to salinity yielded a CTD salinity of: $S = 0.99691 * (\text{CTD } S) - 0.05745$, with a standard deviation of ± 0.0047 .

Hydrographic data are presented in the form of vertical sections, scatter plots (e.g., T-S diagram) and data listings. The bulk of the illustrations within this paper were obtained by gridding and plotting the corrected CTD data using the **SURFER** contouring program by Golden Software, Inc (1989). All grids were constructed using the kriging method with a quadrant search of three points per quadrant. Shallow-layered profiles (surface-500 m depth) employed a grid spacing of 5 km horizontally and 20 m vertically. Deep-layered profiles (surface-3000 m depth) were made

with a grid spacing of 8 km horizontally and 20 m vertically, with the exception of geostrophic velocity, where the grid spacing was 5 km and 30 m, respectively. All corresponding plots were smoothed using the smooth option offered in the TOPO section in **SURFER**.

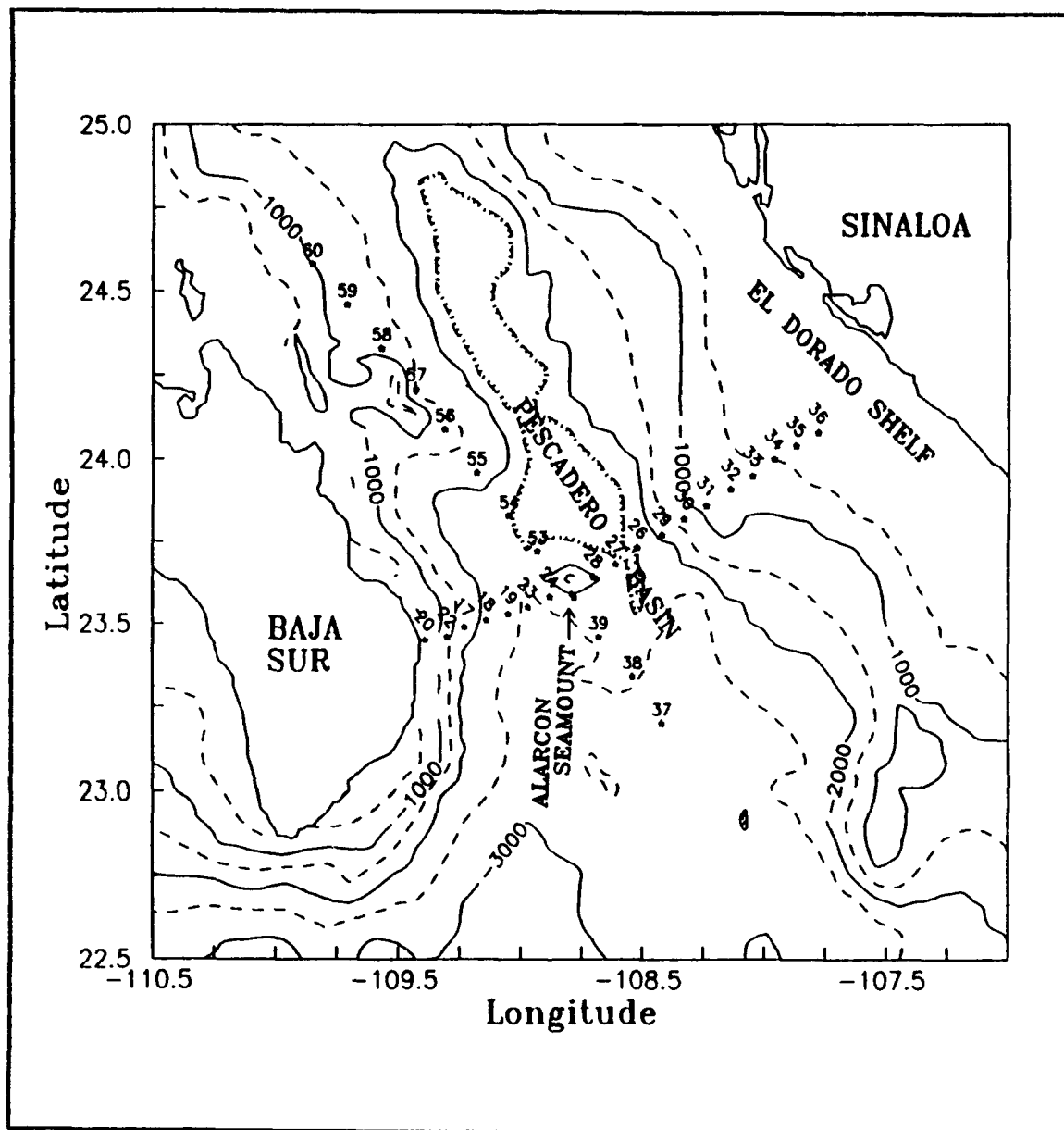


Figure 1. Location of CTD casts on the PESCAR 02 cruise at the entrance to the Gulf of California, December 28, 1992 - January 08, 1993. Labeling of casts 25 and 52 has been omitted to more clearly display Alarcon Seamount. Isobath spacing is 500 m.

III. RESULTS

Analyses of the data will be discussed in two parts. An interpretation of the study area's hydrography will precede discussion of the thermohaline circulation and water exchange balances.

A. HYDROGRAPHIC CONDITIONS

Hydrographic conditions in the region are defined by examining the across- and along-gulf transections of temperature, salinity and density anomaly. Water mass analyses are included to supplement these results. The structural definition gained from the examination of hydrographic properties should help understand the dynamics of the flow.

1. Temperature

Inspection of Figure 2a shows strong stratification in the upper 125 m of the across-gulf section. Surface temperatures across the Gulf's entrance are still warm (exceeding 22 °C) from the

preceding summer's intense insolation. Interesting features of the near-surface temperature structure include the upward bending of the 22 °C isotherm, breaking the surface on the western side of the Gulf between CTD casts #17 and #18. West of this position, surface temperatures are from 2 to 3 °C cooler than observed farther offshore. Depressed isotherms, centered in approximately 50 m of water below casts #17 and #18, indicate the presence of a warm-water core. On the eastern side of the Gulf, 140-160 km offshore from the Baja peninsula, elevated isotherms above 50 m depth mark the presence of a cooler core of water. Also, in the upper structure, between 100 and 200 m, warmer waters are found closest to Baja. Below 200 m, warmest waters are found next to shore, while it is cooler offshore in the open Gulf. A final point about the upper 500 m water column regards the wavy character of the isotherms as they stretch across the Gulf's mouth. Because of limited data, it's difficult to prove what exactly the wavy isotherms imply, but

they may be indicative of internal waves. The deep layers, depicted in Figure 3a, reveal no unusual details. Below 200 m, the temperature is uniform and decreases monotonically towards the bottom. At about 750 m the isotherms appear level. At 2250 m depth, water temperatures have cooled to 2 °C.

Examination of Figures 4a and 5a, the along-gulf temperature data sets (PESCAR 02, Leg III), reveal that the near-surface structure just described stretched some 40 km north into the Gulf's interior. North of cast #54, the isotherms slope down to the north, breaking the continuity of the upper ocean structure observed over the southernmost stations. This introduces an extensive surface core structure of 50 km length and 100 m depth between casts #55 and #60. These core waters are about 2 °C warmer than corresponding waters south of cast #54. In the subsurface waters below this section, the isotherms gently rise to the south and begin to level. The deep-layer structure again shows monotonic decreasing of

the isotherms and leveling below 1500 m. Observed as a whole, the along-gulf isotherms are sloped negatively across the transection, indicating slightly cooler subsurface waters to the south.

2. Salinity

The vertical salinity structure across the Gulf's entrance is shown in Figures 2b and 3b. The profile is characterized by salinity maxima and minima layers in the upper water column. The contouring illustrates that these layers are not uniform horizontally. The observed cores are distinct and prominent in the strongly temperature / density stratified upper 100 m layer. The best defined high-salinity core is centered near-surface in the westernmost realm of the transection (casts #20 to #18), reaching from the surface to about 75 m depth. Salinities within the core are in excess of 34.9 psu, with maximum values reaching 35.1 psu. Temperatures corresponding to this saline core exceed 20 °C. Owing to its high salinity, this core of water is easily

traceable to water of Gulf origin, and will often be referred to as Gulf Water. Examination of the central and eastern regions of the transection reveal intermittent surfacing of both saline and fresher water. Between casts #24 and #28, a relatively fresh pool of 34.6 psu salinity breaks the surface from 25 m depth. Farther east, originating at cast #27 and extending 60 km east, saline water of 34.8 psu pools at the surface from 75 km depth. The diversity of surface water salinity across the study area reflects mixing of the water masses comprising the near-surface layer (Stevenson, 1970). Across the central sector of the transection, several cores of low-salinity water embody the lower half of the upper 125 m layer. Indicated by hatching, the cores are observed 40-150 km offshore from the Baja peninsula in waters from 50 to 125 m deep. Salinities decrease from 34.6 to 34.3 psu within the cores. Associated temperatures range from 14 to 18 °C, and the isotherms show doming where the cores exist. The cores appear highly structured

and seem not to mix significantly with the surrounding water.

Plotting salinity on density anomaly surfaces offers another perspective of the salinity structure (Figure 2d). It delineates the location of the isohaline curves with respect to the density surfaces at each cast. This structure removes the presence and associated influences of internal waves, which in turn, allows closer inspection of the salinity cores. Also, spreading the density surfaces uniformly expands the upper layer, thus helping to distinguish the independent identifiable salinity cores there. Waters below this layer reveal less variability of salinity on a given density surface. The shallow salinity minimum (shaded triangles in Figure 2b) identified by Griffiths (1968) and Roden (1972) crosses through the heart of the cores. The nodes of low-salinity water ($S \leq 34.6\%$) have clear origins from the California Current Water (Griffiths); and the matrix of higher salinity water ($34.65 \leq S \leq 34.85\%$) is representative

of subsurface components of the Eastern Tropical Pacific Water (Stevenson, 1970). The latter extends to more than 350 m, forming parcels of higher salinity water that occupy the entire cross section. The deep salinity minimum is observed in the next underlying layer, stretching across the Gulf in waters ranging between 500 and 650 m deep (Figure 3b). Characterized by a salinity minimum of 34.5 psu and temperatures varying between 5 and 7 °C, this water mass is Pacific Intermediate Water (Reid, 1965). Beyond the deep salinity minimum, the Pacific Deep Water is distinguished by increasing salinity with depth, that reaches a maximum value of 34.65 psu near the bottom (Robles and Marinone, 1987). The deep layer T-S signature resembles that found in the Eastern Pacific, suggesting that there are no processes occurring in the Gulf to modify the deep waters. The waters that are modified in the Gulf are only apparent above the 11 °C mark, or approximately 250 m.

The along-gulf salinity structure is seen in Figures 4b and 5b. The most striking feature observed in the upper 500 m layer is the sudden and sharp descension of the isohalines north of station #54. This, in effect, outlines a large body of high-salinity water to the north that reaches from the surface to 175 m depth. The plot of salinity on density anomaly surfaces, Figure 4d, shows high-salinity Gulf Water ($S \geq 34.9$ psu) settled between the 24.25 and 25.25 kg/m^3 density surfaces. This observation appears to coincide with the same Gulf Water signature found on similar density surfaces in the western section of the across-gulf transection (Figure 2d). Such would imply that the origin of the high-salinity water isolated at the across-gulf transection is the inner-Gulf. Also, in the shallow subsurface waters below cast #53 (Figure 4b), a prominent vertical salinity boundary is disclosed. Reaching to 200 m depth, the boundary marks the dividing line between the higher salinity northern

waters and the less saline southern waters. Below the 200 m layer, the isohalines steadily decrease towards the deep salinity minimum at 650 m depth. The deep layer structure closely resembles that observed with the across-gulf transection. Below the deep salinity minimum, at a given depth, salinity to the north of Alarcon Seamount is less than that to the south.

3. DENSITY ANOMALY (γ_0)

The density anomaly discussed in this section was calculated from algorithms in Volume 4 of the International Oceanographic Tables (UNESCO, 1987). Commonly referred to as the potential density anomaly, with units of kg/m^3 , it is the density of water (ρ) calculated as a function of potential temperature (θ) referenced to the ocean surface, pressure (p), and in situ salinity (s) minus 1000 kg/m^3 . In equation form: $\gamma_0 = \rho(\theta, s, p) - 1000 \text{ kg/m}^3$ (UNESCO, 1991).

The density field, shown in Figure 2c, closely resembles that of the temperature

distribution. Isopycnal curves in the upper 150 m layer have the same character as the isotherms. The tight packing of the isopycnals indicates the strong stratification existent in the upper layers. Of particular interest is the abrupt shoaling of the 24.0 kg/m³ isopycnal curve, observed breaking the surface near cast #23. This feature marks a near-surface frontal boundary dividing denser water west of the curve from less dense surface water to the east. East of the Baja peninsula, between 75 to 175 m depth, are two sections of depressed isopycnals divided by an upward bulge or ridge centered 50-70 km offshore. The ridge approximately overlies the Alarcon Seamount located a few hundred meters below. The presence of the ridge implies water of lesser density along its flanks; and consequently, opposing geostrophic flows. Waters east of the ridge would flow north and into the Gulf, while waters west of the ridge flow in a southerly direction. Seasonal upwelling may be occurring on the eastern side of the Gulf as indicated

by the general upslope pattern of the near-surface isopycnals (Warsh and Warsh, 1973). Between 200 to 500 m depth, the isopycnal surfaces become less stratified and assume a bowed shape, bending downward towards the coasts. This feature supports the assumption that cyclonic subsurface exchanges occur as water flows into the Gulf along eastern boundaries and flows out along western shores. Predictably, the flow pattern would appear to circumscribe the mid-basin Alarcon Seamount. As with the temperature distribution, the density structure levels with depth, implying little or no motion at depths below 1500 m (Figure 3c).

The along-gulf density anomaly structure (Figures 4c and 5c) parallels that of the temperature, indicating a continuous upper layer structure stretching some 40 km into the Gulf. North of cast #54, the isopycnal surfaces tilt sharply down towards the north, before bending upward at about cast #58. The tilting isopycnals persist down through the upper subsurface layers, resulting in broadening with depth

of the area bounding their slope endpoints. The area defined by the sloped isopycnals represents a frontal boundary that consequently widens and protrudes south with depth. This boundary represents a transition zone separating less dense waters to the north from slightly denser waters south. Examination of the deep layer section (Figure 5c) shows that the isopycnals level at about 1250 m. This suggests a depth of no horizontal pressure gradient; and, may in turn suggest a good depth for establishing the level of no motion (LNM) when determining geostrophy. Approaching the bottom, the isopycnals show slight downward tilting towards the north. Such reflects that benthic waters north of the seamount are less dense than deep waters to the south. These features, when considered collectively, are indicative of westward flow onto the Baja banks, and further suggest the existence of a cyclonic horizontal circulation pattern.

4. Water Mass Analyses

Stevenson (1970) wrote that at the entrance to the Gulf of California Eastern Tropical Pacific Water, California Current Water and Gulf of California Water converge and interact. Isolating these water masses discloses to what extent they interact and how each influences the structure. Identifying them is achieved via the hydrographic relationships specific to each.

In the following sections, temperature - salinity (T-S) and density anomaly - salinity (σ_t -S) diagrams are examined in order to resolve the water masses comprising the area of study. The T-S diagram, plotting temperature ($^{\circ}\text{C}$) versus salinity (psu), is first addressed. A succeeding discussion of the σ_t -S relationship should offer an additional perspective on the water structure. Spiciness (π) analysis is

consistent with previous discussion and is included as an appendix (Appendix B).

a. T-S Diagram

The T-S diagram (Figure 6a) reveals three regimes of water. The regimes are: the surface layer (0-50 m); mid-layer (50-250 m); and, deep layer (250 m-bottom). Waters of the upper 50 m regime are clearly warm and high in salinity ($T \geq 22^{\circ}\text{C}$; $S \geq 34.7$ psu). Examination of the CTD data (Table C3 of Appendix C) shows that along the across-gulf transection there exists a varying surface mixed layer of 10 to 30 m within the surface layer. There is some resolution in the regime via a small break where salinity is about 34.9 psu. The break divides the well-mixed, warmer and less saline Tropical Surface Water from slightly cooler higher salinity water. The latter is conceivably Gulf of California Water (Gulf Water), high-salinity water from the inner-Gulf, and cooled by the seasonal southward winds as it moves south along the Baja banks.

The second regime of water extends from the bottom of the upper layer down to the 11 °C temperature break, which corresponds to a depth of 250 m. In this subsurface section, salinities range from the low extreme ($S \leq 34.4$ psu) to maximum salinity values ($S \geq 34.9$ psu). The section is a region of strong vertical stratification with minimal vertical mixing occurring. Citing Stevenson's classifications, the 34.6 psu salinity mark distinguishes California Current Water (where $S \leq 34.6\%$) from the more saline subsurface composites of the Eastern Tropical Pacific Water, or Subtropical Subsurface Water ($34.65 \leq S \leq 34.85\%$). Both masses were observed previously as independent cores in the salinity distribution diagrams. To a lesser degree, Gulf Water (where $S \geq 34.9\%$) is observed at the top of the section.

Proceeding deeper, the third and final regime is characterized by uniformity. A deep salinity minimum is reached at about 6 °C, corresponding to 700 m depth. This water corresponds

to the oceanwide Pacific Intermediate Water (Reid, 1965). Below the minimum, salinities increase slightly with depth, marking Pacific Deep Water (Robles and Marinone, 1987).

b. γ_θ -S Diagram

The γ_θ -S diagram (Figure 6b) is similar to the T-S plot. The diagram is also characterized by a three regime structure: extensive mixing is observed near the surface of the uppermost regime (where $\gamma_\theta \leq 24.75$ kg/m³); uniformity occurs at depth (where $\gamma_\theta \geq 26.50$ kg/m³); and, considerable variability occurs in between. The upper layer regime offers the same conclusions derived from the T-S diagram. Regarding the identification of Gulf of California Water, the 34.9 psu salinity break separates a pocket of more saline, slightly denser water from lighter, less saline water. The former likely corresponds to the dense Gulf Water from the inner-Gulf. The remainder of the layer appears well-mixed when compared to the

underlying stratified layers of the middle regime ($24.75 \leq \gamma_0 \leq 26.50 \text{ kg/m}^3$), where greater variability in salinity is observed.

The middle regime extends to more than 250 m from the surface, embodying separate cores of high-salinity water and water of lesser salinity. Classification by salinity is used to determine along which isopycnal surfaces the elemental water masses are dispersed. Subsurface California Current Water has densities ranging from $24.75 - 25.50 \text{ kg/m}^3$. Densities representing the subsurface regime of the Eastern Tropical Pacific Water (Subsurface Subtropical Water) range between $24.75 - 26.50 \text{ kg/m}^3$. The increased variability observed in the subsurface layer is consistent with the strong stratification there. The stability of the layer diminishes vertical mixing between the water masses, giving the banded structure observed.

The third regime, corresponding to a depth below 250 m, indicates the water structure

assuming uniformity and stability with depth. The density of the deep salinity minimum of the Pacific Intermediate Water is approximately 27.15 kg/m^3 . Densities increase to 27.75 kg/m^3 approaching the bottom.

5. Summary

The study area's hydrography supports the concept of a two-tiered water exchange process existing at the Gulf of California's entrance. The near-surface vertical structure is interlaced cores of both warm, saline water and cooler, less saline water. The former is believed to represent equatorward flow exiting the Gulf, while the latter is generally associated with poleward flow into the Gulf. A warm (but cool at the surface) saline layer, penetrating down to 75 m depth and centered 25 km offshore from the Baja peninsula, is suggestive of equatorward flow believed to have originated within the Gulf's interior. Fresher salinity cores were observed east of a ridged transition zone centered approximately 45 km

from Baja. These cores, with salinities less than 34.7 psu, are thought to be northward intrusions of admixtures of California Current Water with the surrounding subsurface Eastern Tropical Pacific Water (Subtropical Subsurface Water). Combined with the influx of an unchanging deep layer Pacific Intermediate Water ($S \leq 34.6$ psu, $T \leq 10$ °C), these cool and fresher waters account for nearly all of the inflow into the Gulf. An along-gulf transection indicates a large frontal boundary stationed near the across- and along-gulf intersection. The front, besides marking a transition of saltier near-surface, but less dense, northern waters from southern waters, also lends credence to the existence of a large cyclonic horizontal circulation encompassing the entire field of study.

B. BAROCLINIC FLOW

CTD station data were used to compute dynamic height, which was in turn used to examine the geostrophic flow field. Three techniques, each distinguished on the basis of where the level of no motion (LNM) was assumed, were employed and compared.

1. Geostrophy Using Deepest Common Depth

The first technique established the LNM at the deepest common depth (DCD) between stations. The resulting geostrophic velocity transection in Figure 3d shows four distinct currents. Baroclinic outflow, observed as negative (southward) flow, is predominant in the western part of the Gulf as a narrow high-speed core. The flow width stretches eastward from cast #18 some 25 km and extends down to 1250 m deep. Current velocities within the core reach a maximum of 58 cm/sec at the surface, while a subsurface maximum of 72 cm/sec was recorded at 60 m depth. Less prominent incidences of southward flow are observed in the eastern part of the transection at cast #27 and as a

wedge along the Sinaloa coast shoreward of cast #32. These flows are less intensive and only penetrate the upper layer of the water column, producing minimal outflow. According to Roden (1972), the intense and deep running outflow hugging the Baja banks should be high-salinity water of northern Gulf of California origin. The observations made previously regarding the salinity distribution give support to this.

Baroclinic inflow into the Gulf is observed as cores of positive (northward) flow. The first of two of these northward flows is centered 70 km east of the Baja peninsula. The core of this northward flow is confined to the upper 100 m layer of the water column and is approximately 20 km wide. Currents near the surface reach a maximum speed of 56 cm/sec, while weaker currents are observed with depth. The location of the velocity core coincides with the position of the cool, low-salinity cores examined previously in the temperature and salinity distribution diagrams, suggesting intrusion of California Current Water into

the Gulf. The second incidence of northward flow is observed between casts #26 and #29. This core has a maximum width of about 15 km and extends to nearly 500 m depth. Highest speeds (approaching 35 cm/sec) are observed near the center of the upper 100 m layer.

Isotachs of .0 cm/sec separate regions of northward and southward flow. In Figure 3d, three 0 cm/sec isotachs are observed extending vertically from the surface, then almost merging as they level between 1250 and 1500 m. This infers that geostrophic velocities in the vicinity of 1500 m approximate zero. Below 1500 m, weak currents are observed. The currents in this deep layer vary in direction and have speeds seldom exceeding 5 cm/sec.

2. Geostrophy Using 1500 m Reference Level

From the preceding observance of near zero velocities at 1500 m, the second technique for determining the geostrophic velocities was applied. In this procedure, while it was still necessary to use the DCD method for shallow water casts, deep casts of

the transection were referenced to a 1500 m LNM (Figure 3e). This technique provided no significant change over using the DCD technique independently. Minor differences in the results include expected leveling of the 0 cm/sec isotachs at the 1500 dbar level. The 0 cm/sec isotachs below the 1500 dbar level appear to have greater distortion. This feature results from velocity changes below the LNM associated with the weak horizontal and vertical gradients which occur there.

3. Geostrophy Using Reid and Mantyla

The third and final technique used in determining the geostrophic velocities was derived from Reid and Mantyla (1976). In its simplicity, the gradient of the offshore dynamic height field (with respect to the 1500 dbar level in this application) is repeatedly extrapolated shoreward along the deepest common standard pressure surface between station pairs. The technique was derived in order to explain variations of coastal sea level and, hence, achieve a

better representation of the geostrophic flows occurring in the shallower water. The Reid and Mantyla method, depicted in Figure 3f, did accelerate the geostrophic velocities in the eastern half of the Gulf. East of station #26, several small-scale cores of both inflowing and outflowing water are revealed in the upper 100 m layer. The other distinctive contrast is the descension of the 15 cm/sec isotach from the surface (cast #26) to 750 m depth. Such implies substantial deep-layer current activity occurring in the eastern section of the Gulf.

Of the three techniques used, it is of the writer's opinion that the first method provided the most realistic representation of the baroclinic velocity. Establishing the LNM at the DCD between stations offers a procedure that is consistent over an entire deep/shallow water transection. Adjustments to the LNM are simply made at the individual station pairs, allowing a fuller and more customized representation of the vertical structure. The computed

velocity distribution in turn more accurately portrays the entire current field.

4. Along-gulf Geostrophy

Examination of Figure 5d, the along-gulf transection using the DCD method, reveals a number of weak upper layer and mid layer velocity cores within the water column. North of cast #54 and flowing in the upper 250 m is a broad negative (westward) flow with maximum velocities of 47 cm/sec occurring near the surface. North of this flow is a similarly broad positive (eastward) flowing current characterized by maximum velocities of 39 cm/sec at the surface. These adjacent, but opposing, current bands may mark the presence of an anticyclonic eddy in the region. The enclosed 0 cm/sec isotachs north of cast #52 disclose additional but slower (velocity ≤ 15 cm/sec) flowing eastward currents. South of cast #52, at the position marking the intersection of the across- and along-gulf transections and Alarcon Seamount, westward flowing currents (15 cm/sec isotach) are observed extending

from the surface to about 500 m depth. Below 1500 m, regimes of westward flow to the north of the Alarcon Seamount and eastward flow to the south predominate. Observed together, these velocity cells are indicative of a circulation system scattered with eddylike features in the upper layer structure overlying a larger cyclonic system organized at depth.

5. Volume Transport

The baroclinic volume transports occurring over the entire across-gulf transection were calculated using the cut-and-fill option of **SURFER**. The program calculated positive/negative volumes in units of km^3/sec . The volume calculations were then divided by 10^5 to give volume transports in Sverdrups (Sv). The volume transports are listed in Table 1. Transports were calculated for the full section water column, and then subdivided horizontally into the following three sections: 1) 0-50 m surface layer, 2) 50-250 m mid-layer, and 3) 250-3000 m deep layer. The DCD method yielded a net inflow of

1.9 Sv, the difference between a northward transport of 8.4 Sv and a southward transport of 6.5 Sv. These values are larger than expected, and also indicate a 23 % imbalance between outflow and inflow.

When the water column is divided into subsections, the resulting values would appear to suggest that the greatest source of transport in or out of the Gulf originates in the deepest section (@ 250 - 3000 m). The upper two sections show significantly less transport activity than the deep section. The upper two sections combined yielded a net outflow of -0.7 Sv, the difference between a total northward transport of 2.5 Sv and a total southward transport of 3.2 Sv. These values appear reasonable, and the -0.7 Sv net outflow is in generally good agreement with the ± 0.9 Sv total suggested by Bray (1988a).

The deep layer section yields a net inflow of +2.7 Sv, the difference between an inflow of 6.0 Sv and 3.3 Sv. The uncertainty over the large magnitude

of the full section transport values and exchange imbalance appears to be related to the deep layer analyses. It is conceived that any inaccuracy in estimating the sluggish speeds occupying the voluminous deep layer would translate into considerably larger error in the associated transports.

For the 1500 m LNM calculation, transport results were nearly opposite of those observed using the DCD method. The full section analyses yielded a net outflow from the Gulf of -1.7 Sv, the difference between an inflow of 6.5 Sv and outflow of 8.2 Sv.

The final results are from application of the Reid & Mantyla technique. This resulted in a significantly higher inflow (12.0), and hence a positive net transport value (+3.7).

The transport balance is defined by the following equation: $V_i + R + P = V_o + E$ (Pickard and Emery, 1990). The inflow and outflow transports are given by V_i and V_o , respectively, with runoff (R),

precipitation (P) and evaporation (E) being the other variables. Experimentally, inflows and outflows have not always balanced (Roden and Groves, 1959 and Roden, 1972). Anticipating that evaporation in the Gulf (≈ 0.95 m/yr by Bray (1988a)) to be considerably greater than runoff and precipitation, would suggest an expected small net inflow to balance Gulf processes. The +1.9 Sv full section net inflow is again larger than was expected, and is credited to having included the deep layer section in the results. Still, the weaker currents of the voluminous deep layer do appear to be organized into regions of inflow and outflow. Taken collectively, they are responsible for an appreciable amount of the transport activity occurring at the Gulf's entrance, and should thus be considered.

TABLE 1. PESCAR 02 ACROSS-GULF VOLUME TRANSPORT

Volume Transport:

	Ref. wrt <u>1500 m</u>	Deepest Common <u>Depth</u>	Reid & <u>Mantyla</u>
Full Section			
Pos. Volume [Inflow] →	6.5	8.4	12.0
Neg. Volume [Outflow] →	8.2	6.5	8.3
[Inflow]-[Outflow] →	-1.7	+1.9	+3.7
=====	=====	=====	=====
Upper 50 m Section			
Pos. Volume [Inflow] →	0.6	0.6	1.0
Neg. Volume [Outflow] →	0.9	0.8	0.9
[Inflow]-[Outflow] →	-0.3	-0.2	+0.1
50 - 250 m Section			
Pos. Volume [Inflow] →	1.8	1.9	3.5
Neg. Volume [Outflow] →	2.6	2.4	2.5
[Inflow]-[Outflow] →	-0.8	-0.5	+1.0
250 - 3000 m Section			
Pos. Volume [Inflow] →	4.2	6.0	7.7
Neg. Volume [Outflow] →	4.9	3.3	5.0
[Inflow]-[Outflow] →	-0.7	+2.7	+2.0

• units are in Sv (Sverdrup)

6. Salt Budget

A salt budget analysis was performed as a tool to help interpret transport values, and also confirm the most suitable geostrophy technique. The salt budget for the study region can be estimated by simply multiplying the volume transports into (V_i) and out of (V_o) the Gulf by their corresponding salinities, S_i and S_o . A reasonable balance of salt should exist, as defined by the following conservation principle: $V_i \rho_i S_i = V_o \rho_o S_o$ (Pickard and Emery, 1990). The densities of the above relation, ρ_i and ρ_o , can be ignored since their variation is not appreciable (less than 3 %).

The cut-and-fill option of **SURFER** performed the necessary operations, producing the salinity transports (or salt fluxes) presented in Table 2. Units of $\text{psu} \cdot \text{Sv}$ were obtained by dividing computed results by 10^5 . The $\text{psu} \cdot \text{Sv}$ were subsequently converted to more conventional units of metric tons salt per

second (tonne/sec), approximating the seawater density as 10^3 kg/m^3 and using g salt per kg water for psu.

Review of the full section results in Table 2 reveals that the DCD method provided the best results for this experiment. The Reid and Mantyla method gave the greatest imbalance of the three techniques, over twice that observed with the other techniques. And the negative-valued net salt balance (-5.0×10^4 tonne/sec) obtained using the 1500 m LNM, questions its use as the best option. Given the exchange processes governing the Gulf, where inflow replenishes evaporative loss with water and accompanying salt, a net loss of mass, as calculated above, would seem highly improbable. The salinity transports derived using the DCD method are higher than anticipated (with a net imbalance of $+6.0 \times 10^4$ tonne/sec), but are the most reasonable results from the techniques tried. Predictably, as with the volume transports, the most significant figures were obtained from the deep, 250-300 m layer. Again, the deep layer processes are no

doubt real; however, the lack of balance in the salt transports calculated there seem too high, and should be considered as the most likely source of the wide, full section imbalance.

TABLE 2. PESCAR 02 ACROSS-GULF SALT FLUX

Salinity Transport:

	Ref. wrt <u>1500 m</u>	Deepest Common <u>Depth</u>	Reid & <u>Mantyla</u>
Full Section			
Pos. Volume [Inflow] →	2.3×10^5	2.9×10^5	4.1×10^5
Neg. Volume [Outflow] →	2.8×10^5	2.3×10^5	2.8×10^5
[Inflow]-[Outflow] →	-5.0×10^4	$+6.0 \times 10^4$	$+1.3 \times 10^5$
-----	-----	-----	-----
Upper 50 m Section			
Pos. Volume [Inflow] →	2.0×10^4	2.1×10^4	3.4×10^4
Neg. Volume [Outflow] →	3.1×10^4	2.9×10^4	3.0×10^4
[Inflow]-[Outflow] →	-1.1×10^4	-8.0×10^3	$+4.0 \times 10^3$
50 - 250 m Section			
Pos. Volume [Inflow] →	6.2×10^4	6.6×10^4	1.2×10^5
Neg. Volume [Outflow] →	8.9×10^4	8.2×10^4	8.5×10^4
[Inflow]-[Outflow] →	-2.7×10^4	-1.6×10^4	3.5×10^4
250 - 3000 m Section			
Pos. Volume [Inflow] →	1.5×10^5	2.1×10^5	2.7×10^5
Neg. Volume [Outflow] →	1.7×10^5	1.2×10^5	1.7×10^5
[Inflow]-[Outflow] →	-2.0×10^4	$+9.0 \times 10^4$	$+1.0 \times 10^5$

* units are in tonne /sec

7. Summary

Three geostrophic velocity regimes comprise the circulation occurring at the entrance to the Gulf of California. A large flux of deeply-penetrating southward flow was prevalent in the western Gulf along the slopes of the Baja shelf. This current exhibited maximum speeds of about 70 cm/sec in the near-surface layer, and was correlated with high-salinity water from the northern Gulf. In the central and eastern sections of the Gulf, a combination of both northward (inflow) and southward (outflow) currents were observed in the upper 500 m layer. Two prominent inflow currents were isolated. One, centered just 20 km east of the large outflowing core, was constrained to the upper 100 m layer and had maximum velocities near the surface, approaching 56 cm/sec. The other, a less intense but larger core, had maximum current speeds of about 35 cm/sec flowing within the core. Centered approximately 75 km off the Mexican mainland, the core extended 400 m deeper into the water column

than the other inflow core. Both inflowing cores entrained cool, low-salinity water, likely originating from California Current Water. Although not as evident as the high-intensity cores found in the upper layers, deep water currents in both directions were prevalent in the voluminous abyssal layer. Rarely exceeding speeds of 5 cm/sec, these currents, when considered as a whole, move immense volumes of water; and therefore, should be recognized as having an integral role in the advective processes occurring in the Gulf. However, the low current speeds prevent an accurate computation of the baroclinic flow. Deep waters to the north of the Alarcon Seamount moved westward towards the Baja shores, while corresponding waters south of the seamount flowed east towards the Sinaloa coast. This implies a cyclonic circulation pattern.

Of three geostrophic techniques tried, the DCD method proved to be the most suitable for the area of study. It minimized the net salt transport and provided a reasonable volume transport in the

upper 250 m. Applying the DCD method produced a volume inflow of 8.4 Sv and outflow of 6.5 Sv, corresponding to a net volume transport of +1.9 Sv. Salinity transports using DCD method resulted in an overall salt imbalance of $+6.0 \times 10^4$ tonne/sec. This value, as well as the residual volume transport, are too high. The obvious source of errors coincide with the included integration of the deep layer (@ 250-3000 m) section. This implies that either I failed to resolve the mass field or there are higher order dynamics. Waves trapped by the deep bathymetry along both coasts and Alarcon Seamount could induce noise in geostrophic estimates, inhibiting efforts to accurately balance mass and salt. From these results, it would appear using geostrophy can provide useful estimates in the upper layers, but has limitations at depth.

C. SATELLITE IMAGERY

The satellite image shown in Figure 7 was taken by the NOAA-11 satellite's Advanced Very High Resolution Radiometer (AVHRR) sensor on 15 December 1992. The image exemplifies the SST structure prevalent at the entrance to the Gulf of California two weeks prior to the PESCAR 02 survey. It shows SSTs ranging between 21-25 °C dominating the region, with the highest temperatures offshore and equatorward. But it's the anomalous features in the image that offer the most insight on the circulation processes occurring in the region.

In the western Gulf, along the southern shores of the Baja peninsula, surface waters of 19-20 °C are apparent. A narrow band of slightly cooler water, traced back to the inner-Gulf, is seen hugging the contours of the southern Baja banks (below 24 °N latitude) before meandering into the Pacific. South of Cabo San Lucas, the cooler surface signature gradually fades in the surrounding warmer waters. This

observation lends support to a previous assumption made from the across-gulf temperature structure (Figure 2a). That is, the low temperature cores located just offshore from the Baja peninsula represent equatorward flow of high-salinity Gulf of California Water.

Similarly, across the Gulf and alongshore the Sinaloa coast, another cool tongue of surface water is isolated. Starting at about the 24 degree parallel, the tongue's signature widens and becomes more enhanced as it's traced northward into the Gulf. Coastal SSTs north of 25 °N decrease to approximately 17 °C. According to Roden and Groves (1959), the observance of this cold water tongue may be attributed to localized upwelling brought on by seasonal northwesterly winds.

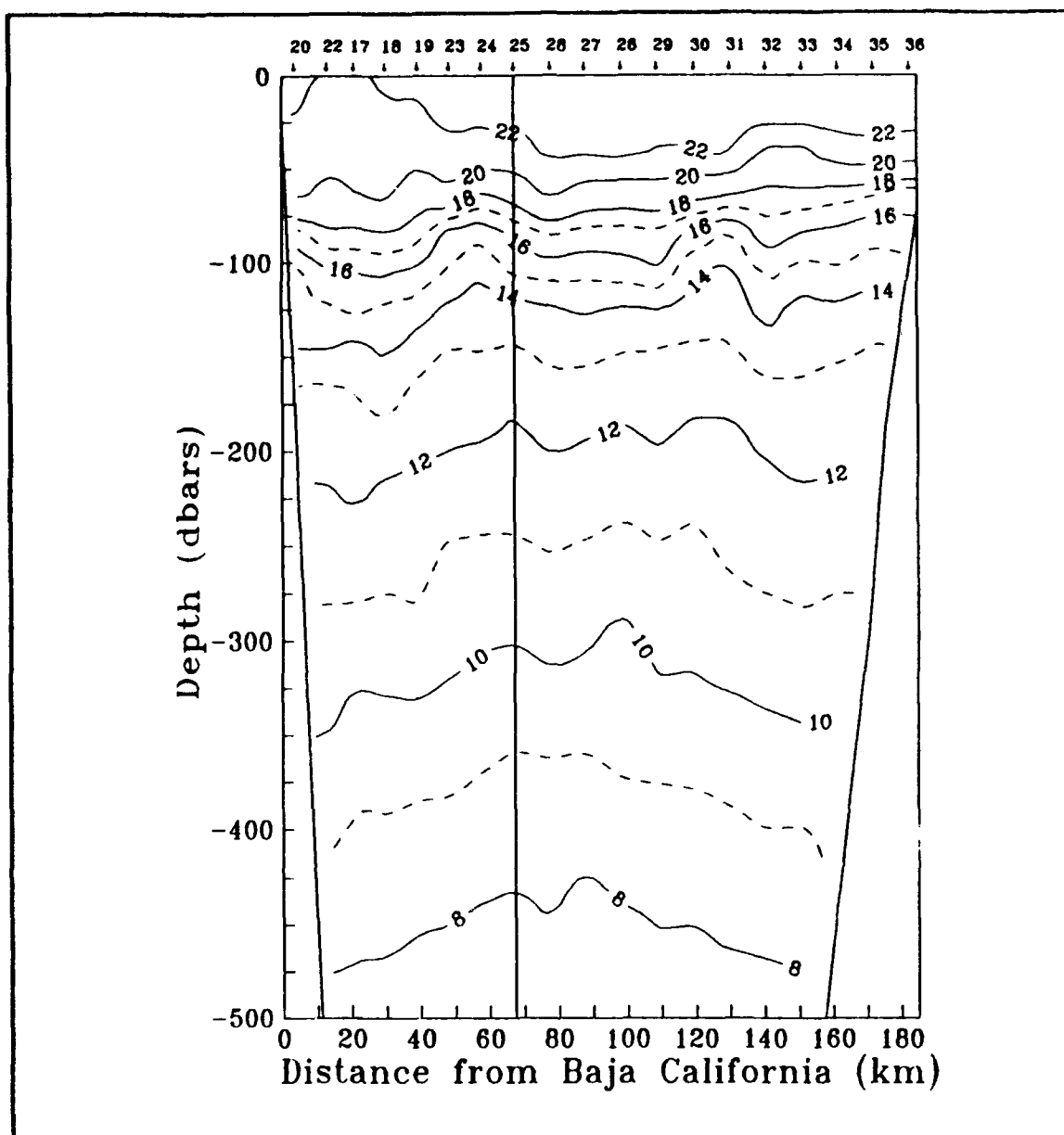


Figure 2. 500 dbar across-gulf transections for PESCAR 02 (28 December 1992 - 02 January 1993). Cast location and number are given at the top of the figure. Vertical line at cast #25 marks the position of intersection with along-gulf transection. It also denotes the location of the Alarcon Seamount. (a). Temperature. Isotherm spacing is 1 °C or as labeled.

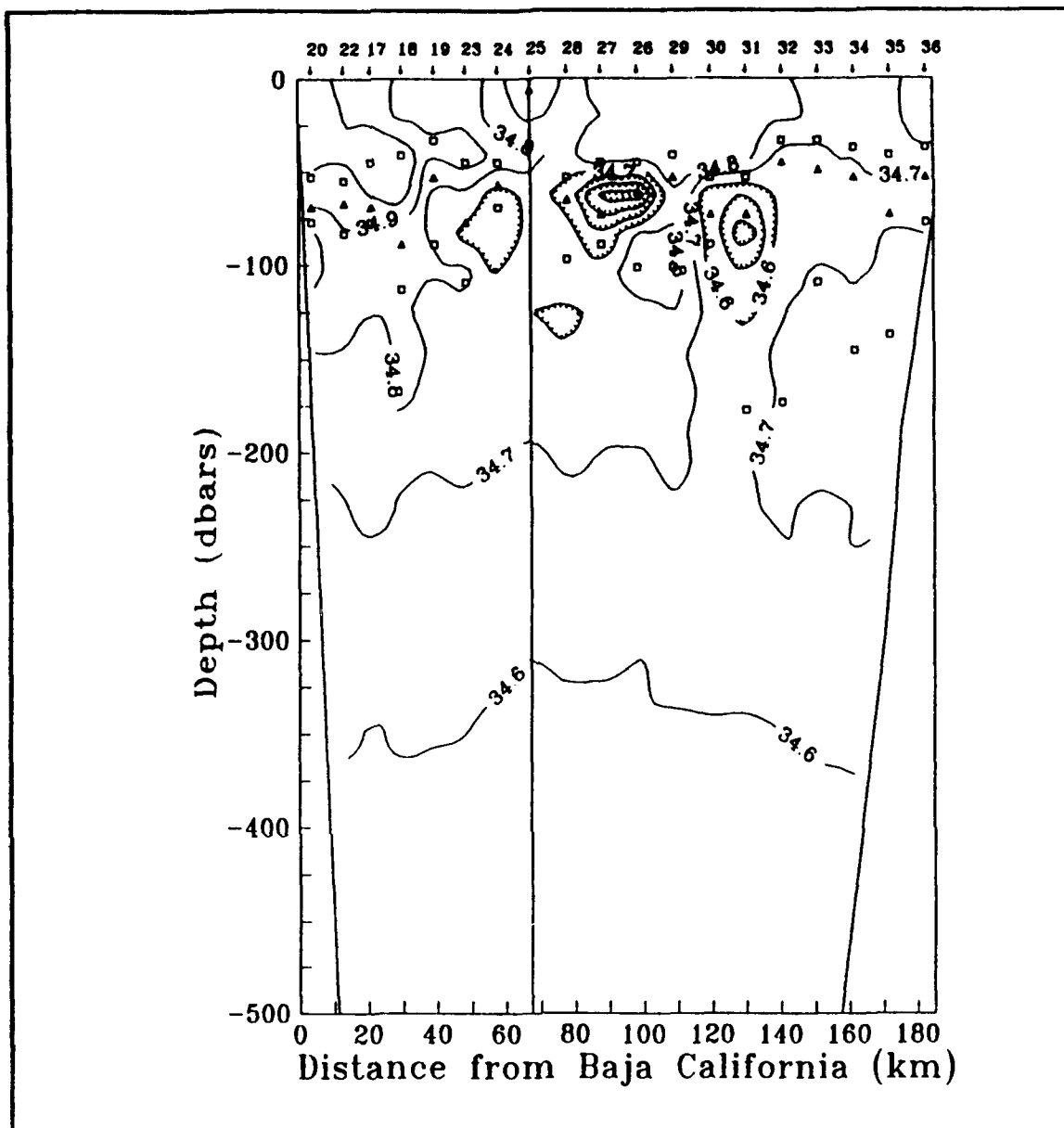


Figure 2(b). Salinity. Isohaline spacing is 0.1 psu. Cores of less saline water are denoted by hatching. The shallow layer salinity minimum is denoted by shaded triangles. Both the shallow and deep layer salinity maxima are denoted by open squares.

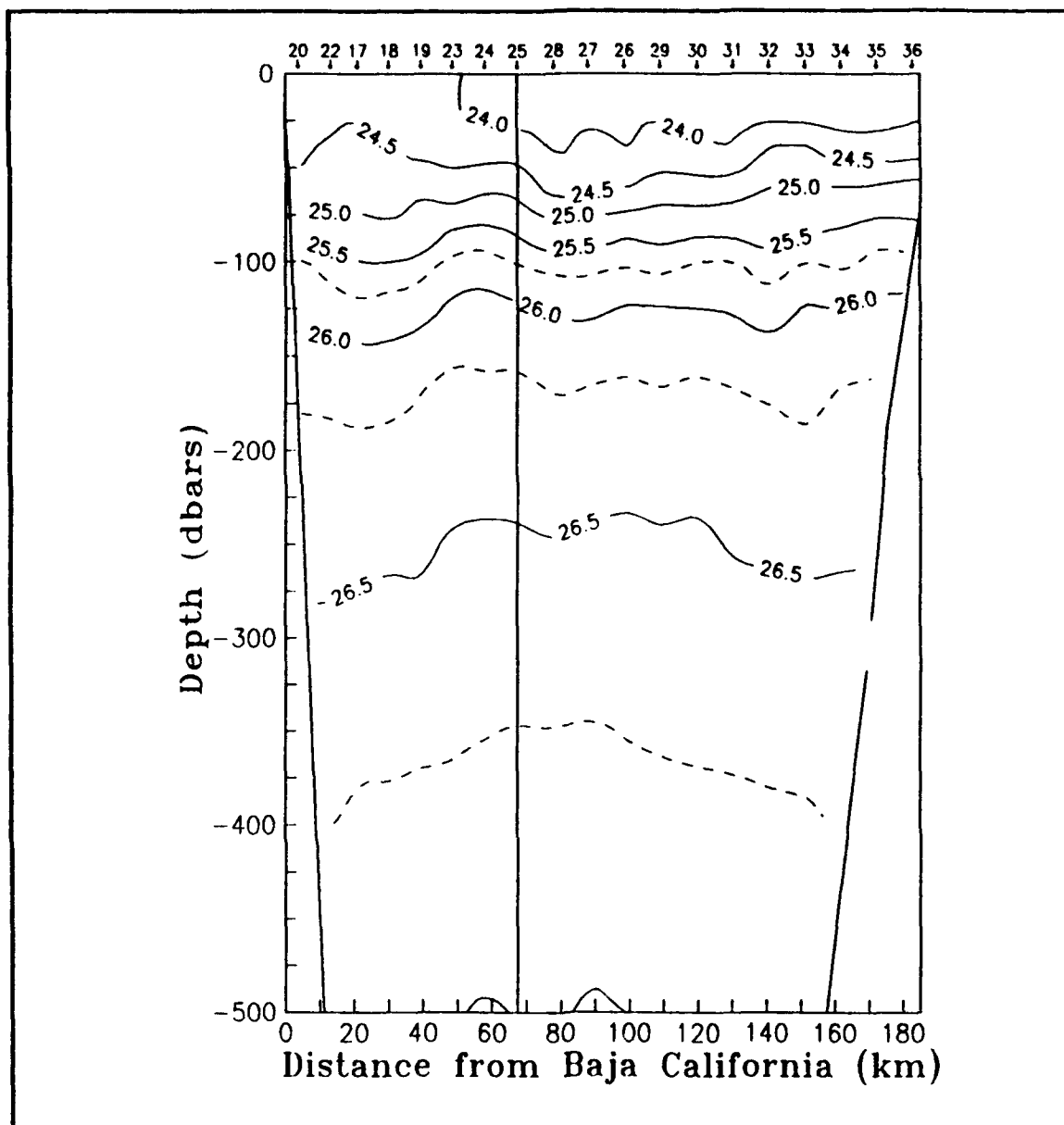


Figure 2(c). Density anomaly. Isopycnal spacing is 0.25 kg/m³ or as labeled.

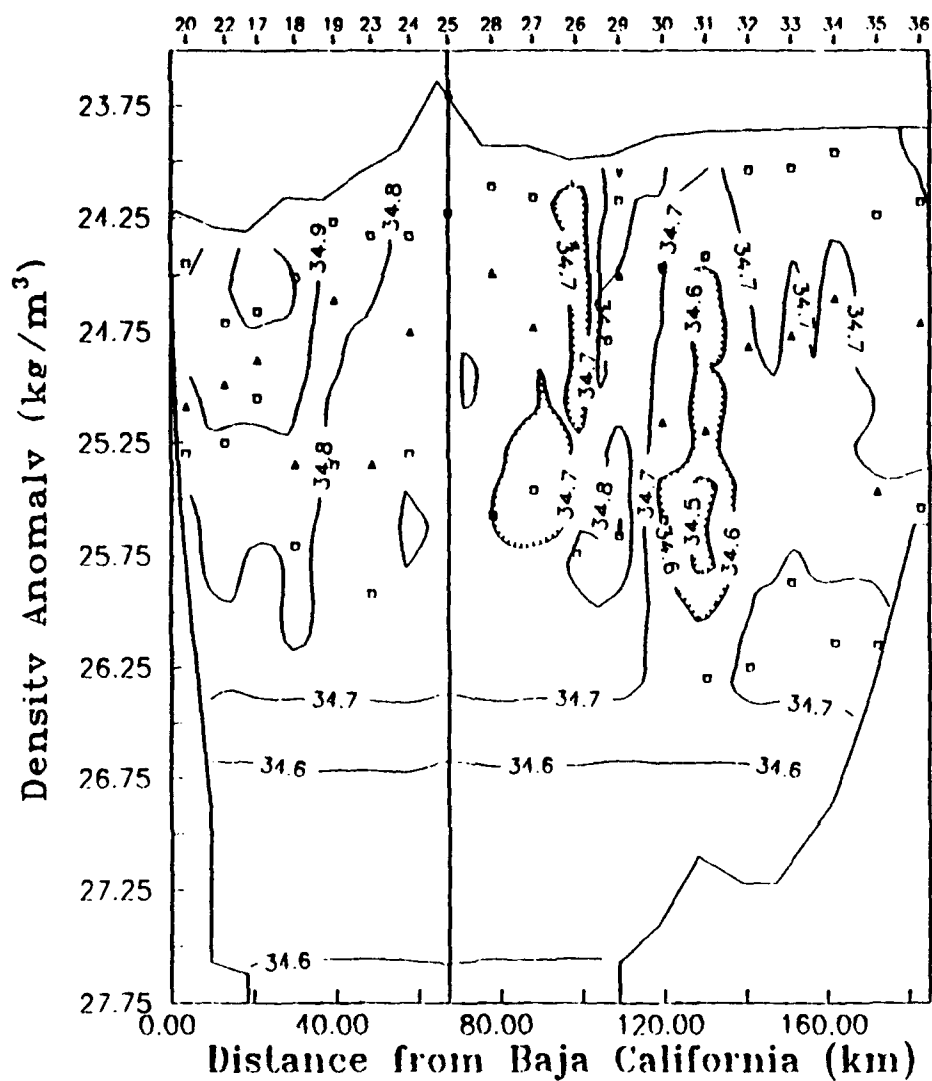


Figure 2(d). Salinity plotted on density anomaly surfaces. Isohaline spacing is 0.1 psu. Cores of less saline water are denoted by hatching. The shallow layer salinity minimum is denoted by shaded triangles. Both the shallow and deep layer salinity maxima are denoted by open squares.

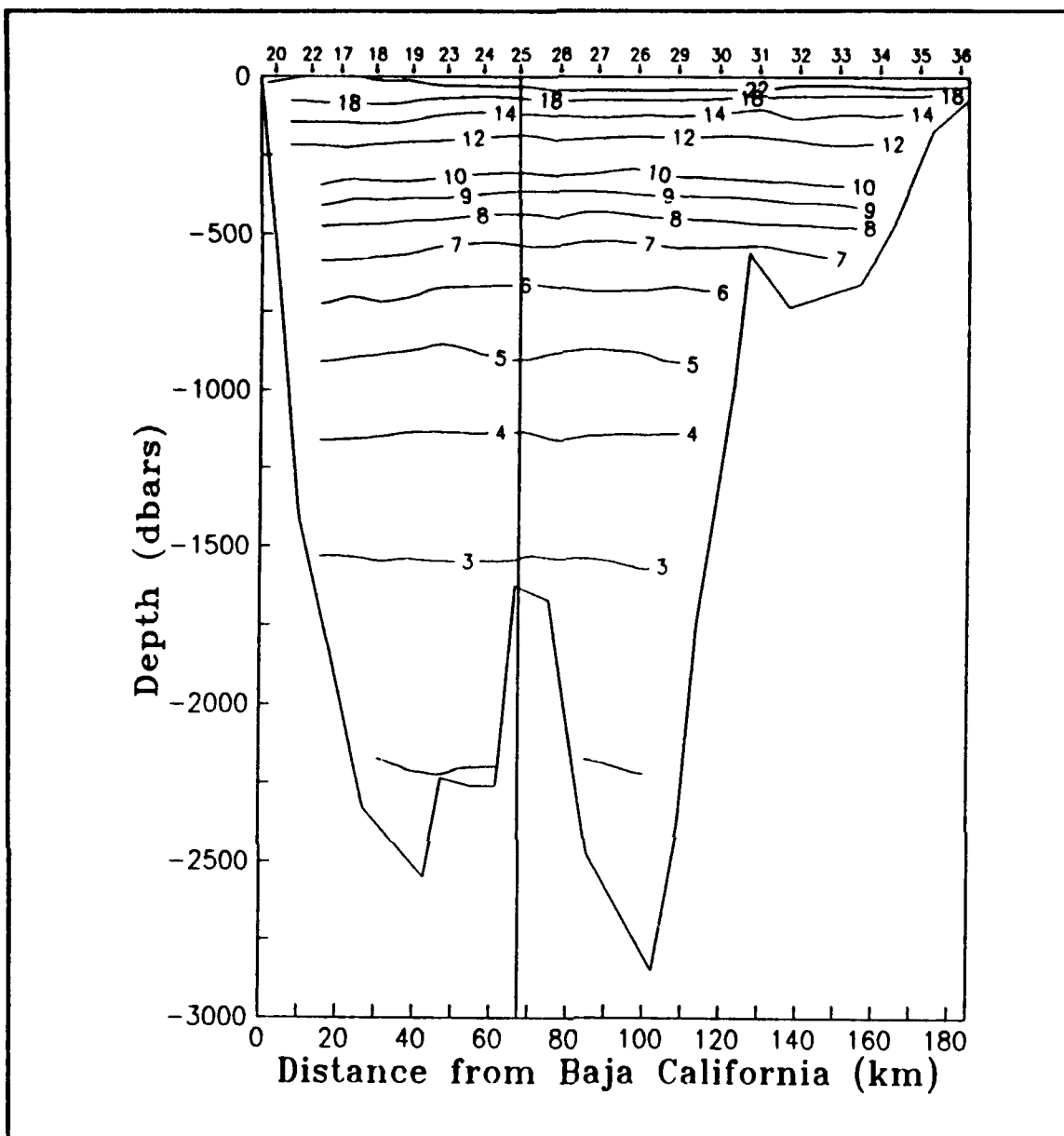


Figure 3. 3000 dbar across-gulf transections for PESCAR 02 (28 December 1992 - 02 January 1993). Cast location and number are given at the top of the figure. Vertical line at cast #25 marks the position of intersection with along-gulf transection. It also denotes the location of the Alarcon Seamount. (a). Temperature. Isotherm spacing is 1 °C or as labeled.

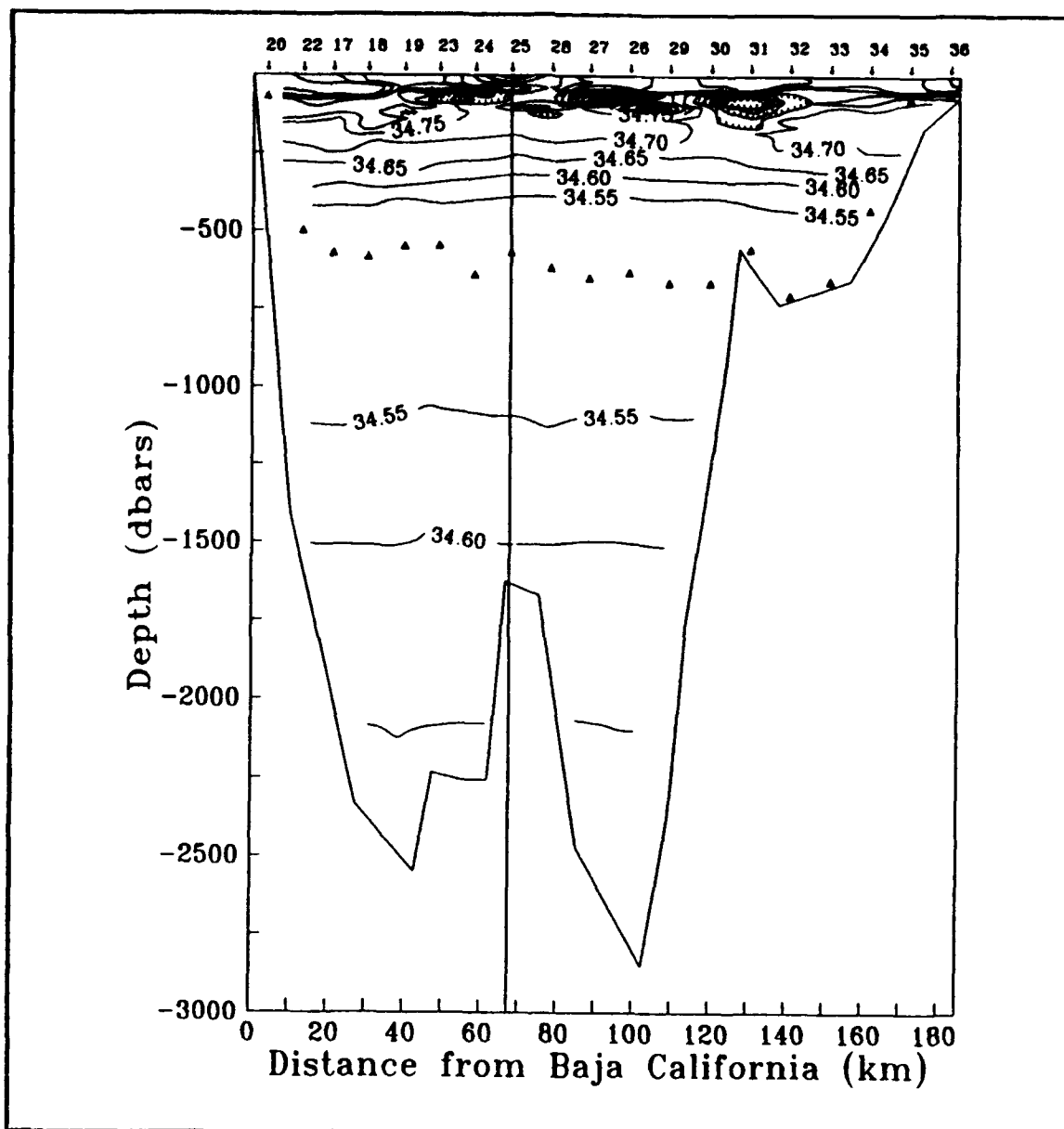


Figure 3(b). Salinity. Isohaline spacing is 0.05 psu. Cores of less saline water are denoted by hatching. The deep layer salinity minimum is denoted by shaded triangles.

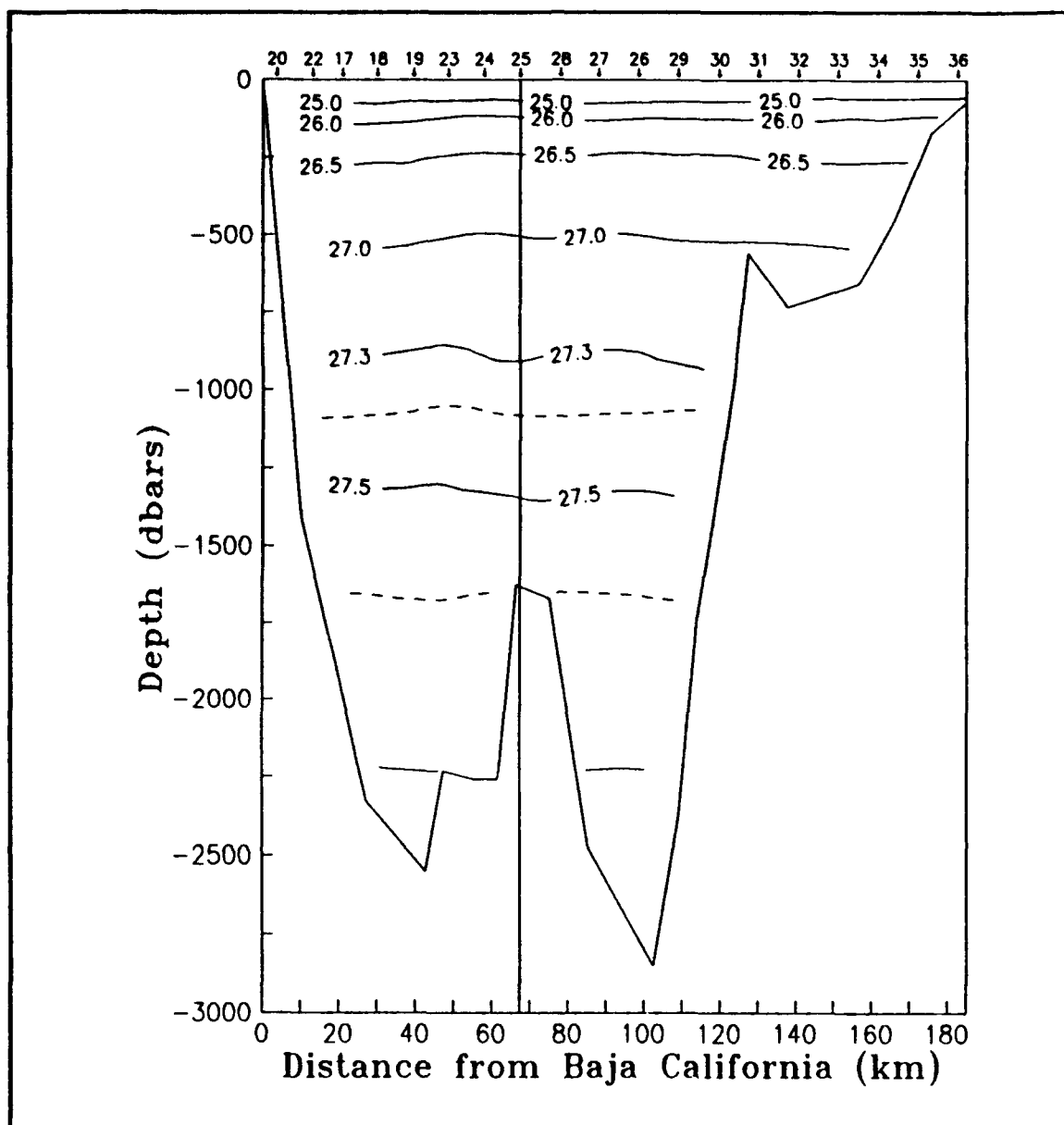


Figure 3(c). Density anomaly. Isopycnal spacing is 0.1 kg/m^3 or as labeled.

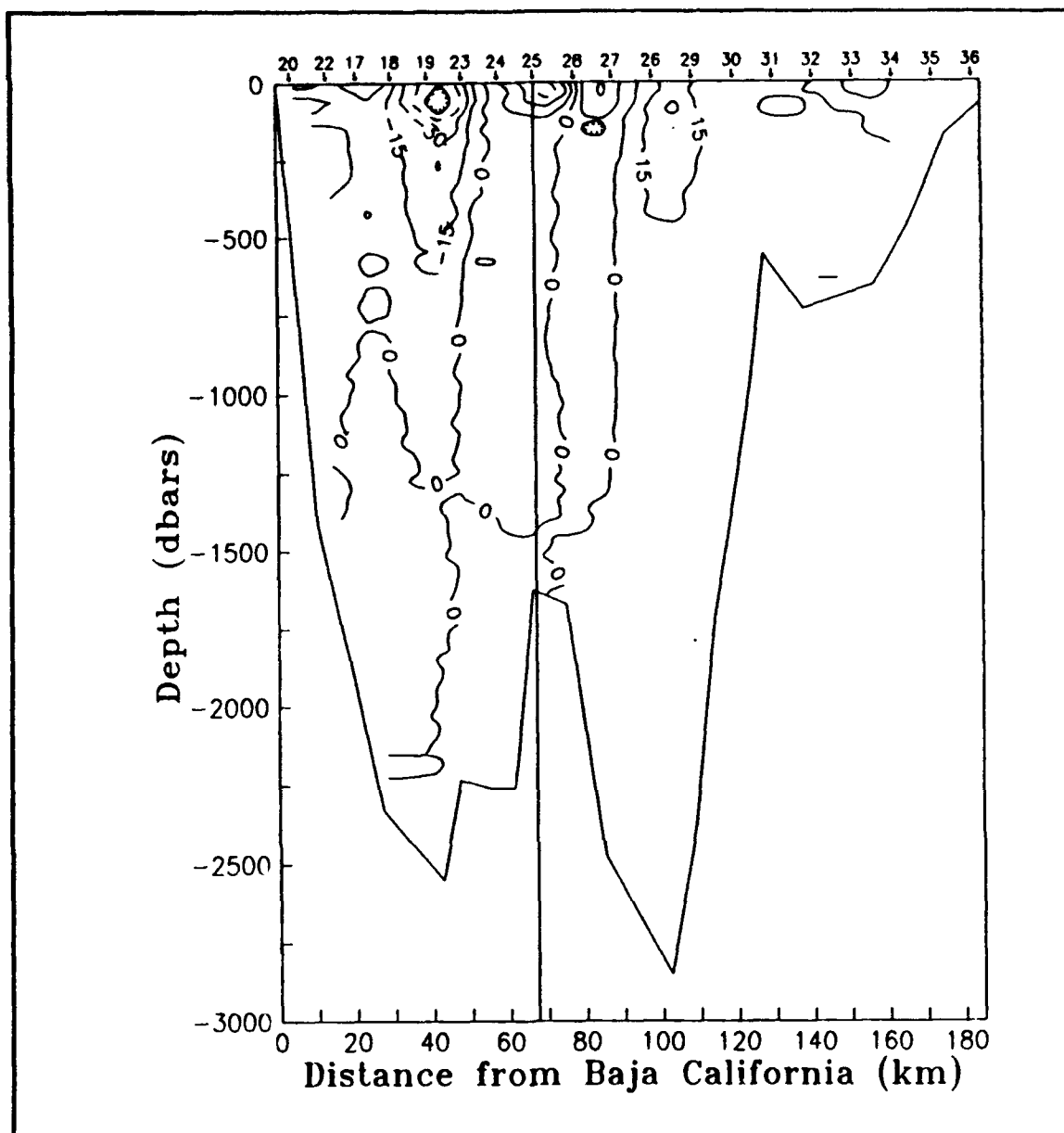


Figure 3(d). Geostrophic velocity using deepest common depth (DCD) method. Isotach spacing is 15 cm/sec.

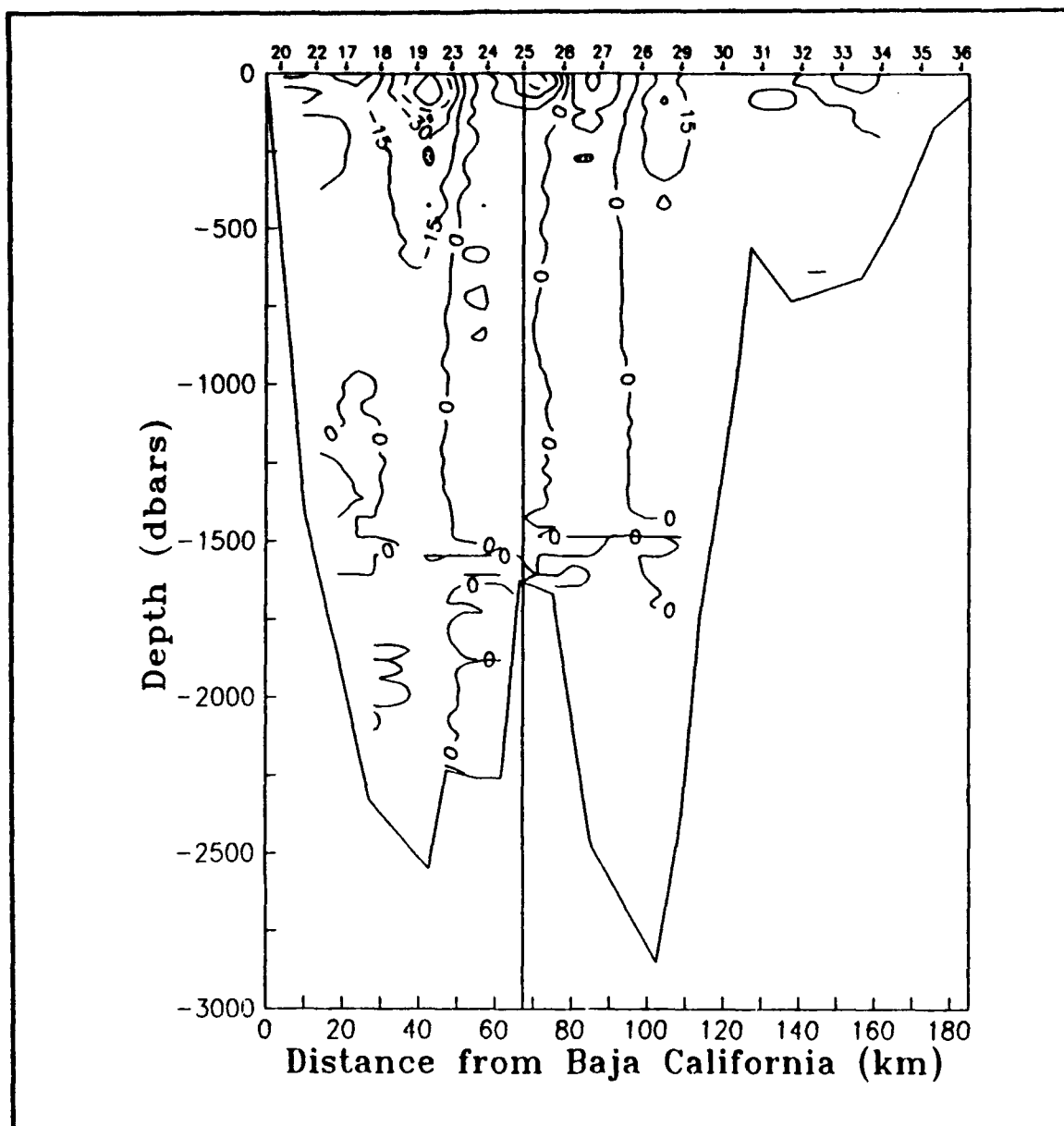


Figure 3(e). Geostrophic velocity using 1500 m as the level of no motion (LNM). At shallower casts, the DCD method was used. Isotach spacing is 15 cm/sec.

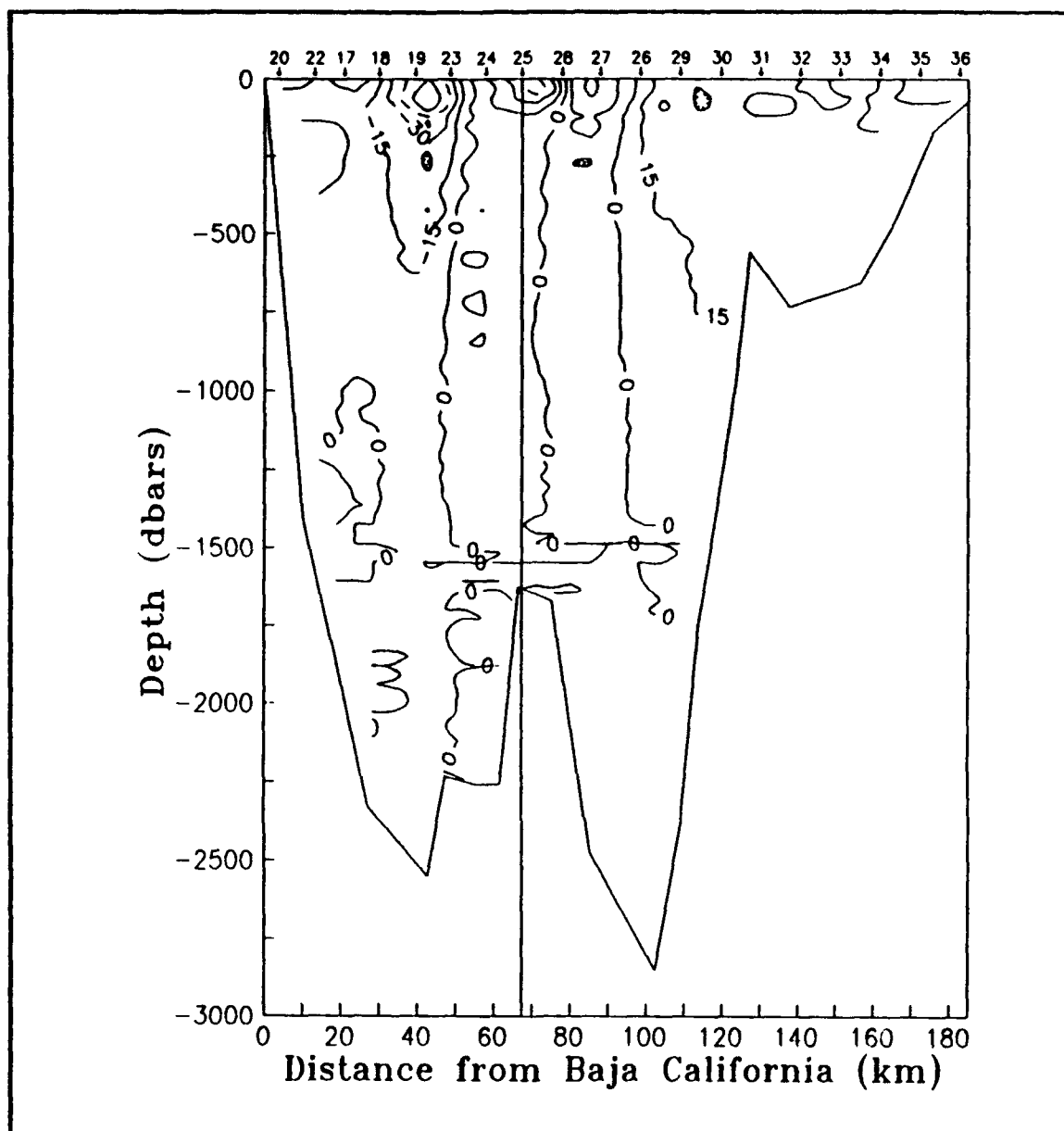


Figure 3(f). Geostrophic velocity using the Reid and Mantyla (1976) method, with 1500 dbar chosen as the reference pressure. Isotach spacing is 15 cm/sec.

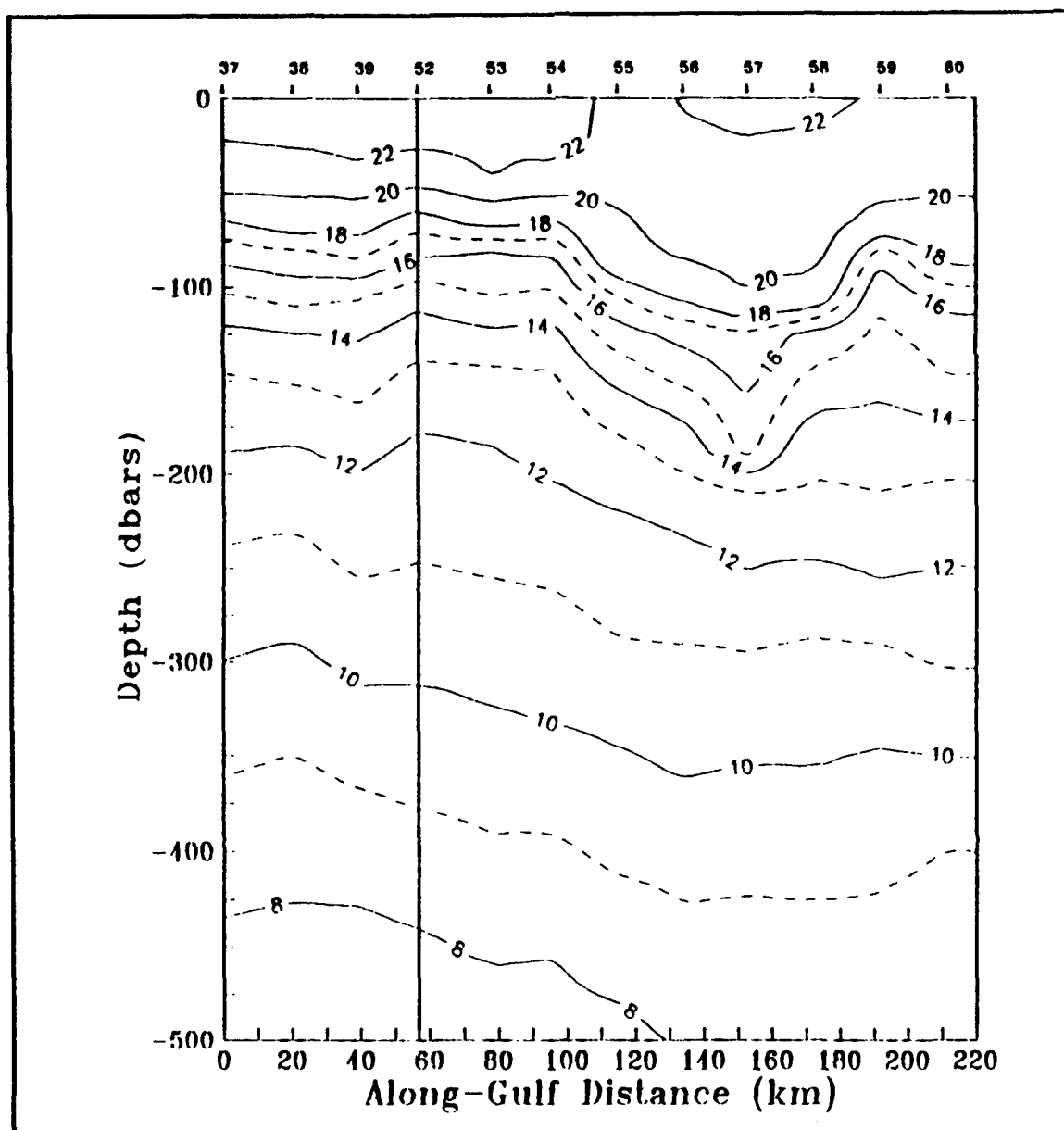


Figure 4. 500 dbar along-gulf transections for PESCAR 02 (03 - 08 January 1993). Cast location and number are given at the top of the figure. Vertical line at cast #52 marks the position of intersection with across-gulf transection. It also denotes the location of the Alarcon Seamount. (a). Temperature. Isotherm spacing is 1 °C or as labeled.

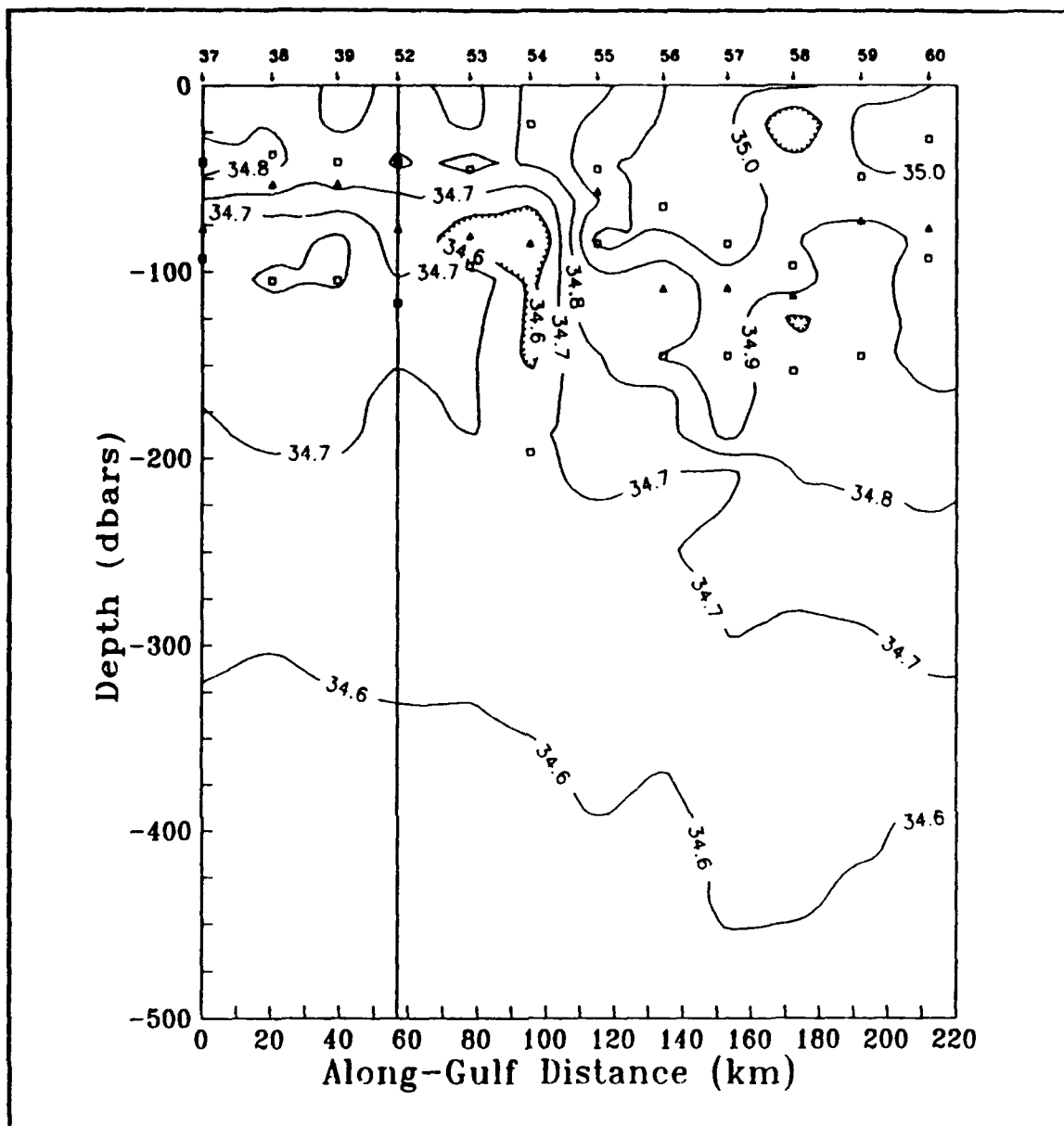


Figure 4(b). Salinity. Isohaline spacing is 0.1 psu. Cores of less saline water are denoted by hatching. The shallow layer salinity minimum is denoted by shaded triangles. Both the shallow and deep layer salinity maxima are denoted by open squares.

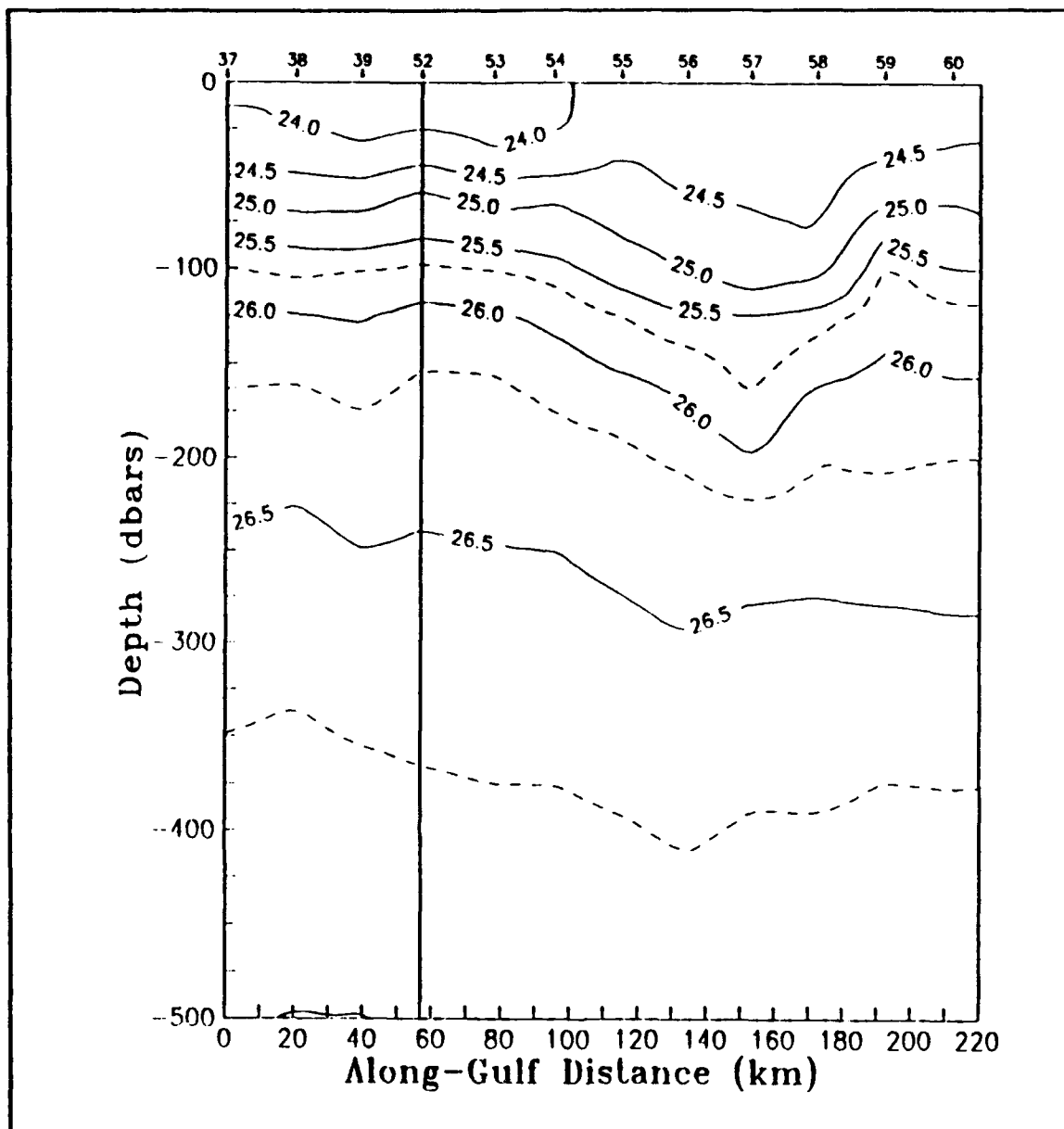


Figure 4(c). Density anomaly. Isopycnal spacing is 0.25 kg/m^3 or as labeled.

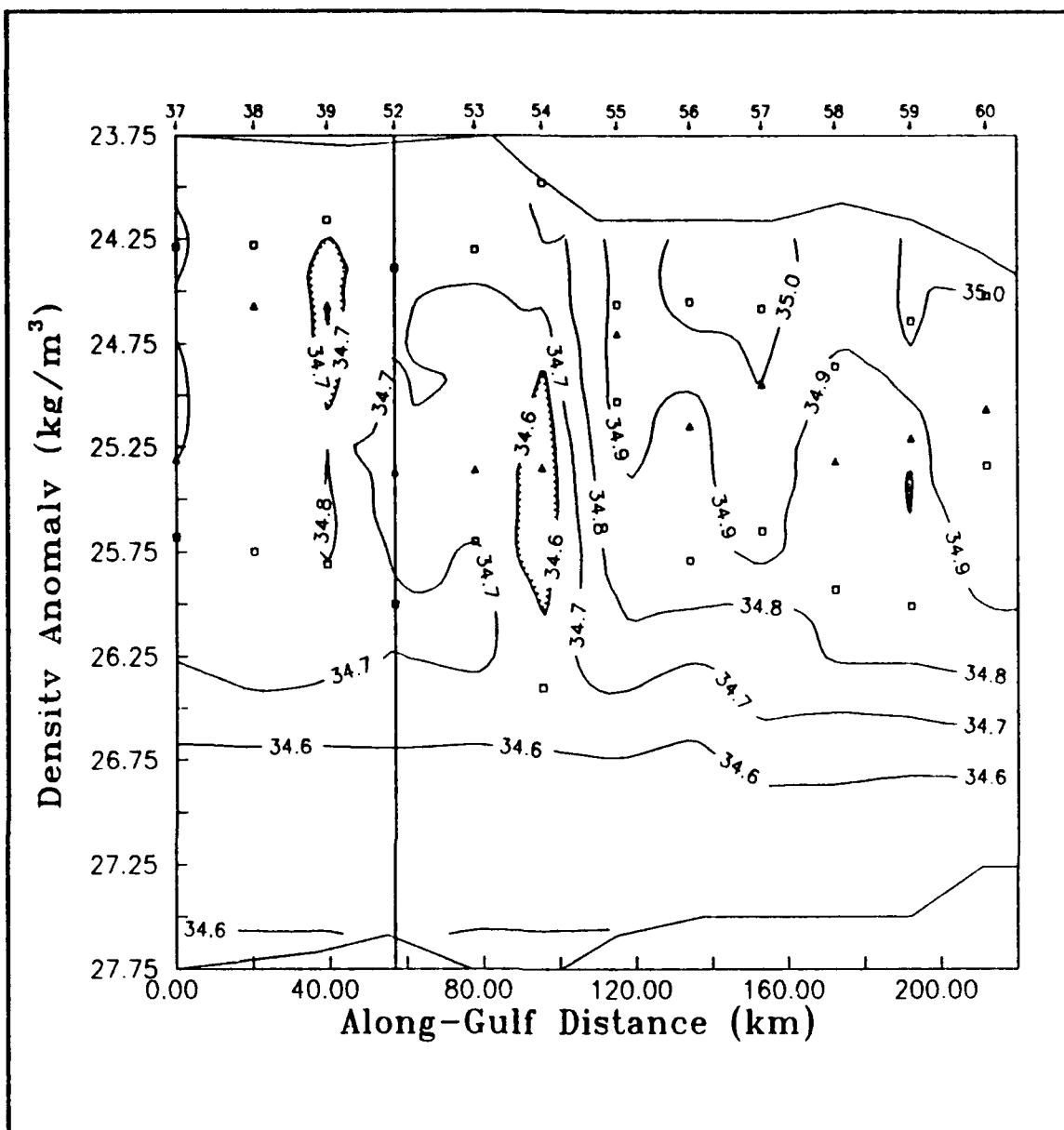


Figure 4(d). Salinity plotted on density anomaly surfaces. Isohaline spacing is 0.1 psu. Cores of less saline water are denoted by hatching. The shallow layer salinity minimum is denoted by shaded triangles. Both the shallow and deep layer salinity maxima are denoted by open squares.

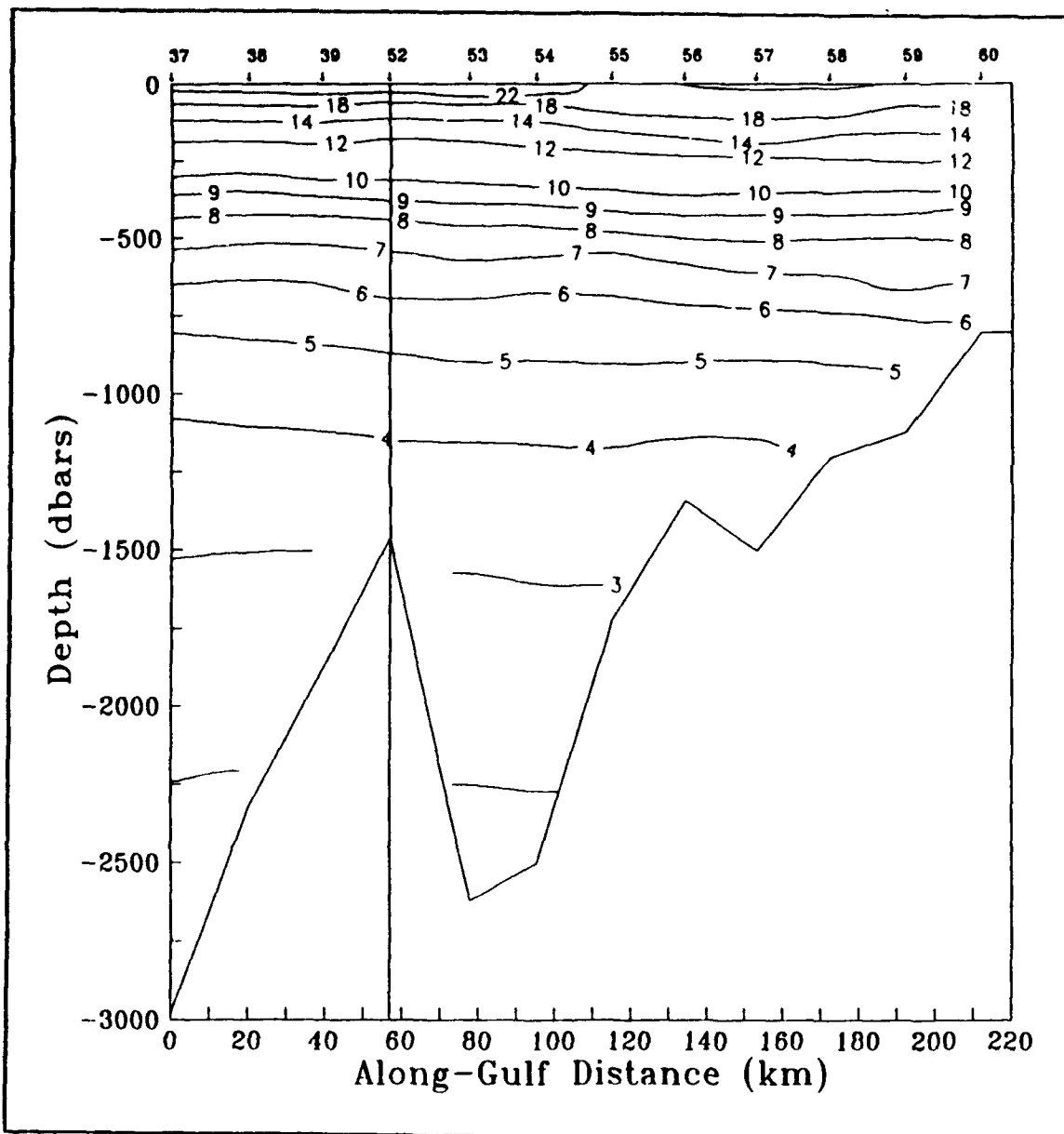


Figure 5. 3000 dbar along-gulf transections for PESCAR 02 (03 - 08 January 1993). Cast location and number are given at the top of the figure. Vertical line at cast #52 marks the position of intersection with across-gulf transection. It also denotes the location of the Alarcon Seamount. (a). Temperature. Isotherm spacing is 1 °C or as labeled.

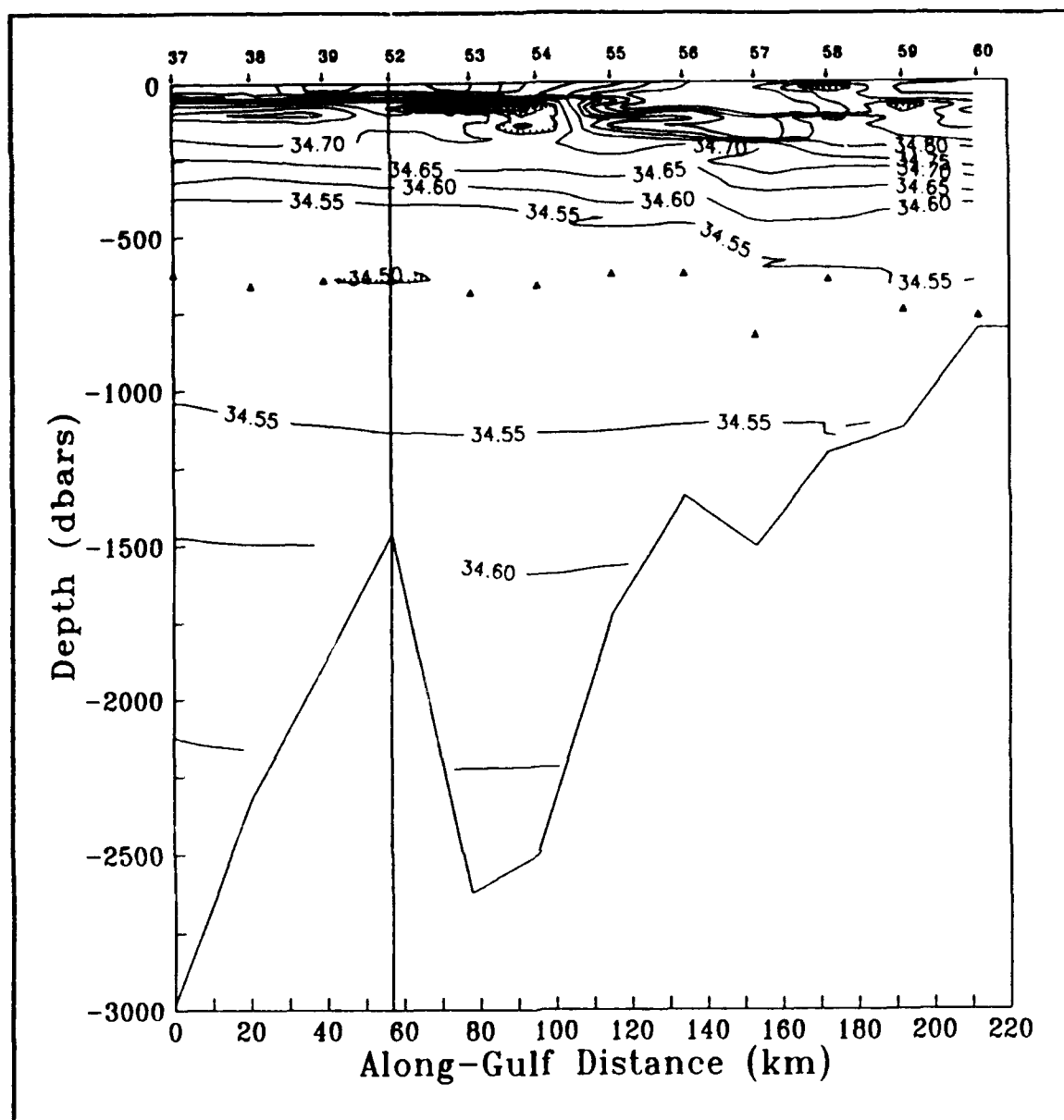


Figure 5(b). Salinity. Isohaline spacing is 0.05 psu. Cores of less saline water are denoted by hatching. The deep layer salinity minimum is denoted by shaded triangles.

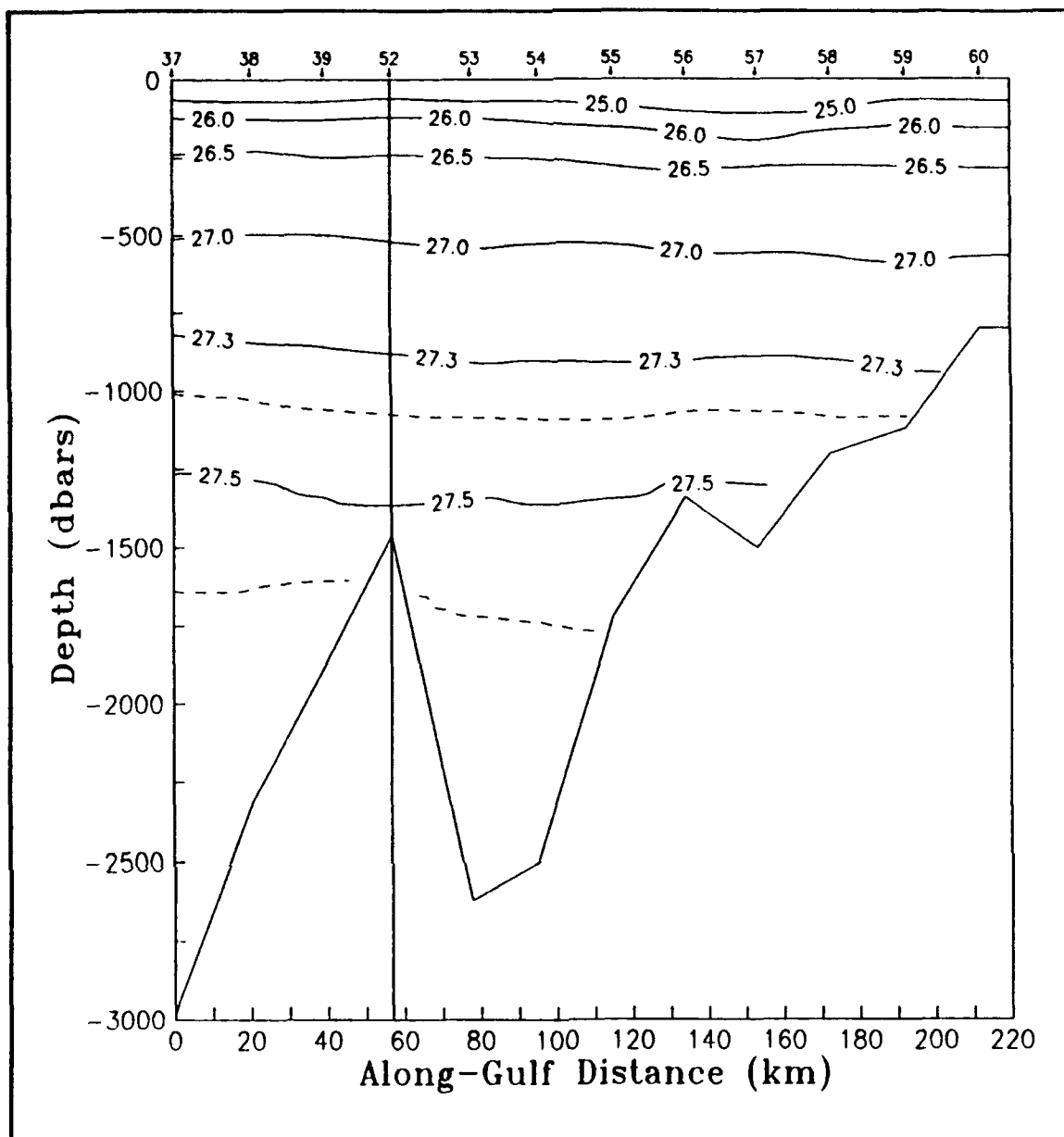


Figure 5(c). Density anomaly. Isopycnal spacing is 0.1 kg/m³ or as labeled.

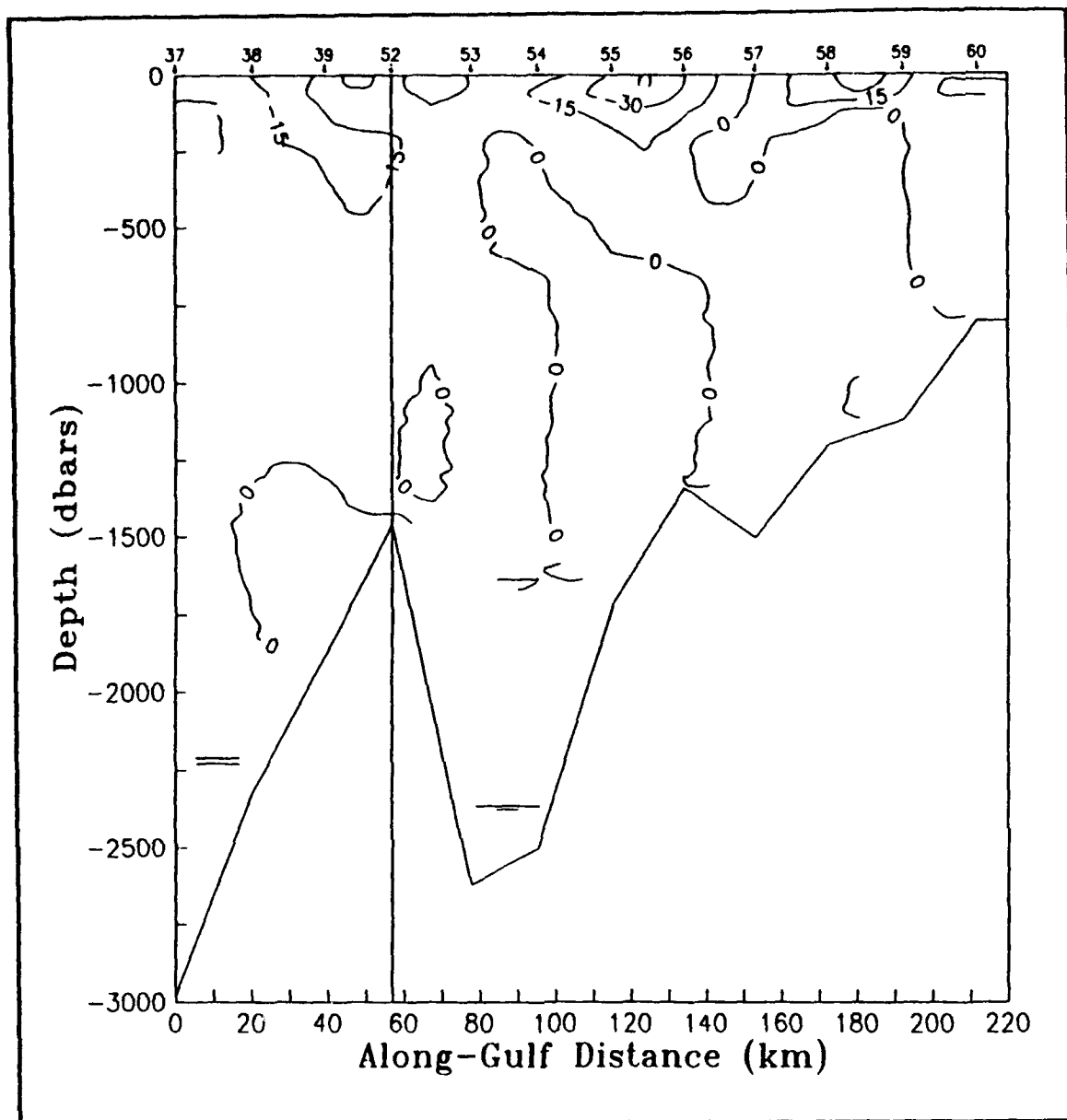


Figure 5(d). Geostrophic velocity using deepest common depth (DCD) method. Isotach spacing is 15 cm/sec.

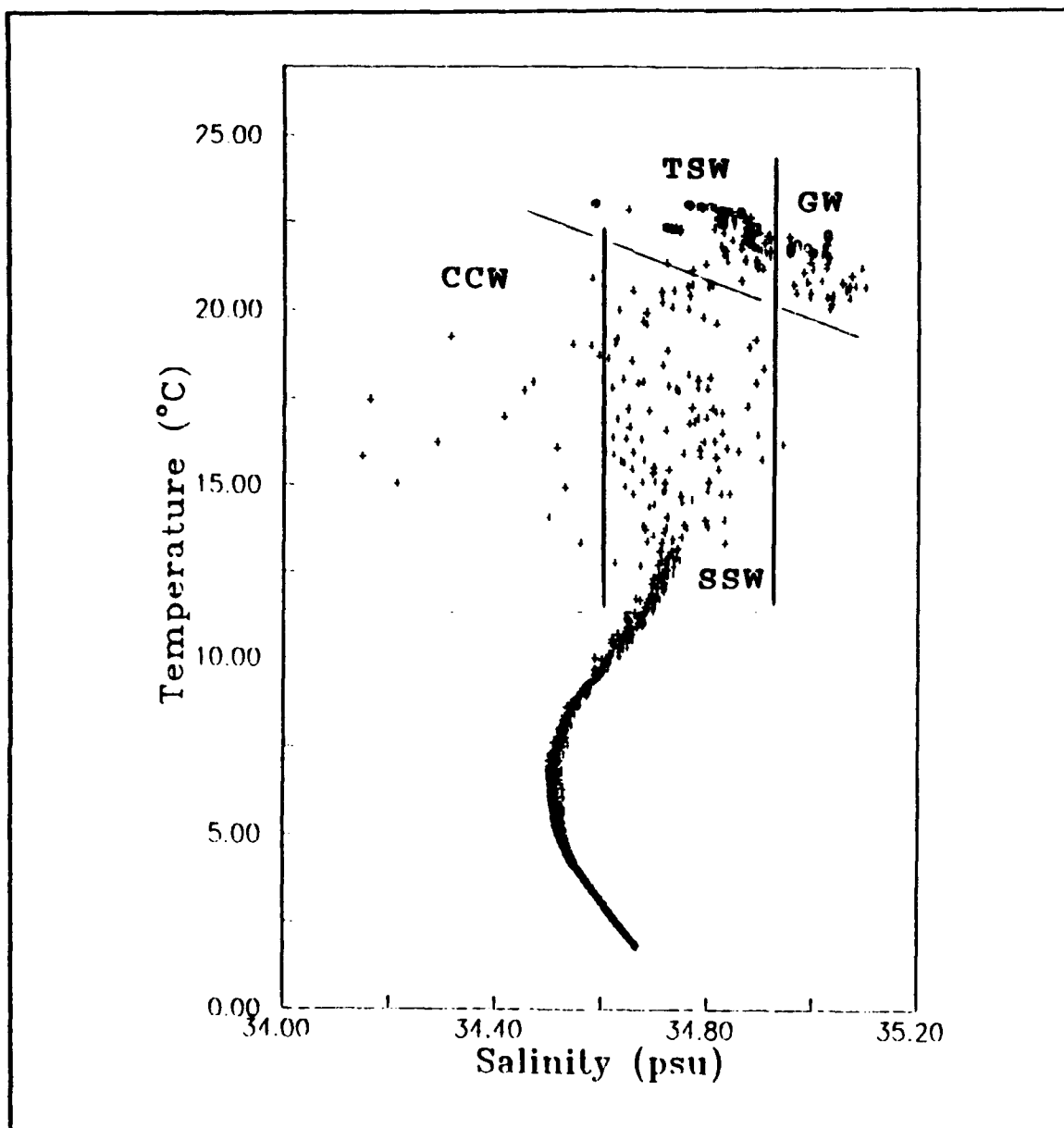


Figure 6. Full section scatter plot for across-gulf transections for PESCAR 02 (28 December 1992 - 02 January 1993). Plot is subdivided into sections by water mass: 1) **TSW** denotes Tropical Surface Water, 2) **GW** denotes Gulf Water, 3) **CCW** denotes California Current Water, and 4) **SSW** denotes Subtropical Subsurface Water. The top 10 m section is denoted by circles. (a). Temperature-Salinity (T-S) diagram.

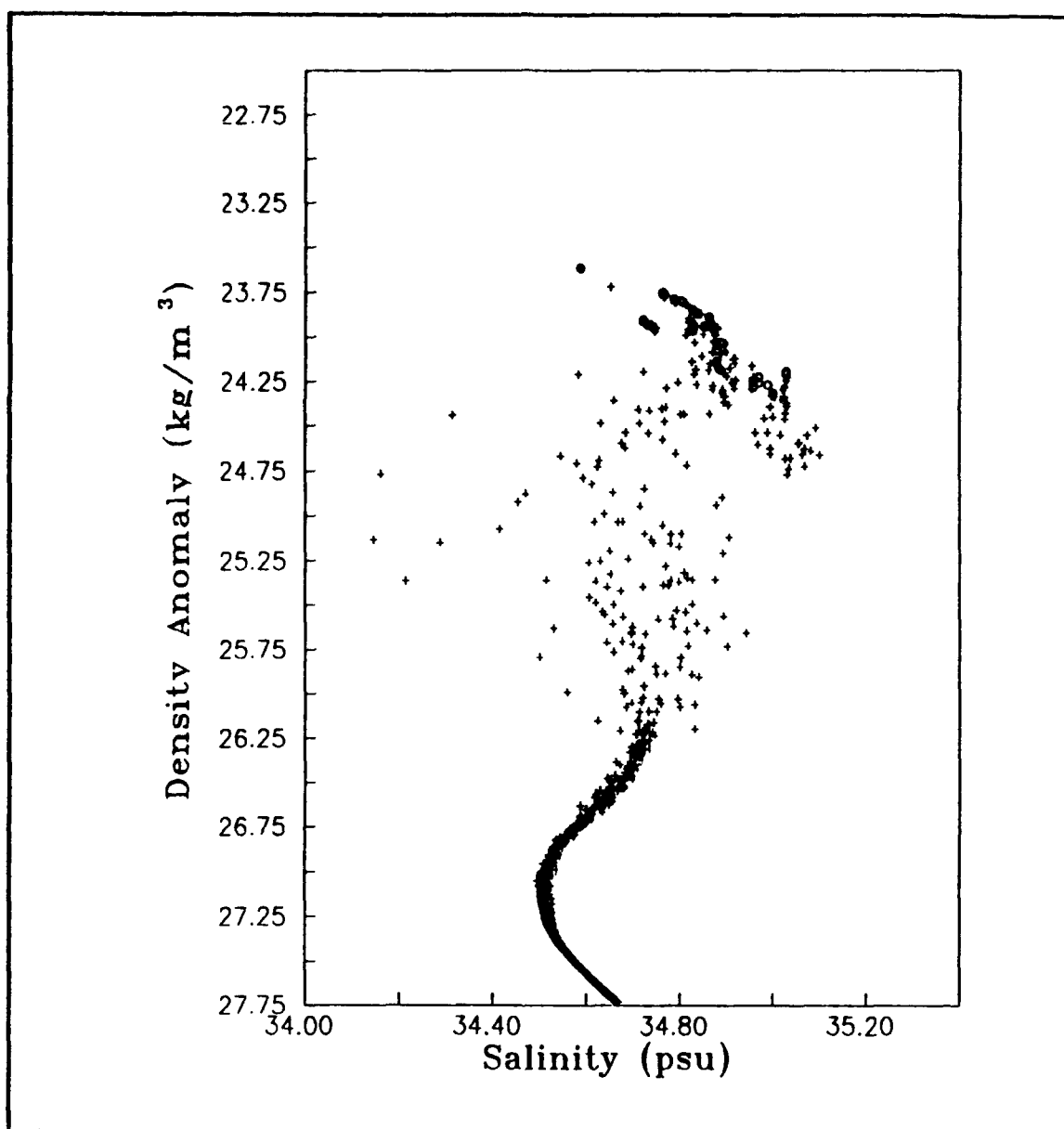


Figure 6(b). Density anomaly - Salinity (σ_t -S) diagram.

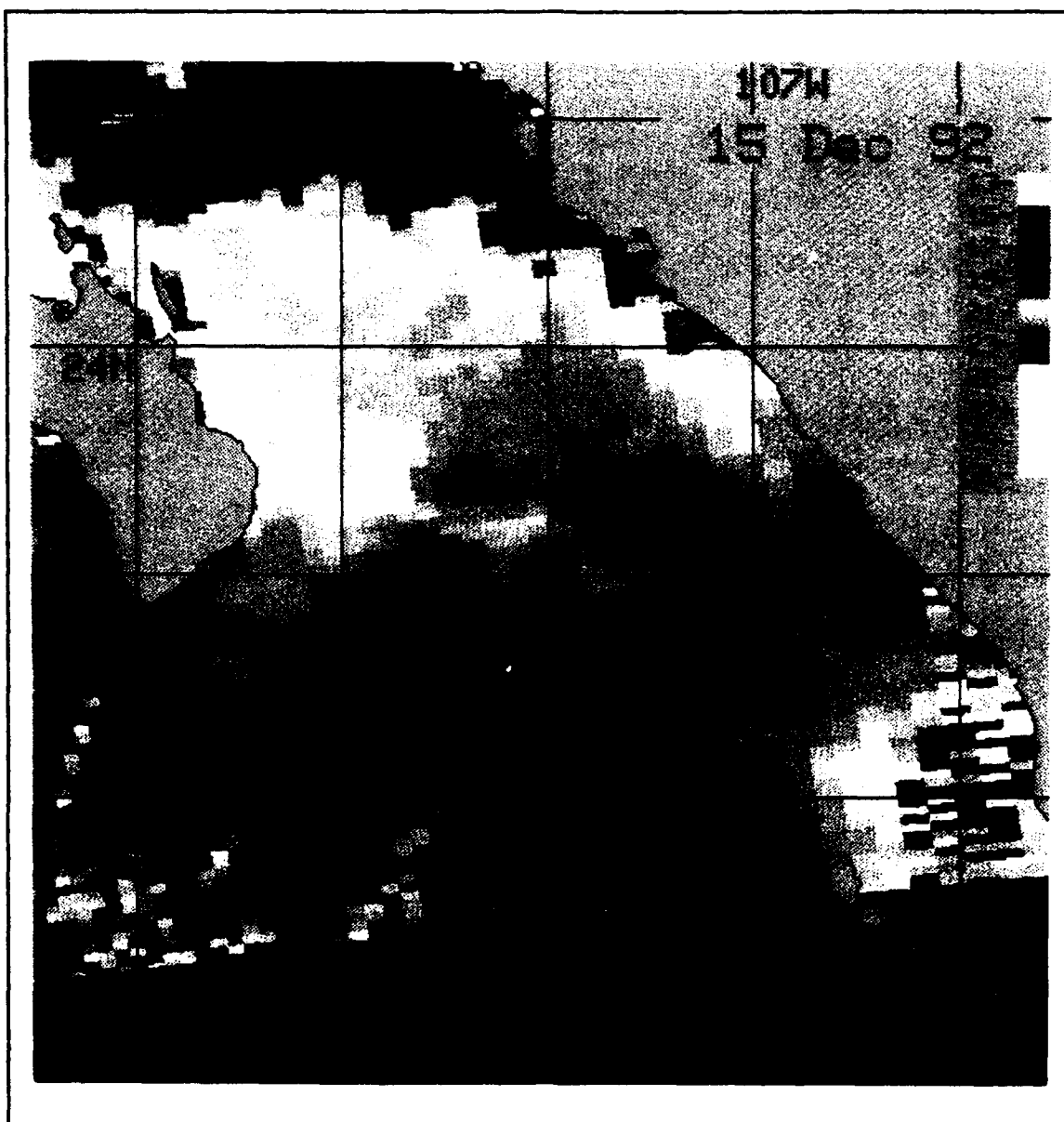


Figure 7. Sea surface temperatures ($^{\circ}\text{C}$) in the Gulf of California on December 15, 1992. Image is from the AVHRR sensor aboard the NOAA-11 satellite.

IV. CTD DATA FROM APRIL 1992

A. APRIL-MAY 1992 RESULTS

The PESCAR 01 data set was collected from 21 April-08 May 1992 aboard the *USNS DeSteiguer*. The ship performed a total of 17 CTD casts along the same across-gulf transection that was later examined during the December 1992 cruise. A Neil Brown MK-IIIB CTD was employed to collect the data. Data collection and processing procedures were similar to the PESCAR 02 cruise, with the exception that a different software package was used to process the raw data. This difference in the processing of the data had no effect in the comparison of the two cruises' data results. However, the contrasting seasonal conditions associated with the two cruises did result in appreciable differences between the data. Unlike the December cruise, which had cool, blustery winds and confused seas, the April cruise was conducted during a period of warming and was characterized by calm with

flat seas. The following paragraphs describe the observations from that survey.

The PESCAR 01 temperature structure is shown in Figures 8a and 9a. Sea surface temperatures (SSTs) were in excess of 25 °C across the entire region, with those in the eastern one-third of the Gulf measuring 1-2 °C warmer than those in the west. The isotherms reveal strong stratification of the upper layer, persisting down to about 150 m. Perhaps the most dominant feature of the shallow subsurface layer is the sudden shoaling of the 8-12 °C isotherms occurring approximately 65 Km off the Baja peninsula. The detail that makes this observation especially interesting is the fact that the doming occurs in waters overlying the mid-basin Alarcon Seamount. Whether the seamount entirely forces or even contributes to the doming is subject to conjecture. Below 500 m, the isotherms leveled and decreased uniformly with depth.

The vertical salinity structure during this period is depicted in Figures 8b and 9b. Two striking

features are seen in the upper 100 m layer. One is the broad 110 km long, shallow core of relatively low salinity (defined by hatching where $S \leq 34.5$ psu) that stretches across the entire central section of the Gulf. The other is a significantly smaller low-salinity core (defined by hatching where $S \leq 34.5$ psu) centered 25 km offshore from Baja. Defining a gradient between these two cores is a narrow higher salinity 34.6 psu region. The shallow layer salinity minimum (symbolized by shaded triangles) cuts through the center of both cores. What makes the latter core particularly interesting is that it is a core of low-salinity water situated in a region generally associated with high-salinity Gulf of California Water (Gulf Water). The presence of a salinity front may be suggested, judging from the abrupt shoaling of the 34.6 and 34.7 psu isohalines below cast #5. The low-salinity waters observed in the eastern Gulf interleaving the slightly deeper, higher salinity waters to the west (identified by the 34.8 psu

isohaline) could produce such a front. The plotting of salinity on density anomaly surfaces (Figure 8d) also depicts this boundary, existing between the 24 and 25.5 kg/m³ density surfaces. Also of interest is that the shallow salinity maximum (symbolized by squares) is found at the surface. Below 200 m, the isohalines dome sharply near the center of the transection. This feature persists down to the bottom and may be associated with flow around the Alarcon Seamount.

Strong stratification reaching to the surface characterizes the upper 150 m layer of the density anomaly structure (Figures 8c and 9c). The isopycnals remain tightly packed throughout this entire upper layer. Surface layer densities across the Gulf exceed 23.0 kg/m³. Just below the surface and penetrating to about 125 m, a broad section of depressed isopycnals in the western half of the Gulf (between casts 6-10) separate two domed regions of isopycnals. East of cast #14 the isopycnals slope downward towards the Mexican mainland, indicating generally less dense waters in

the eastern region of the Gulf. These observations may suggest a two-celled cyclonic gyre system within the near-surface structure, or possibly an eddy over the seamount imbedded in general cyclonic flow. In the subsurface waters underlying the upper layer where the isopycnals are depressed, dramatic shoaling of the isopycnals occurs. The rising isopycnals produce impressive doming features that persist as deep as 1000 m. This subsurface representation may be indicative of a large cyclonic gyre system circumscribing the mid-basin seamount.

The temperature - salinity (T-S diagram) and density anomaly - salinity (σ_t -S diagram) relationships for this cruise (Figures 10a and 10b, respectively) reveal both expected and some surprising results. The associated insolation increase of April and May increased SSTs as expected, with maximum temperatures reaching about 26.5 °C. However, a more interesting observation is the apparent lack of Gulf of California Water in the region. Both diagrams

indicate salinity maxima of about 34.85 psu, clearly below the 34.9‰ used to isolate Gulf Water. Waters at the surface are a probable mixture of Tropical Surface Water with some influence from California Current Water ($S \leq 34.6\text{‰}$). Near-surface waters of the upper 50 m layer indicate far greater influence from California Current Water. These waters correlate with the immense across-gulf expansion of low-salinity cores seen previously in Figure 8b. Underlying this layer and descending to depths where temperature cools to 11 °C and density anomaly increases to 26.50 kg/m³ (approximately 250 m) is a regime showing some California Current Water influence, but which is more characteristic of Subtropical Subsurface Water. The deep layer regime, as with the PESCAR 02 diagrams, shows the distinct deep salinity minimum of the Pacific Intermediate Water occurring at a corresponding depth of about 650 m.

The velocity transection of the April 1992 cruise placed outflowing current from the Gulf occurring over

a range of 10-60 km from the Baja shores (Figure 9d). Maximum velocities in excess of 70 cm/sec are observed near the surface, with less intense velocities contoured as deep as 400 m. A transition region, centered over the Alarcon Seamount and defined where the vertical descension of the 0 cm/sec isotach occurs, is observed separating this equatorward flow from an even broader poleward flow to the east. Surface cores within the latter show maximum speeds in excess of 60 cm/sec. As observed with the equatorward flow, this current penetrates deeply into the water column's upper layer. Even below 500 m, there's still some indication of significant current flow occurring around the transition region, as evidenced by the 15 cm/sec isotach to the east and hatched areas west. The associated volume transports of the PESCAR 01 cruise are provided and compared against the PESCAR 02 transports in Table 3. Using DCD method, the calculated PESCAR 01 volume transports include: a net

inflow of 11.7 Sv, net outflow of 9.2 Sv and an overall net transport of +2.5 Sv.

TABLE 3. VOLUME TRANSPORT

Volume Transport:

	Ref. wrt <u>1500 m</u>	Deepest Common <u>Depth</u>	Reid & <u>Mantyla</u>
PESCAR 01			
Pos. Volume [Inflow] →	9.5	11.7	9.1
Neg. Volume [Outflow] →	7.4	9.2	8.2
[Inflow]-[Outflow] →	+2.1	+2.5	+0.9
PESCAR02			
Pos. Volume [Inflow]→	6.5	8.4	12.0
Neg. Volume [Outflow] →	8.2	6.5	8.3
[Inflow]-[Outflow]→	-1.7	+1.9	+3.7

•units are in Sv (Sverdrup)

B. Differences Between April and December 1992

Perhaps the most obvious distinction between the April and December 1992 cruise results is observed in the velocity transections (Figures 9d and 3d, respectively). Two distinct and large regimes of current characterized the April results. In the upper 500 m layer, east of the Alarcon seamount (feature centered at 70 km from Baja), a broad cross section of inflowing (poleward) current was observed. West of the seamount, a correspondingly large cross section of outflow occurs. This depiction differs conspicuously from the December results where similarly intense but frequently alternating bands of current flow were observed. During the December cruise at least three transition zones separating narrower cores of inflowing and outflowing currents were observed. The most prominent of the cores was the outflowing (equatorward) core centered 40 km from the Baja coastline. Penetrating deeper and more structurally defined than the outflowing section observed during

the April cruise, this core is similarly unique in that it entrained the more saline ($S \geq 34.9\%$) Gulf Water, which was not apparent in the April cruise. The stronger winds and higher seas of the December cruise are undoubtedly related to the greater variability observed in the upper layer currents.

Why was Gulf Water not observed during the April cruise? One possible explanation is derived from the predicted time it would take for Gulf Water to appear at the Gulf's entrance following its formation in the northern basins (Bray, 1988b). Assuming an average flow speed of 20 cm/sec, it would take about 50 days for the subject water mass to transit the estimated 900 km. Along with the seasonal formation (Gulf Water is first formed from intense summer and fall heating), this may account for the December prominence of Gulf Water at the mouth. Alternatively, the lack of wind forcing during the April cruise, may lead to a reduction of Gulf Water being pushed southward.

Another distinction related to the baroclinic flow results involves the volume transports calculated for the two cruise periods (Table 3). Focusing on the results using DCD method, the table shows an increase in transport for the April-May cruise (PESCAR 01). This includes a net influx that is 20% larger than that determined from the December cruise. Outside of the seasonal variability that leads to density modification, the reasons for this additional transport are uncertain. However, from the comparison of the two cruises' velocity transections and volume transport results, it's reasonable to assume that more water was exchanged at the Gulf's entrance during the April-May period.

The temperature and salinity transections along with the corresponding T-S diagrams likewise delineate marked differences between the two cruise periods. The April SST's were 3-5 °C warmer than those observed during December. This elevation in temperatures was expected, a consequence of the associated seasonal

heating. A related feature was the increase in the near-surface stratification. The differences in the salinity transections were particularly pronounced and included at least one very distinct difference: the absence of Gulf Water. Besides shoaling of the shallow water salinity maximum and minimum layers, the April transection also revealed a low-salinity core water in the upper 50 m, again suggesting stronger stratification in the upper layers. These broad, low-salinity cores with salinities ranging from 33.3 - 33.6 psu likely reflect the influence of California Current Water and are gravitationally maintained in the strongly stratified near-surface layer. As previously discussed, the most striking difference between the cruise sets may have been the absence of high-salinity Gulf Water from the April transection! Such could infer that Gulf Water at the mouth is seasonal in occurrence; and hence, outflowing waters leaving the western Gulf in April may represent simple recirculation of eastern Gulf waters.

Salinities typical of sections in the Gulf can be used to calculate an estimate of the water mass ratios integral to the formation of Gulf Water. Taking the outflow at the mouth to have a salinity of 34.9 psu, inflow at the mouth on the same density surface to average 34.65 psu and the salinity of the northern basin waters to average 36 psu, it's then estimated that there is a 1 to 4 ratio of highly saline northern waters to fresh, Pacific-origin inflow involved in the formation process. This value points to the importance of mixing in the Gulf, in addition to providing an idea of the exchange balance required to drive the Gulf's thermohaline circulation.

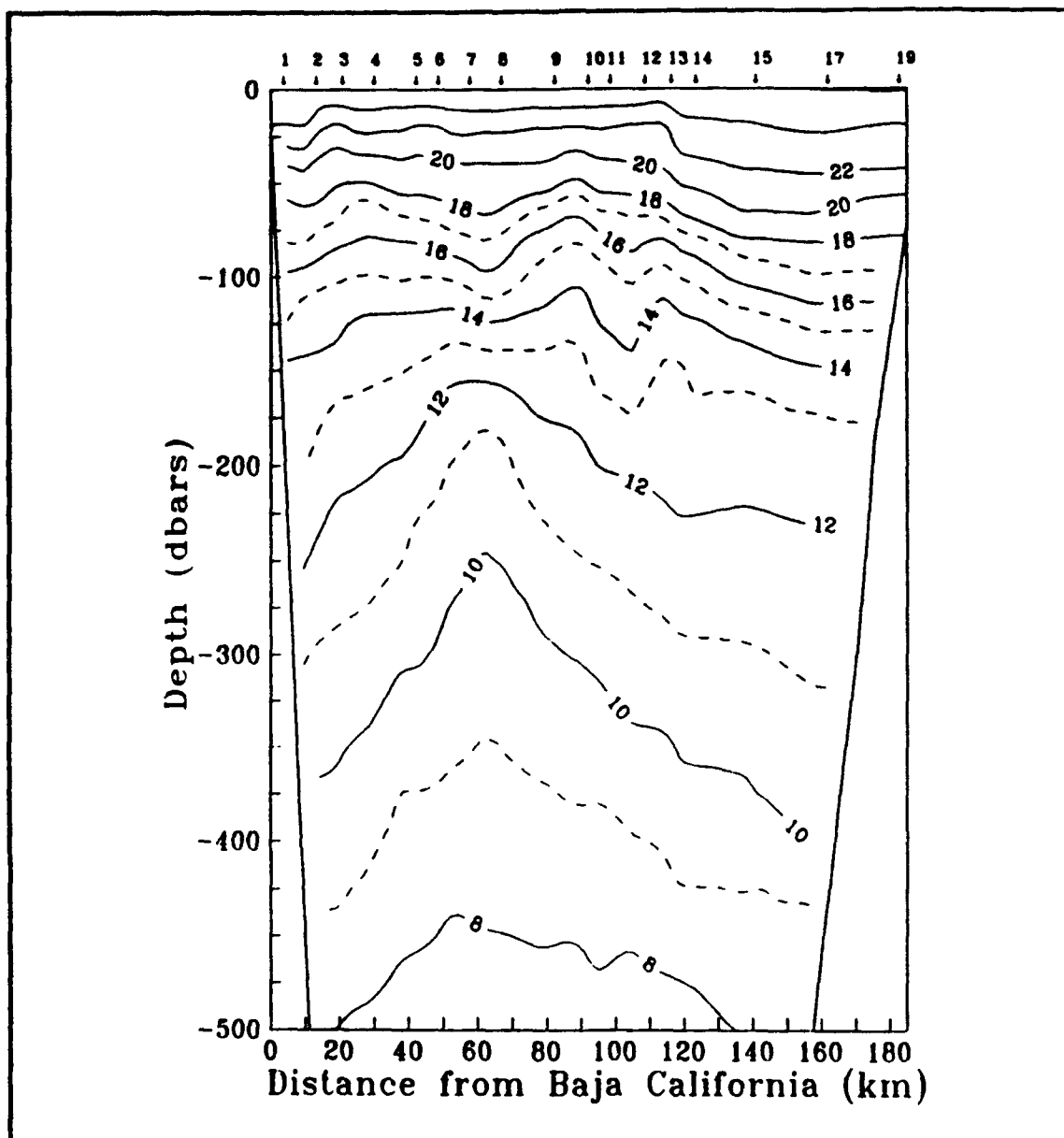


Figure 8. 500 dbar across-gulf transections for PESCAR 01 (21 April - 08 May 1992). Cast location and number are given at the top of the figure. (a). Temperature. Isotherm spacing is 1 °C or as labeled.

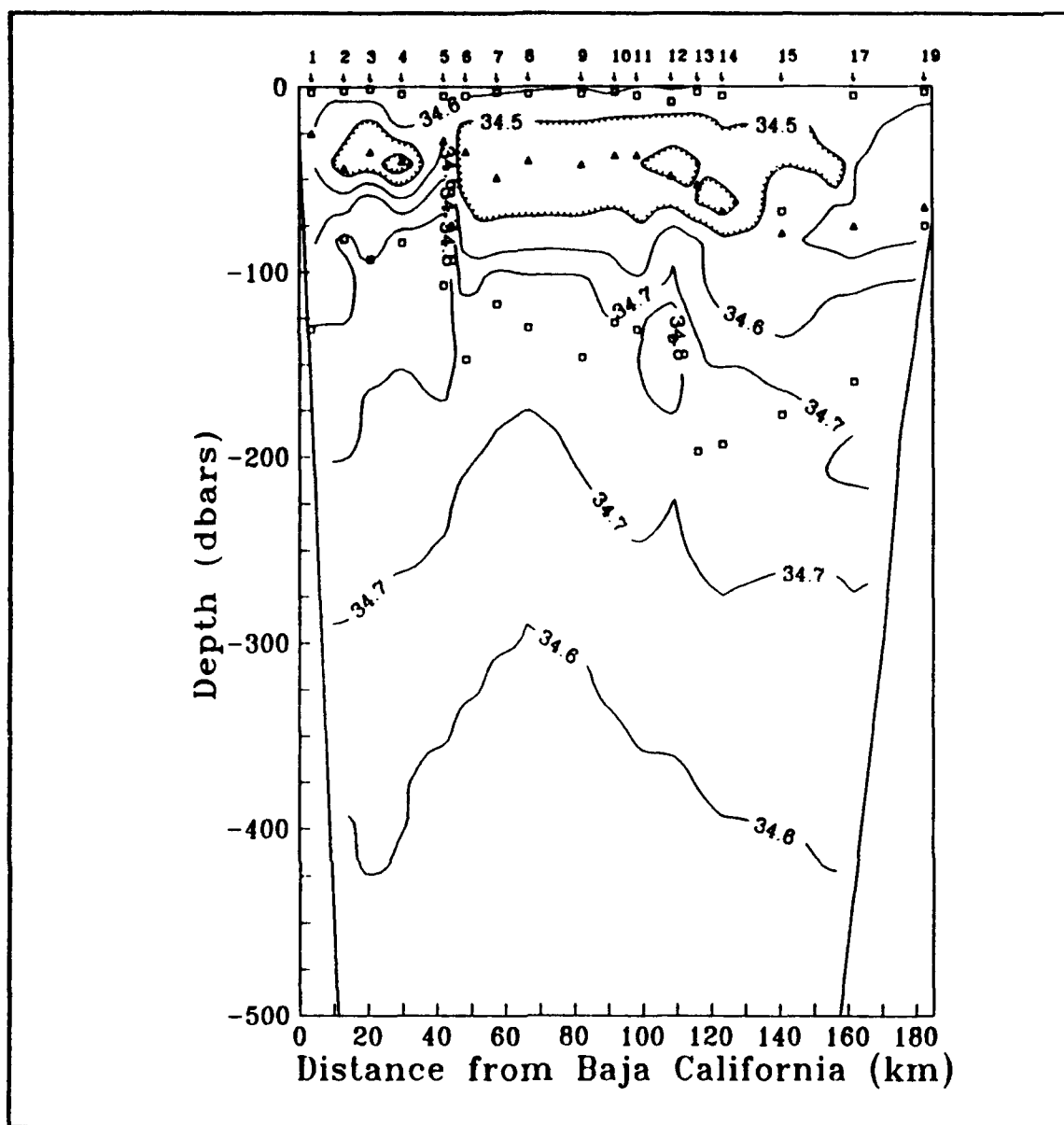


Figure 8(b). Salinity. Isohaline spacing is 0.1 psu. Cores of less saline water are denoted by hatching. The shallow layer salinity minimum is denoted by shaded triangles. Both the shallow and deep layer salinity maxima are denoted by open squares.

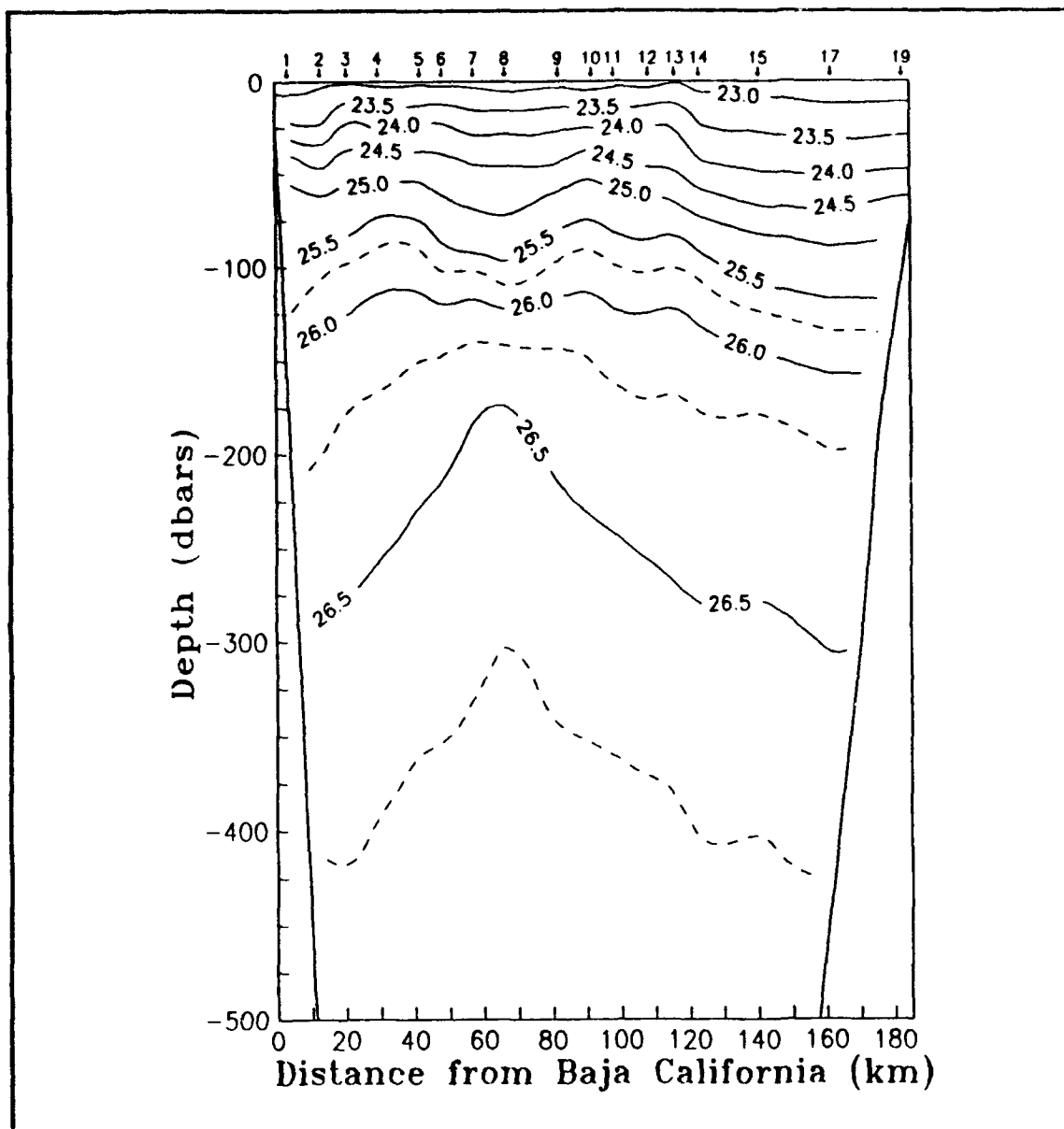


Figure 8(c). Density anomaly. Isopycnal spacing is 0.25 kg/m³ or as labeled.

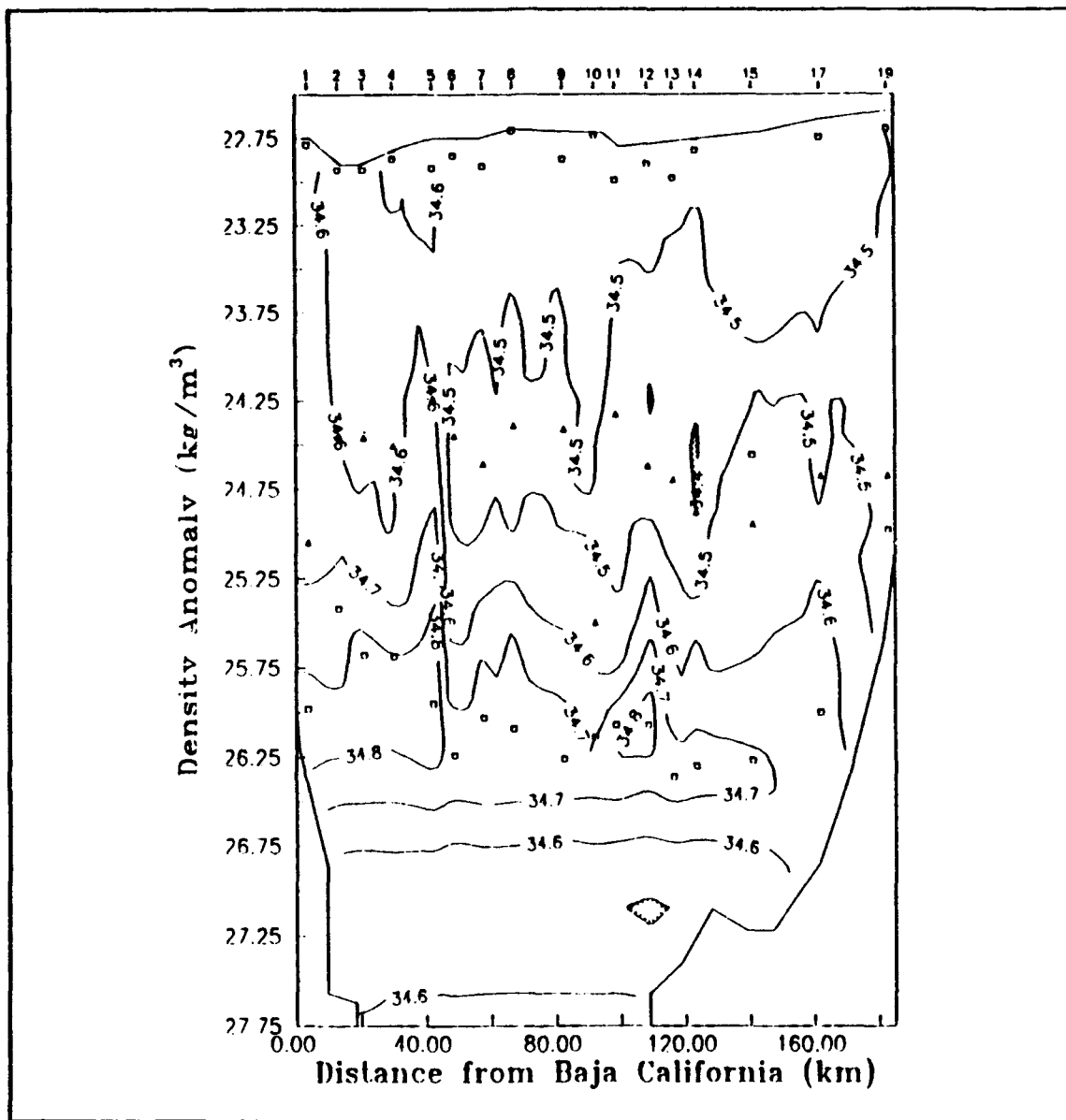


Figure 8(d). Salinity plotted on density anomaly surfaces. Isohaline spacing is 0.1 psu. Cores of less saline water are denoted by hatching. The shallow layer salinity minimum is denoted by shaded triangles. Both the shallow and deep layer salinity maxima are denoted by open squares.

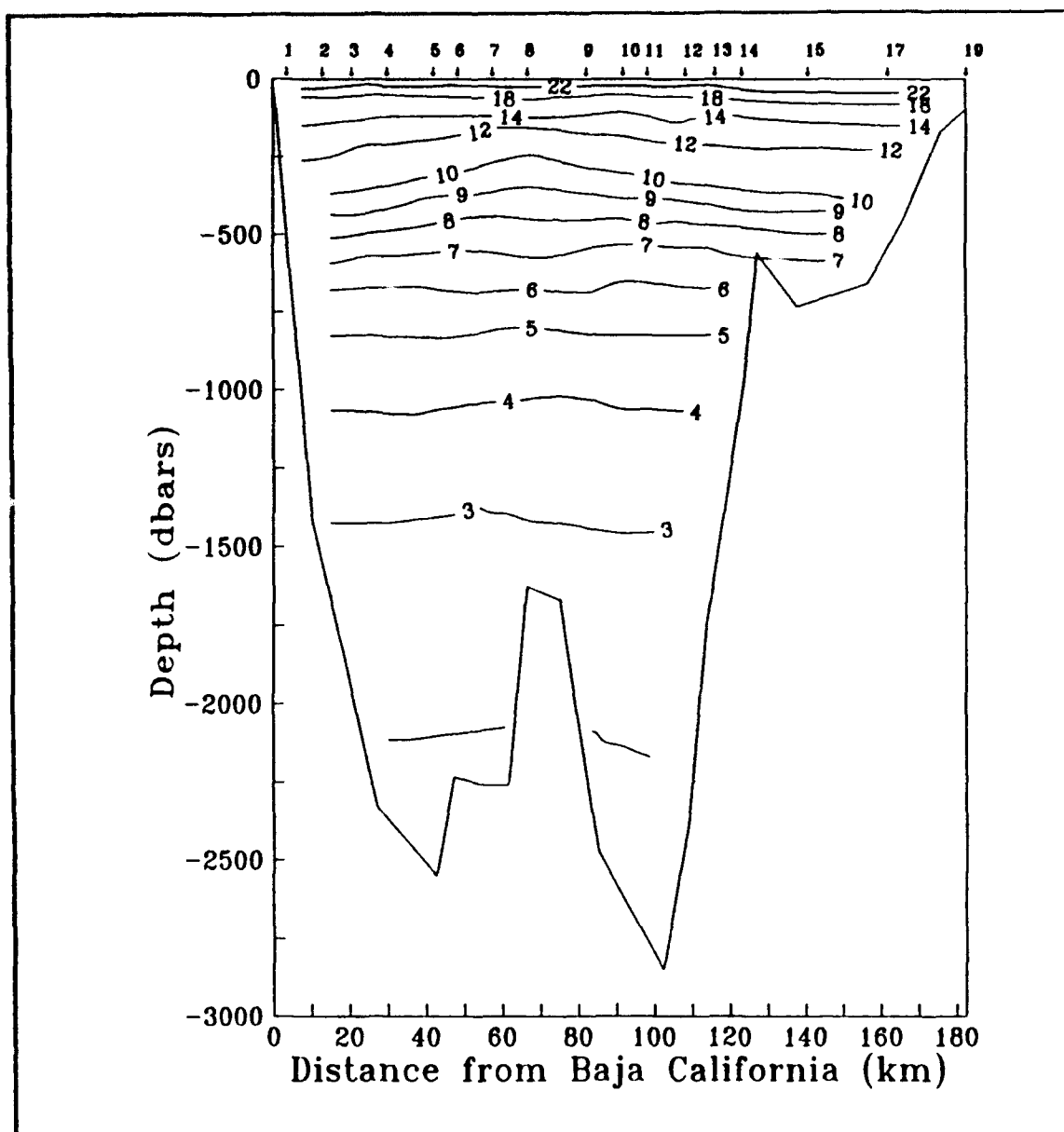


Figure 9. 3000 dbar across-gulf transections for PESCAR 01 (21 April - 08 May 1992). Cast location and number are given at the top of the figure. (a). Temperature. Isotherm spacing is 1 °C or as labeled.

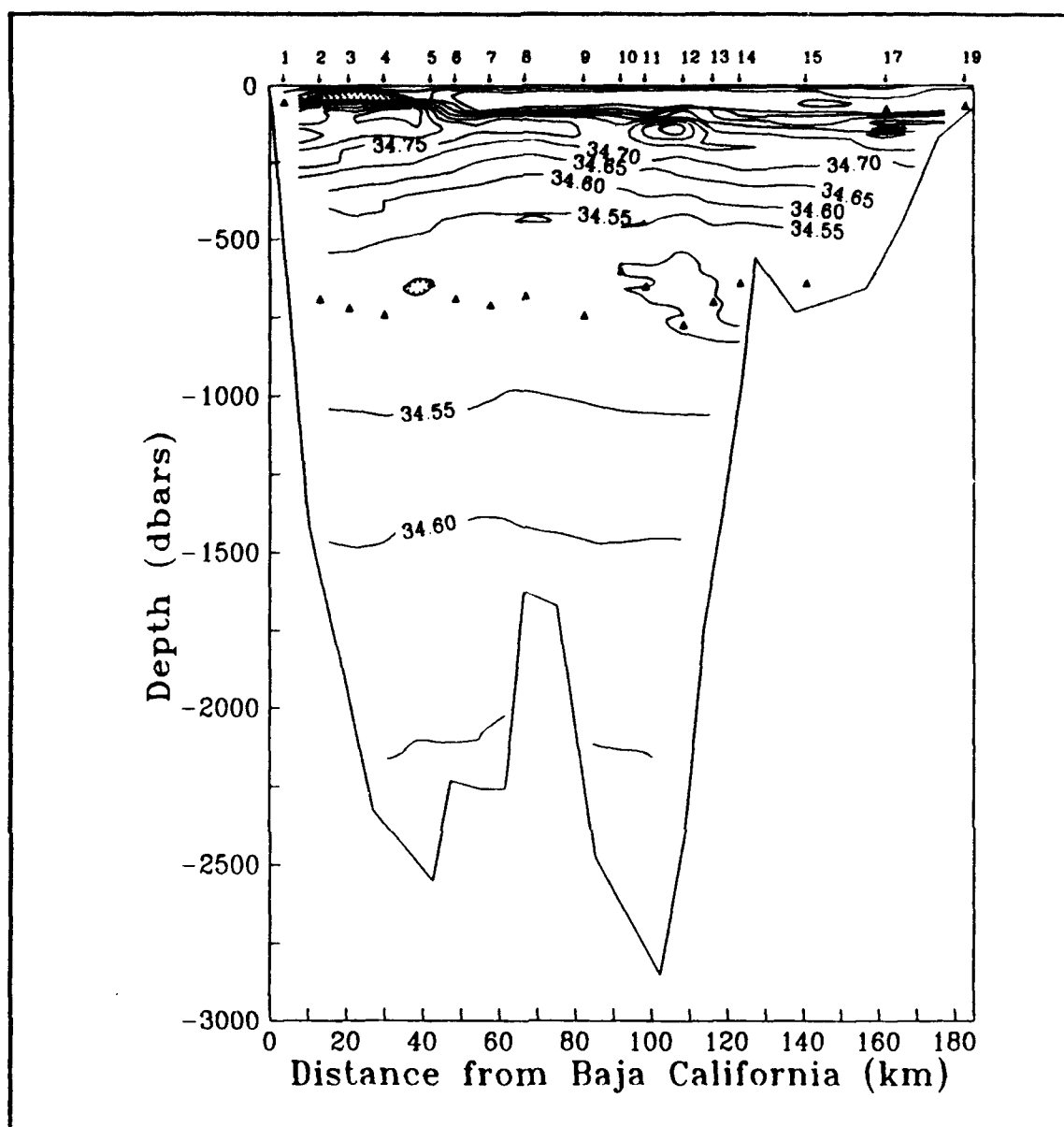


Figure 9(b). Salinity. Isohaline spacing is 0.05 psu. Cores of less saline water are denoted by hatching. The deep layer salinity minimum is denoted by shaded triangles.

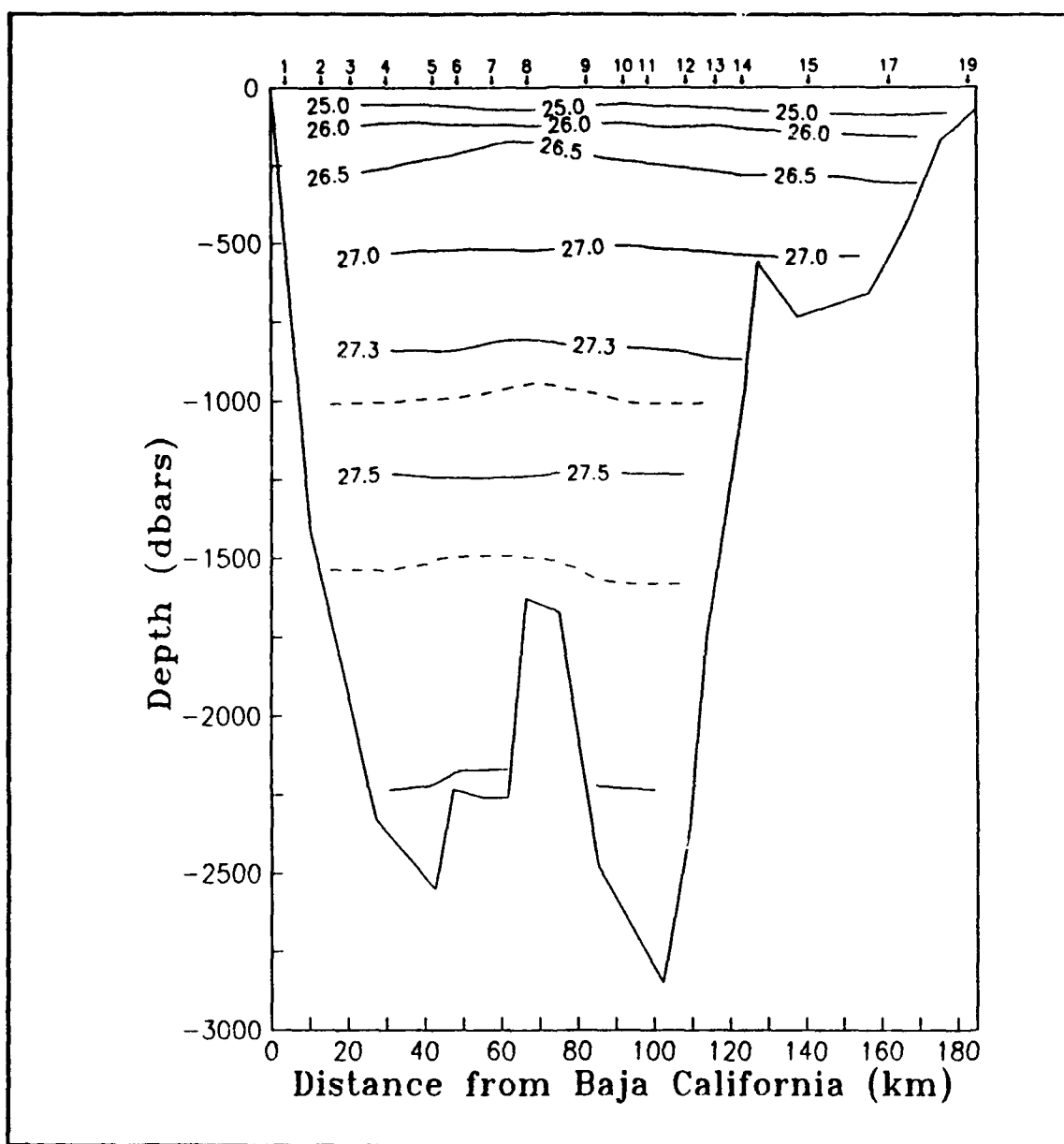


Figure 9(c). Density anomaly. Isopycnal spacing is 0.1 kg/m^3 or as labeled.

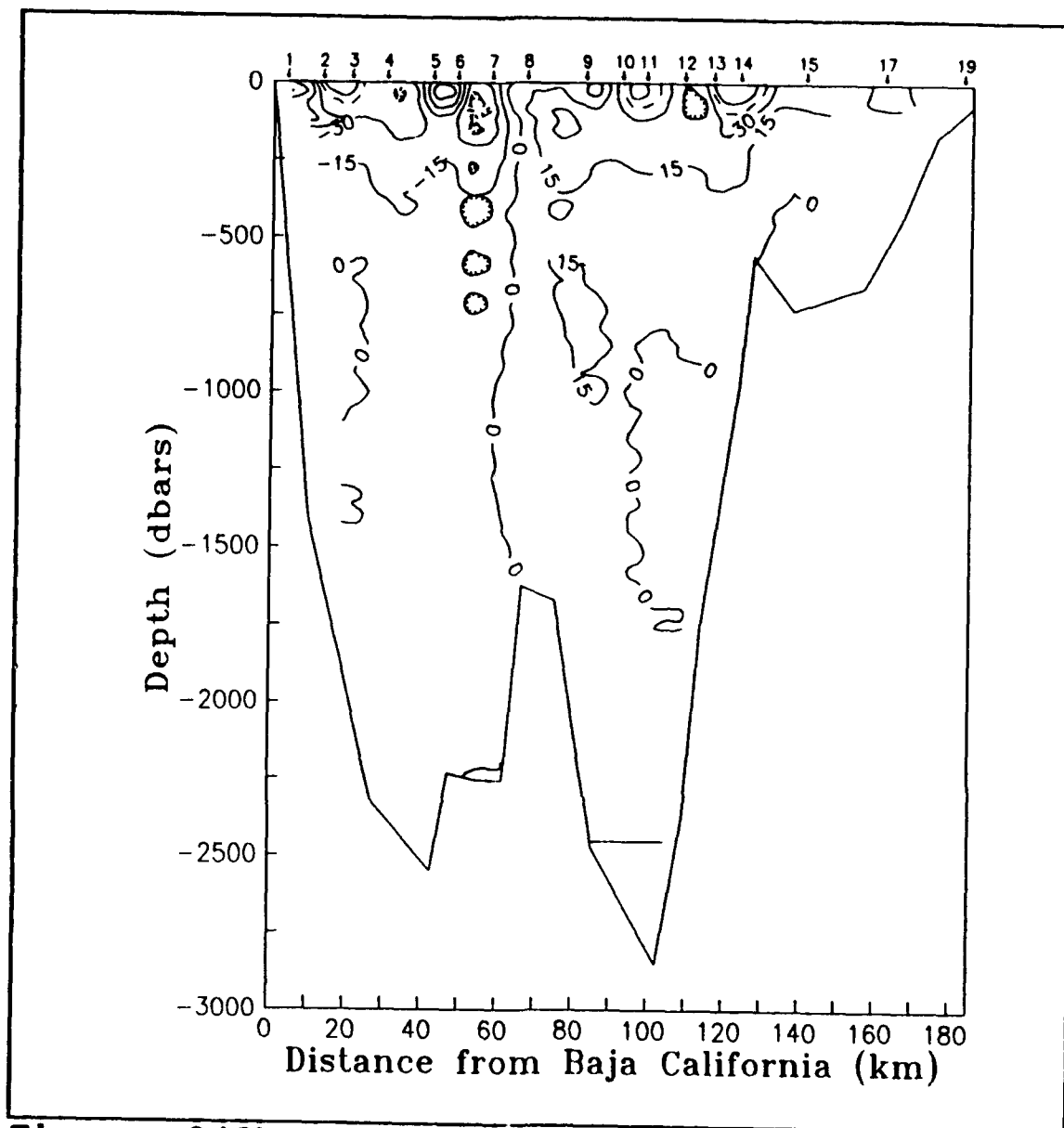


Figure 9(d). Geostrophic velocity using deepest common depth (DCD) method. Isotach spacing is 15 cm/sec.

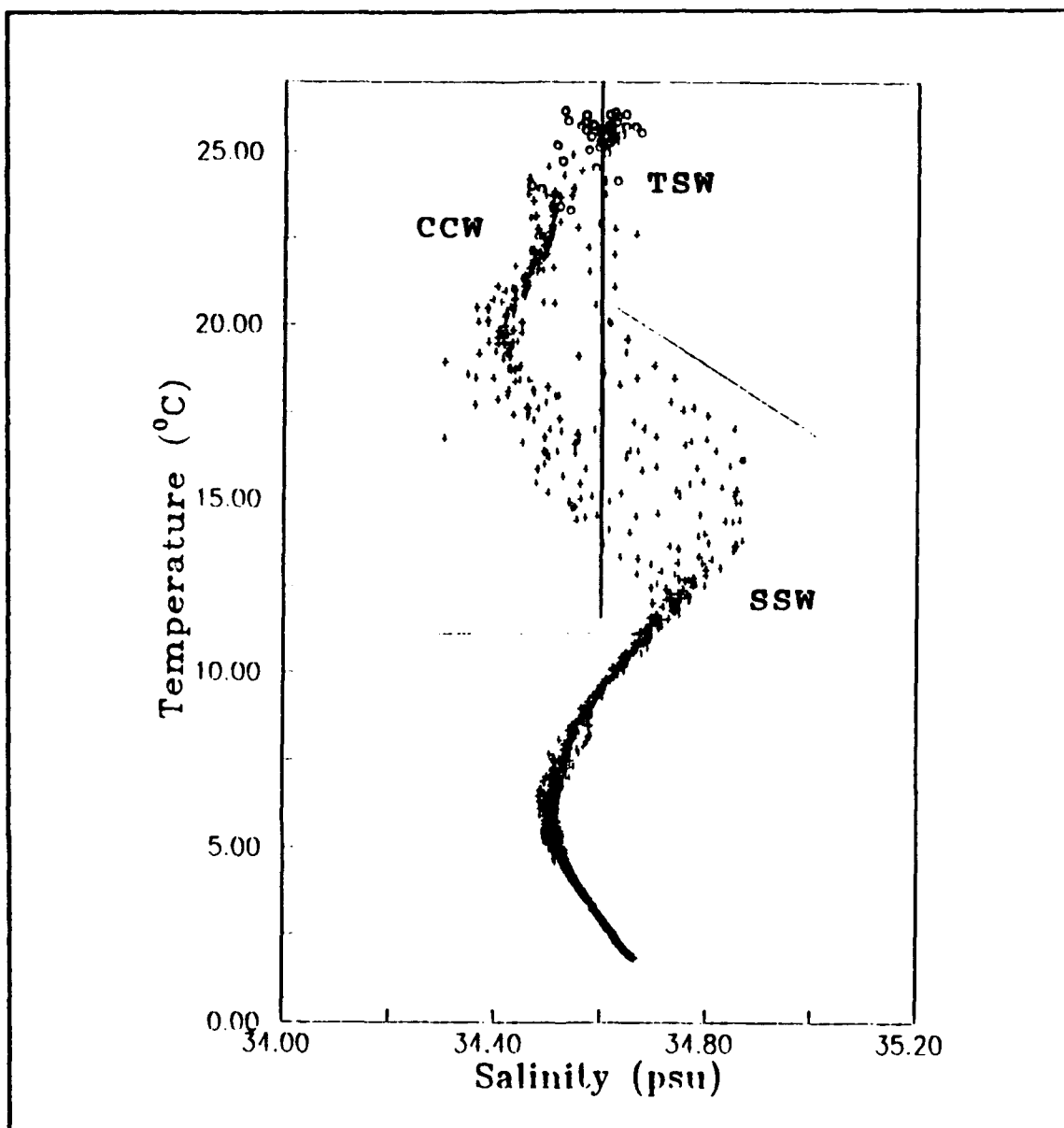


Figure 10. Full section scatter plot for across-gulf transections for PESCAR 01 (21 April - 08 May 1992). Plot is subdivided into sections by water mass: 1) **TSW** denotes Tropical Surface Water, 2) **CCW** denotes California Current Water, and 3) **SSW** denotes Subtropical Subsurface Water. The top 10 m section is denoted by circles. (a). Temperature-Salinity (T-S) diagram.

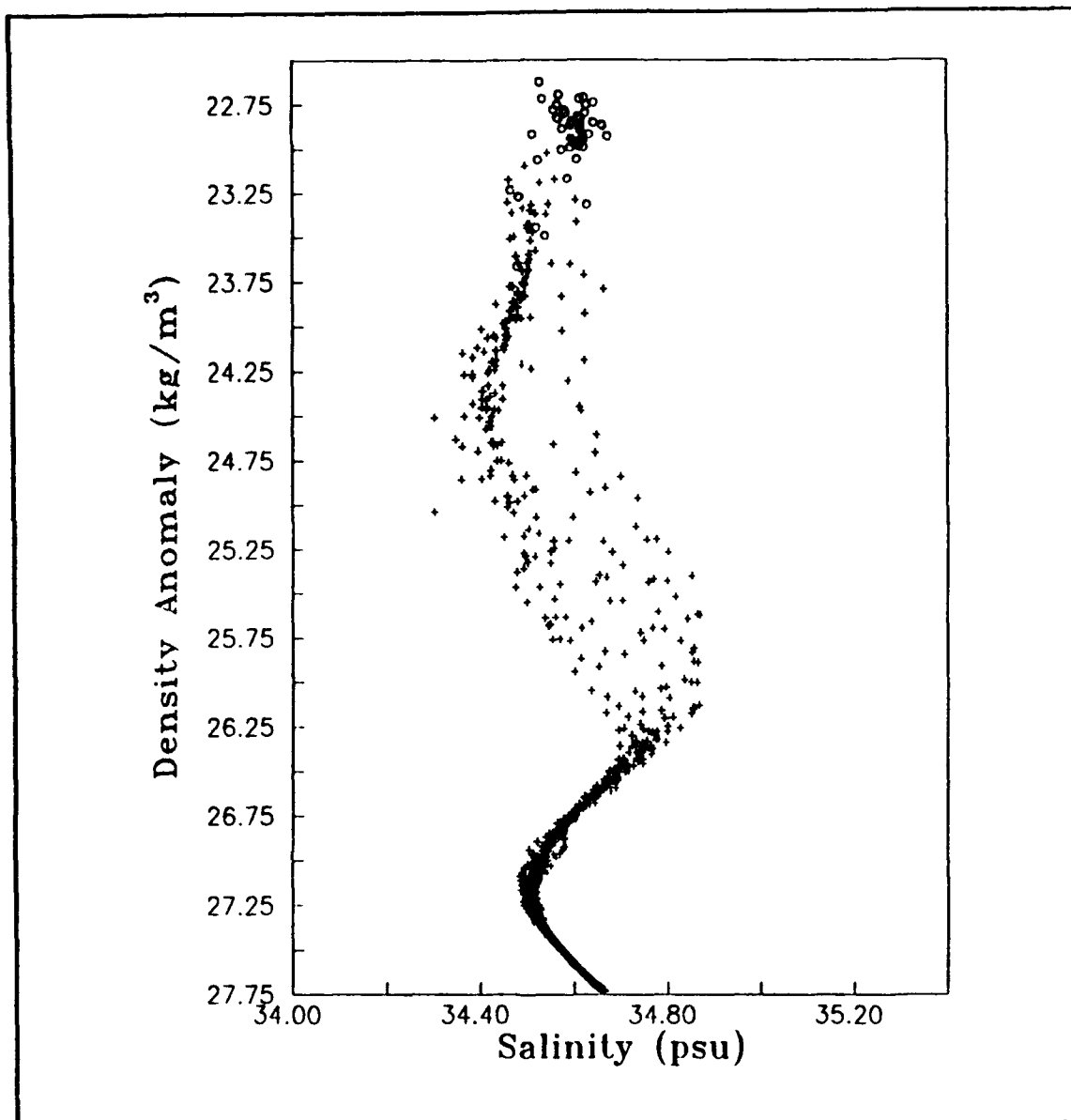


Figure 10(b). Density anomaly - Salinity (σ_t -S) diagram.

V. CONCLUSIONS

The circulation pattern observed at the entrance to the Gulf of California was generally cyclonic and characterized by occasional and opposing eddies in the near-surface layers and by consistent deep cyclonic circulation around the mid-basin Alarcon Seamount. Water generally entered the Gulf east of the seamount and exited the Gulf leaving the seamount to the east.

The late December 1992 - early January 1993 cruise results (PESCAR 02) show a system largely influenced by the strong seasonal winds (directed south). The surface waters at the Gulf's entrance during this period appeared to be well-mixed, and the upper layer currents banded. Just below the surface and extending down to about 200 m, the vertical temperature and density structure showed strong stratification. Within these layers, independent cores of both warm, saline and cooler, less saline water

were observed. The salinity signature of the warm water cores ($S \geq 34.9$ psu), suggest they originated from the inner-Gulf. The most pronounced of these warm, equatorward flows was observed along the southern flanks of the Baja banks, positioned 25-40 km offshore with maximum velocities of 68-72 cm/sec. Satellite imagery taken near the time of the December cruise supports this presumed movement of inner-Gulf water (Gulf Water) towards the mouth. During the 21 April-08 May 1992 cruise (PESCAR 01), a period when weather and sea conditions were generally calm, the high-salinity signature marking this core was not evident, even though a similarly positioned and broader equatorward flow existed. This April-May outflow likely represents simple recirculation of the waters comprising the eastern Gulf. The presence of Gulf Water at the entrance appears to be seasonally influenced, and could be related to either: 1) a temporal effect, due to the period between the water's formation in the northern Gulf and its estimated time

of transit to the entrance, or 2) simply the presence (or lack thereof) of wind forcing to drive upper layer water masses. Both conclusions support the observed Gulf Water at the entrance in December.

East of the Alarcon Seamount (centered approximately 70 km offshore from Baja), independent cores of cooler, low-salinity ($S \leq 34.7$ psu) water dominated the near-surface stratified layer. These poleward flowing cores, believed to consist of admixtures of California Current Water and subsurface composites of Eastern Tropical Pacific Water (often referred as Subtropical Subsurface Water), are undoubtedly a partial source for the advection of cooler and fresher water into the Gulf. The cores appear dispersed and only marginally organized during the December cruise, but broad and uniform during April-May. Current speeds were comparable in intensity to those of the outflowing cores, with slightly stronger currents (maximum speeds of 70 cm/sec) observed for April-May.

The deepest common depth (DCD) method proved to be the most suitable of three techniques compared in determining the geostrophic velocities. Besides suggesting a more complete depiction of the currents running through this highly diverse bathymetric region, it also gave the most reasonable results for volume and salinity transports.

Volume transports calculated for the two cruise periods indicated less transport occurring during the December-January period. For PESCAR 02, a net inflow of +1.9 Sv, the difference between a northward transport of 8.4 Sv and a southward transport of 6.5 Sv, was determined. Corresponding salinity transports were a net inflow of $+6.0 \times 10^4$ tonne/sec, the difference between a northward transport of 2.9×10^5 tonne/sec and a southward transport of 2.3×10^5 tonne/sec. Why more water was exchanged over the April-May period was not readily apparent. The differences are presumably due to seasonal processes.

This experiment opened new ground and raised additional questions concerning the circulation and exchange processes occurring at the Gulf's entrance. The inclusion of the deep layer structure in this examination established the importance of the processes occurring at depth. Unaccounted for in past studies, the deep layer structure revealed both interesting hydrography and appreciable transports relative to the transections analyzed. It was from the deep hydrography sections that the cyclonic flow pattern influencing the region was determined. Likewise, it was found that the largest percentage of the transports were gained from the deep layers. These observations suggest that the deep layer sections at the Gulf's entrance are very dynamic, and thus integral to the overall exchange balances occurring in the Gulf. The caveat to the above remarks is that the calculated transports for this experiment contained excessive imbalances between inflows and outflows. The problem that remains is how to best account for the

dynamics characterizing the deep layer. Suspected error in the results appears to have resulted from the inclusion of the deep layer analyses; and, none of the geostrophy techniques used in the experiment were totally effective in resolving the deep layer. It may be that the sluggish flows and reversing fields associated with the deep layer regime cannot be accurately measured by CTDs or resolved through simple geostrophic examination. Direct current measuring techniques may be the best approach for resolving the velocity structure.

Many of the hydrography sections indicated possible influence from the presence of the Alarcon Seamount. Were these observations real, and, if so, to what degree does the seamount affect the flow processes there? The answers to these questions are outside the scope of this examination. Perhaps a more detailed look utilizing direct measurements (e.g., Pegasus) can solve this newest of the Gulf's riddles.

APPENDIX A: LITERATURE REVIEW

Water Mass Formation and Thermohaline Circulation in the Gulf of California

This appendix is intended to be a more complete review of research reports investigating the Gulf. This includes summary of the extensive work done in the northern Gulf.

I. INTRODUCTION

The Gulf of California is a semi-enclosed, narrow sea basin bordered by the western shores of Mexico and the east coast of Baja California. The Gulf is the only evaporative basin of the Pacific Ocean and is a very dynamic body of water even though it is comparatively small. Surface currents generally follow seasonal variations of the winds, which are predominantly southeasterly in winter and spring and northwesterly in summer and fall (Roden, 1964). Subsurface circulation is far more complex and is characterized by flow exchanges with the adjoining Pacific Ocean, with outflow occurring between the surface layer and about 250 m and inflow occurring between 250 m and roughly 500 m (Bray, 1988b). This paper examines the regional climatology, underwater topography and water mass formation within the Gulf in

order to examine their influences on thermohaline circulation in the Gulf of California.

Bray (1988a) states the Gulf is uniquely characterized by a vertical salinity gradient (salinity decreases with depth) over the top 700 m water column with only occasional exceptions. This condition occurs as a result of the unusual atmospheric forcing over the Gulf, which leads to a net loss of moisture from the ocean surface but a net gain of heat from the atmosphere. She adds that this process is unlike those observed in similar sea basin enclosures such as the Mediterranean and Red seas, where heat is lost to the atmosphere.

The small heat gain (estimated to be $20-50 \text{ W m}^{-2}$) received in the Gulf of California is balanced by an advective flux of colder, fresher Pacific Intermediate Water into the Gulf as warmer, saline Gulf water is transported out (Bray, 1988a). The warm "Gulf Water", as coined by Roden (1964), transported out is a product of water mass formation occurring within the

Gulf. According to Bray (1988b), water mass formation in the Gulf is a result of the following set of complex mechanisms: winter convection; southern transport of newly convected waters via eddylike features; large-scale anticyclonic circulation of northern shelf waters south; and tidal mixing.

Due to restrictions imposed by the Gulf's topography (i.e., transverse ridges or sills) it is assumed that the thermohaline circulation is constrained to depths above 500 m. This corresponds to the controlling sill depth located between the northern and central regions of the Gulf. Observations suggest that the Gulf's thermohaline circulation is a distinctive three-layered system, comprised of: a seasonally driven surface layer; high-saline outflow layer flowing alongshelf the eastern shores of the Baja peninsula; and a deeper, relatively fresh inflow layer entering the central part of the Gulf's mouth (Bray, 1988a).

II. CLIMATOLOGY

The Gulf of California is located between the arid peninsula of Baja California to the west and the equally arid Mexican states of Sonora and Sinaloa to the east. An almost unbroken chain of mountains, 1-3 km high, situated along the Baja peninsula acts to channel seasonal winds along the length of the Gulf. Additionally, these mountains isolate the Gulf from the oceanic climate of the nearby Pacific to the west (Roden, 1964).

There is a large variation of atmospheric temperature over the Gulf between summer and winter periods. Variations are extreme and may exceed 15°C in the northern Gulf region. In the late summer evaporation rates are at a maximum and correlate with increased sea surface temperatures.

Roden (1964) states that precipitation in the region is more prevalent in the south than in the dry,

desert-like northern Gulf, where precipitation is less than 10 cm/yr. In the southern Gulf precipitation can increase to as much as 100 cm/yr, with most of the rain falling during the rainy season months from June to October. The year-to-year variation of precipitation is large. Also, winds in the Gulf of California are extremely variable. The winds blow predominantly out of the northwest from November to May, and out of the southeast during the rest of the year (Roden, 1964). The winter winds are stronger and less humid than the southerly summer winds and are associated with significant upwelling (≈ 3 m/day) along the western shores of the Mexican mainland. The southerly summer winds also induce upwelling along the eastern coast of the Baja peninsula.

Roden (1964) mentions that the Gulf region is noted for its seasonal storms. Northwest gales of two-three days duration are commonly experienced in the northern Gulf between December and February. Their southern counterparts, *chubascos*, violent gales of

short duration, occur in the rainy season from June to October. Also, the Gulf - particularly the extreme southern region - is susceptible to hurricanes during the period between late May and early November.

Isolated from the Pacific Ocean, the Gulf of California is more continental than oceanic in climate. With a related extreme seasonal variation of temperature and wind, the Gulf behaves as the only evaporative basin of the vast Pacific. According to Bray (1988b), the atmosphere over the Gulf influences oceanic circulation through the wind field, which reverses seasonally, through surface heating and cooling, and through evaporation.

III. TOPOGRAPHY

Bray (1988b) explains: the Gulf of California is approximately 1000 km long and 150 km wide, lying between the mountainous Baja California peninsula and the western shores of Mexico. The bathymetry of the Gulf is quite complex, characterized by numerous basins separated by transverse ridges or sills. Most of the basins are deep and in open communication with the Pacific. Progressing northward, the sills become increasingly shallow. Sills located in the southern and central basins are deeper than 1500 m, thus allowing open exchange between the deeper waters of the Pacific and the Gulf waters. South of the region's midriff islands, the San Esteban sill, rising to about 500 m, effectively isolates the northern Gulf from the central region basins (Figure 1).

Bray (1988b) continues, stating the highest salinities found in the Gulf are in the tidal flats of

the north, where evaporation is the greatest and the Gulf is the shallowest. Interestingly, maximum salinities ($\approx 36\%$) are observed at the head of the Gulf in the Colorado River delta. Due to the low fresh water discharge from the river, river runoff has little influence on diluting the salinity of the Gulf waters there.

IV. WATER MASS FORMATION

As defined by Bray (1988b), the term water mass formation refers to processes which convert surface waters of the ocean into deeper waters removed from direct atmospheric forcing. In this context, a water mass is characterized by a temperature versus salinity relationship, T-S, traceable to some observable set of surface conditions.

Evaporation over the Gulf (0.95 m/yr) is comparable to that of the Mediterranean and Red seas, with surface salinities in the northern Gulf 1-2 psu higher than those found along the same latitude in the open Pacific. But the Gulf differs from the aforementioned evaporative basins in that it **gains heat** at an annually estimated average rate of 20-80 W/m² (Bray, 1988b). An accompanying vertical instability condition is possible because temperature and salinity both decrease with depth (Figure 2). This

vertical structure precludes the expected two-layer thermohaline system of warm, fresh subsurface inflow and cold, salty surface outflow. Water mass formation in the Gulf must somehow compensate for the unusual air-sea forcing occurring there. To balance the air-sea heat gain and the evaporative moisture loss, there must be a net upward transport of cold, fresh inflow water and a net downward transport of warm, saline waters, to intermediate depth. Bray (1988b) states that "these constraints force the new water mass to be intermediate (in depth as well as in T-S properties) between the deep, relatively fresh inflow and the surface layer which has been made saline by evaporation." She adds, the following mechanisms are responsible for this process: 1) winter convection, 2) dispersion of convected water in small eddylike features, 3) an anticyclonic circulation in the northern Gulf, and 4) tidal mixing.

An interpretation of Bray's (1988a) detailed explanation of the water mass formation process begins

by stating that evaporation reaches a maximum in the northern Gulf in late summer and early fall following a summer of intense surface heating. This results in a warm, saline surface mass. Localized winter convection transforms some of this saline surface water into a cold, dense, salty bottom water found only in the deep basins of the northern Gulf. Inclusive, there are associated processes relative to winter convection that are key to the entire process. That is, there must be an explanation for the characteristic destabilizing vertical salinity gradient established as a result of less saline Central Gulf Water (CGW) underlying the high-salinity Colorado Delta Water (CDW). Such occurs as a result of cyclonic inflow of CGW at depth into the deep basins of the far north. At depths greater than 100 m, the only conduit for inflow of CGW into the northern Gulf is through the channel connecting Wagner Basin, via depressions to Delfin Basin. Then, as the surface waters of the northern Gulf (CDW) cool in the winter, thus increasing their

density above that of the advected underlying CGW, the CDW sinks below the CGW. If this "penetrative" convection occurs, an identifiable T-S signature of a subsurface salinity minimum (CGW) overlying a deeper salinity maximum (convected CDW) should be observed. Additional properties of this traceable Wagner Basin Water (WBW) are that surface and bottom salinities should be nearly equal, surface temperatures should be warmer than bottom temperatures, and the bottom salinity maximum layer should have higher temperatures than the salinity minimum layer overlying it. Also, density should be nearly uniform with depth in the salinity minimum and maximum layers.

From evidence gathered from hydrographic data, current meter data, and meteorological data (winter '84-'85) it is suspected that at least one mechanism for dispersing Wagner Basin Water is by "Gulfies", or small diameter eddies emanating from the formation region after major cooling events. Thus, the Gulfies are responsible for advecting the newly formed WBW

away from the formation region. These isolated patches of high-salinity water have been discovered several hundred kilometers south of the convection or formation region, and have been traced back in time to specific cooling events, with patches of greater salinity anomaly associated with stronger cooling. Gulfies result from the process of water mass formation itself. Also, as the Gulfies transit south through the sill-strait system of the central-southern Gulf, they can lose much of their T-S signature via tidal mixing with central Gulf water masses.

Another process considered important in the transportation of high-salinity surface waters south from the northern regions of the Gulf is by means of a strong anticyclonic circulation occurring in late winter. Evident in the hydrographic data from March 1985, the gyre centered over the northern Gulf and extending across the width of the Gulf appears responsible for advecting high-salinity surface water from the shelf regions of the north well into the

central Gulf, some 150 km to the south. The water advected is observed as a horizontally isolated salinity maximum, nearly isohaline and extending to approximately 200 m deep in the gyre center (Figure 3). Consequently, the gyre provides a means of transporting high-salinity water away from the northern shelves as well as a mechanism for mixing saline surface waters with deep, fresh inflow water. As a note, the anticyclonic gyre in the northern Gulf does not appear directly related to convection. The gyre is of much larger horizontal scale and is centered far south of the origin of the Wagner Basin Water. A possible driving force for the gyre is the existence of externally imposed density gradients as a circumstance of the cooling of high-salinity surface waters, resulting in denser waters to the north, and consequently anticyclonic circulation.

Inevitably, mixing must be an important factor in water mass formation in the Gulf. Tides provide energy for mixing during water mass formation processes. In

the northern Gulf, tidal mixing is likely induced by bottom friction. Farther south in the island region, particularly near sills, mixing is probably by the breaking of large vertical scale internal waves. Water mass formation in the Gulf is directly affected by these mixing processes. The shallow waters of the northern shelves are vertically mixed during winter, facilitating convection. Likewise, mixing is responsible for reducing the high-salinity signature of northern Gulf waters as they enter the central Gulf.

Bray (1988b) summarizes her explanation of the water mass formation process, contending that water mass formation in the Gulf of California results from a requirement that there be a net upward transport of deep water properties to balance the air-sea heat gain, and a net downward transport of surface water properties to balance evaporative moisture loss. This is accomplished through a series of complex interactions involving atmospheric forcing, tidal

mixing and topographic constraints. The resultant product is a new water mass that is intermediate in depth as well as in its by T-S properties. This intermediate Gulf Water reflects the properties of both the deep, relatively fresh inflow and the salty surface layer formed by evaporation.

V. THERMOHALINE CIRCULATION

As previously discussed, unlike the Mediterranean and Red seas, the Gulf of California actually gains heat from the atmosphere on an annual average. This heat gain is presumably balanced by an advective flux of colder water into the Gulf and warmer water out of the Gulf. This theory correlates with observed vertical gradients of temperature and salinity and with baroclinically determined circulation patterns (Bray, 1988a).

Hydrographic evidence from moored observations and ship measurements suggests that the Gulf's thermohaline circulation is comprised of the following three-layered system: 1) surface layer which is approximately 50 m thick and reverses transport direction with the seasonally reversing large-scale wind field, flowing north in the summer and south in the winter, 2) baroclinic outflow occurring along the

western shores of the Gulf between the surface layer and about 250 m depth, and 3) baroclinic inflow occurring mainly in the central sector of the Gulf between 250 and 500 m depth (Bray, 1988a). There was insufficient data to resolve the circulation at depths deeper than 500 m. To this she adds, "...thermohaline circulation would be constrained to depths above about 500 m, which is the controlling sill depth between the northern and central sections of the Gulf."

The proposed three-layer system has several implications for circulation in the Gulf. In preceding sections of this paper, the formation of an intermediate water mass was discussed. Outflow from the Gulf predominantly consists of this intermediate Gulf Water. Another point of interest is that at the mouth of the Gulf the density of the outflow is such that it forms a near-surface layer. Upon exiting the Gulf, the Gulf Water signature negligibly influences the adjoining Pacific. Also, the Gulf's receipt of

deep, subsurface, nutrient-rich inflow waters from the Pacific gives a sound explanation for the high biological productivity found in the Gulf (Bray, 1988a).

At the mouth of the Gulf, one prominent feature is a thin (10-30 m thick) but pronounced high stability layer sandwiched between the warm surface layer and cooler subsurface layer. This stability layer, depicted in Figure 4, is identified by Väisälä frequencies (where Väisälä freq. $> 0.02 \text{ sec}^{-1}$), and practically extends across the entire southern Gulf. The top of this high stability layer lies at approximately 50 m depth and may be used as an index of the depth of the upper mixed layer. Of particular interest is that breaks in this high-stability layer, clearly evident on the west side of the Gulf, are indicative of strong baroclinic flow (Roden, 1972).

Baroclinic flow across the entrance to the Gulf of California was computed from STD observations (Figure 5). According to Roden (1972), the flow is

referenced to the 1500 dbar surface or the bottom, whichever was encountered first.

Baroclinic outflow, whose origin is traced to the northern Gulf (salinity maximum $> 35.2\%$), flows near the western shores of the southern Gulf, traveling south in a narrow, high-speed velocity core. This core has a characteristic width of about 30 km and deepens to more than 1000 m at the Gulf's entrance. Maximum velocities within the core occur at the surface, reaching 55 cm/sec.

Baroclinic inflow into the Gulf takes place mainly in the central part. Here there are two observable cores of increased velocity entering the Gulf. One core is about 20 km wide and has a maximum velocity of ≈ 26 cm/sec, occurring between 50 and 450 m depth. The other, slightly wider than the first, has a maximum speed of 46 cm/sec and is confined to the upper layer.

VI. SUMMARY

The Gulf of California's hot, arid summer climate makes it the Pacific Ocean's only evaporative sea basin. Surface currents in the Gulf generally follow seasonal variations of the wind, with northwesterlies blowing from November to May and southeasterlies from June to October.

Unlike similar semi-enclosed sea basins (namely, the Mediterranean and Red seas), the Gulf of California is uniquely characterized by a destabilizing vertical salinity gradient (salinity decreases with depth) over the top 700 m water column. This condition occurs as a result of the unusual atmospheric forcing occurring over the Gulf, which results in a net loss of moisture from the ocean surface but a net gain of heat. Given this condition, an intermediate Gulf Water mass is formed. The mechanisms for the formation of this intermediate

water mass include: winter convection in the northern basins; advection of newly convected water via isolated eddies, referred to as Gulfies; transport of water south from the northern shelves by way of a large-scale anticyclonic gyre; and strong tidal mixing.

The thermohaline circulation pattern proposed for the Gulf to balance the net heat and moisture fluxes consists of three layers. There is the surface layer, whose current field is directly influenced by the seasonally varying wind. Baroclinic outflow transports warm and saline Gulf Water of northern origin out of the Gulf along its western boundary. Baroclinic inflow transports relatively fresh, cold Pacific Intermediate Water into the Gulf at the central sector of its entrance.

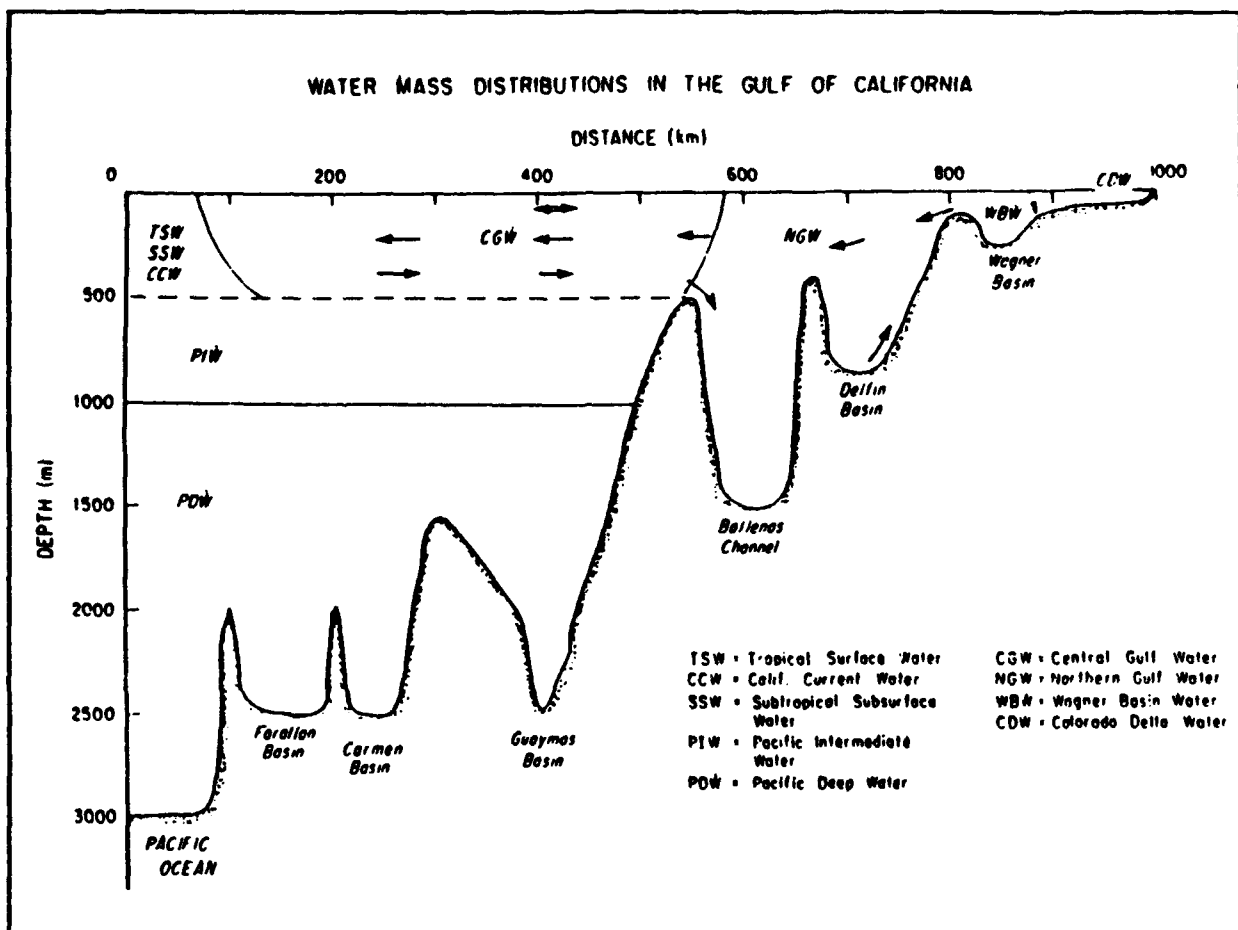


Figure 1. Schematic depicting topography (sills and basins) and water mass distribution in the Gulf of California. Arrows denote hypothesized thermohaline circulation: the open arrow representing the surface wind-driven layer with seasonally reversing transport; solid arrows representing subsurface inflow and outflow; dashed arrow representing deep water formation (Figure 3a., Bray, 1988b).

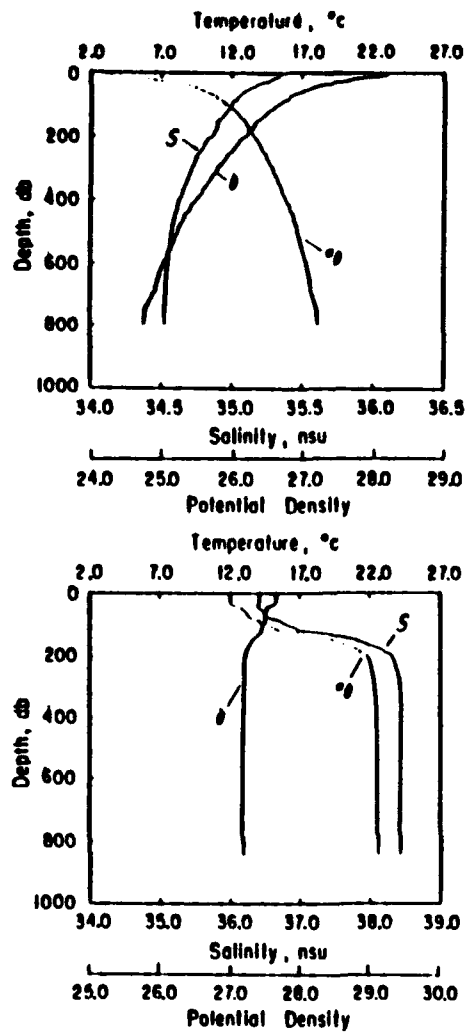


Figure 2. Comparison of the vertical thermohaline structure in the Gulf of California (top graphic, A), and the western Mediterranean Sea (bottom graphic, B). Note that in the case of the Gulf of California, salinity decreases with depth; thus indicating, vertical instability in the water column (Figure 2., Bray, 1988b).

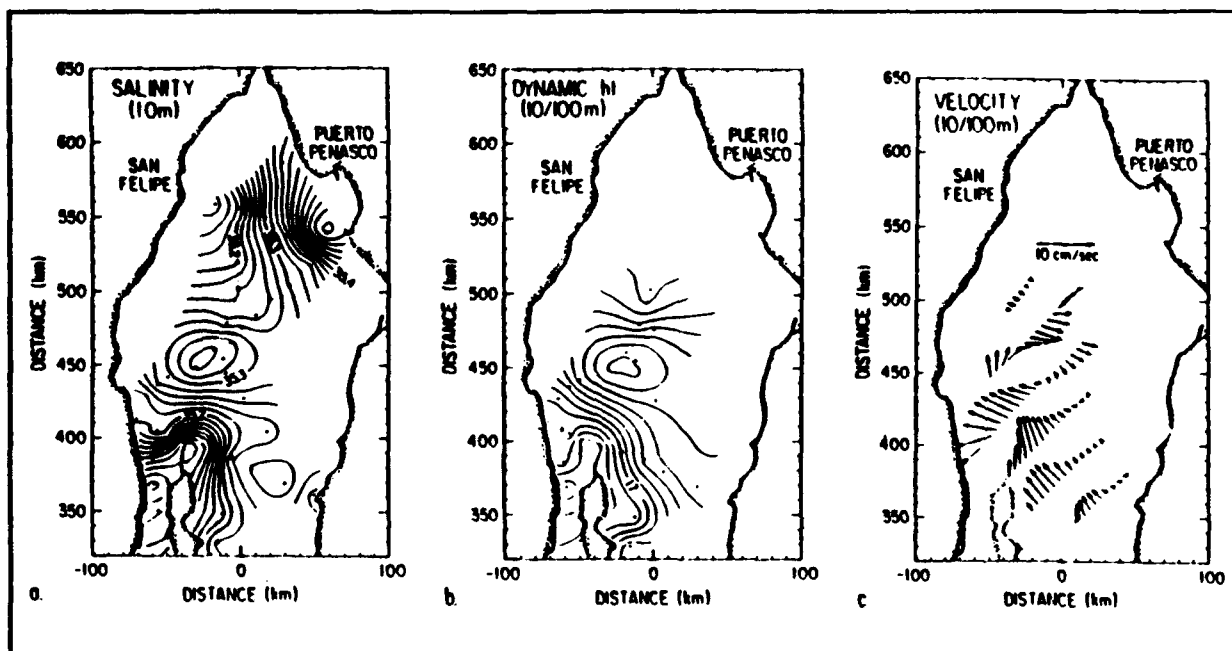


Figure 3. Anticyclonic gyre found in the northern Gulf in March 1985. Plots include: (a) salinity at 10 m, (b) dynamic height at 10 m relative to 100 m, and (c) velocity vectors derived from the dynamic height field. The gyre is presumed to be partially responsible for moving high-salinity waters south from the northern shelf regions. It is also believed to contribute to the mixing processes occurring in the northern Gulf (Figure 15., Bray, 1988b).

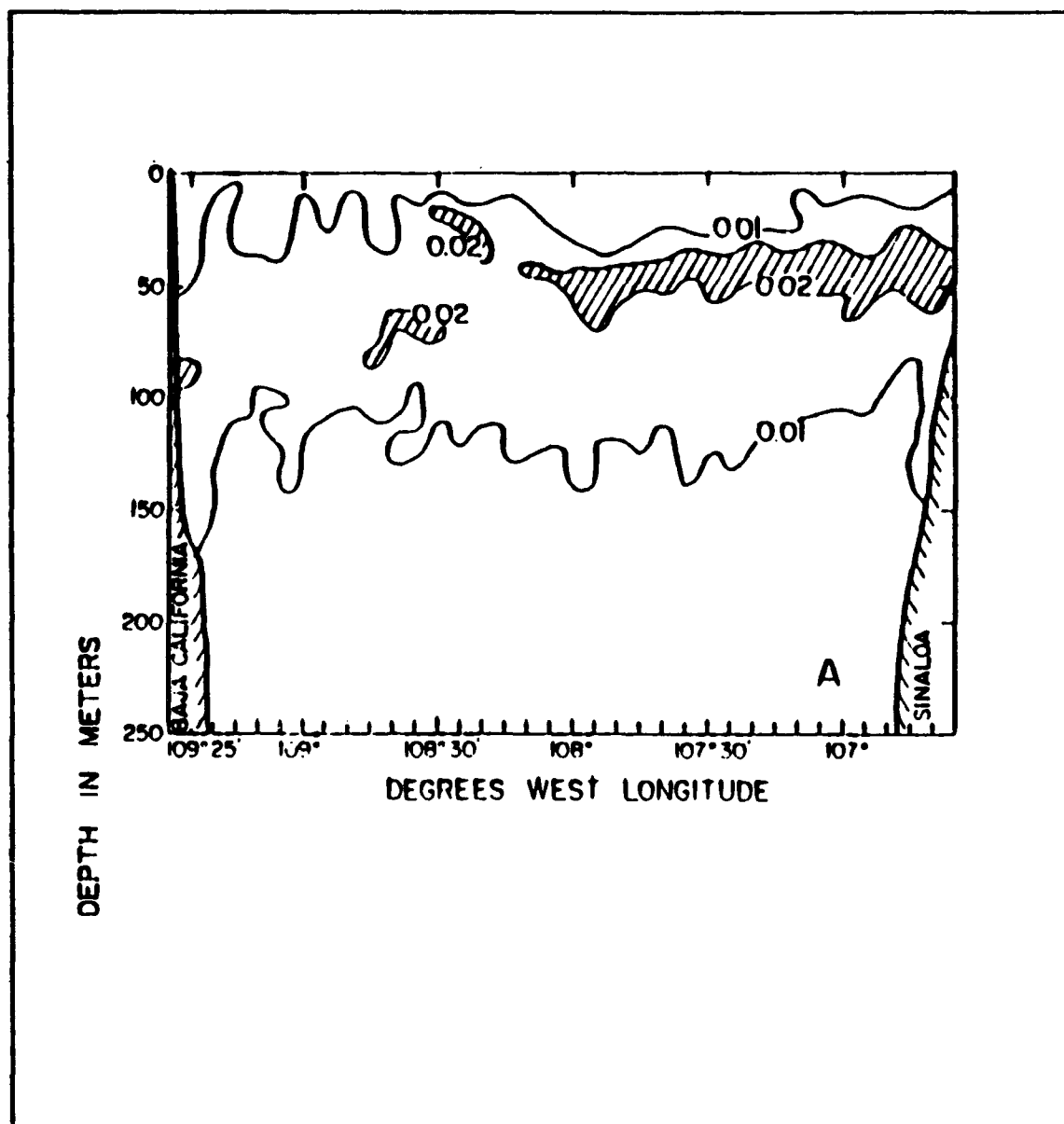


Figure 4. Vertical distribution of Väisälä frequency (sec^{-1}) across the entrance to the Gulf of California. The layer of high stability water is shaded. Breaks in the high stability regions are indicative of baroclinic flow (Figure 2., Roden, 1972).

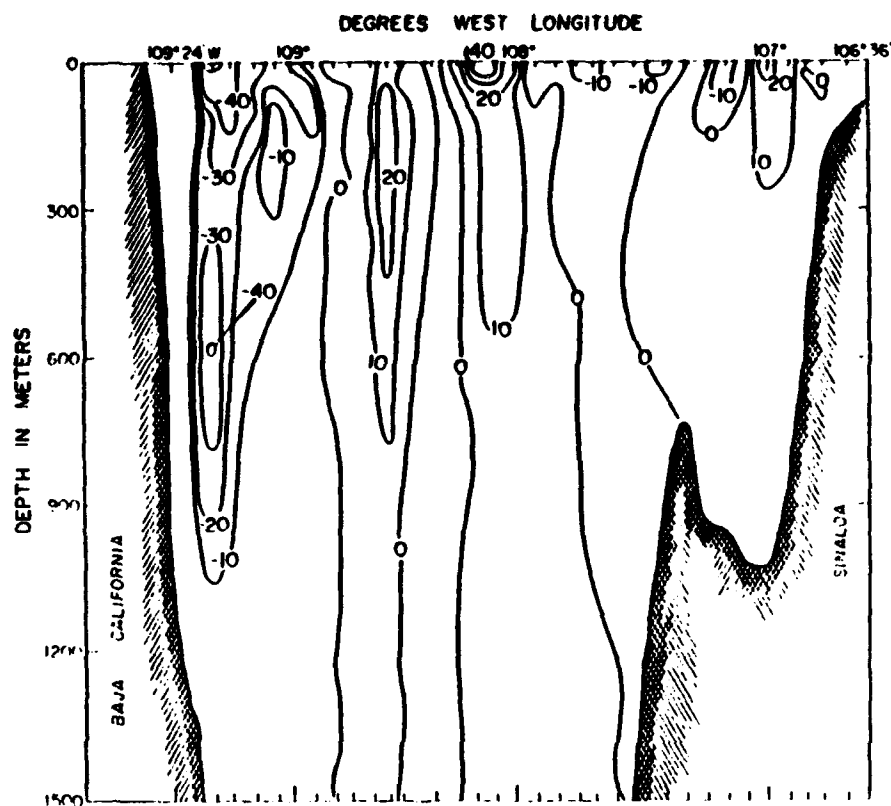


Figure 5. Baroclinic flow (cm/sec) across the entrance to the Gulf of California. The flow is referenced to the 1500 dbar surface. The transection runs from Arroyo de Vinorama, Baja California, to approximately Mazatlán, Sinaloa and was occupied on 5-6 December 1969 (Figure 4., Roden, 1972).

REFERENCES

- Bray, N.A., 1988a: *Thermohaline Circulation in the Gulf of California*, J. Geophys. Res., 93(C5), 4993-5020.
- Bray, N.A., 1988b: *Water Mass Formation in the Gulf of California*, J. Geophys. Res., 93(C8), 9223-9240.
- Roden, G.I., 1964: *Oceanographic Aspects of the Gulf of California*, Marine Geology of the Gulf of California, Amer. Assoc. of Petroleum Geologists, Tulsa, Okla., Memoir No. 3, 30-58.
- Roden, G.I., 1972: *Thermohaline Structure and Baroclinic Flow Across the Gulf of California Entrance and in the Revilla Gigedo Islands Region*, J. Phys. Oceanogr., 2(2), 177-183.

of transit to the entrance, or 2) simply the presence (or lack thereof) of wind forcing to drive upper layer water masses. Both conclusions support the observed Gulf Water at the entrance in December.

East of the Alarcon Seamount (centered approximately 70 km offshore from Baja), independent cores of cooler, low-salinity ($S \leq 34.7$ psu) water dominated the near-surface stratified layer. These poleward flowing cores, believed to consist of admixtures of California Current Water and subsurface composites of Eastern Tropical Pacific Water (often referred as Subtropical Subsurface Water), are undoubtedly a partial source for the advection of cooler and fresher water into the Gulf. The cores appear dispersed and only marginally organized during the December cruise, but broad and uniform during April-May. Current speeds were comparable in intensity to those of the outflowing cores, with slightly stronger currents (maximum speeds of 70 cm/sec) observed for April-May.

The deepest common depth (DCD) method proved to be the most suitable of three techniques compared in determining the geostrophic velocities. Besides suggesting a more complete depiction of the currents running through this highly diverse bathymetric region, it also gave the most reasonable results for volume and salinity transports.

Volume transports calculated for the two cruise periods indicated less transport occurring during the December-January period. For PESCAR 02, a net inflow of +1.9 Sv, the difference between a northward transport of 8.4 Sv and a southward transport of 6.5 Sv, was determined. Corresponding salinity transports were a net inflow of $+6.0 \times 10^4$ tonne/sec, the difference between a northward transport of 2.9×10^5 tonne/sec and a southward transport of 2.3×10^5 tonne/sec. Why more water was exchanged over the April-May period was not readily apparent. The differences are presumably due to seasonal processes.

This experiment opened new ground and raised additional questions concerning the circulation and exchange processes occurring at the Gulf's entrance. The inclusion of the deep layer structure in this examination established the importance of the processes occurring at depth. Unaccounted for in past studies, the deep layer structure revealed both interesting hydrography and appreciable transports relative to the transections analyzed. It was from the deep hydrography sections that the cyclonic flow pattern influencing the region was determined. Likewise, it was found that the largest percentage of the transports were gained from the deep layers. These observations suggest that the deep layer sections at the Gulf's entrance are very dynamic, and thus integral to the overall exchange balances occurring in the Gulf. The caveat to the above remarks is that the calculated transports for this experiment contained excessive imbalances between inflows and outflows. The problem that remains is how to best account for the

dynamics characterizing the deep layer. Suspected error in the results appears to have resulted from the inclusion of the deep layer analyses; and, none of the geostrophy techniques used in the experiment were totally effective in resolving the deep layer. It may be that the sluggish flows and reversing fields associated with the deep layer regime cannot be accurately measured by CTDs or resolved through simple geostrophic examination. Direct current measuring techniques may be the best approach for resolving the velocity structure.

Many of the hydrography sections indicated possible influence from the presence of the Alarcon Seamount. Were these observations real, and, if so, to what degree does the seamount affect the flow processes there? The answers to these questions are outside the scope of this examination. Perhaps a more detailed look utilizing direct measurements (e.g., Pegasus) can solve this newest of the Gulf's riddles.

APPENDIX A: LITERATURE REVIEW

Water Mass Formation and Thermohaline Circulation in the Gulf of California

This appendix is intended to be a more complete review of research reports investigating the Gulf. This includes summary of the extensive work done in the northern Gulf.

I. INTRODUCTION

The Gulf of California is a semi-enclosed, narrow sea basin bordered by the western shores of Mexico and the east coast of Baja California. The Gulf is the only evaporative basin of the Pacific Ocean and is a very dynamic body of water even though it is comparatively small. Surface currents generally follow seasonal variations of the winds, which are predominantly southeasterly in winter and spring and northwesterly in summer and fall (Roden, 1964). Subsurface circulation is far more complex and is characterized by flow exchanges with the adjoining Pacific Ocean, with outflow occurring between the surface layer and about 250 m and inflow occurring between 250 m and roughly 500 m (Bray, 1988b). This paper examines the regional climatology, underwater topography and water mass formation within the Gulf in

order to examine their influences on thermohaline circulation in the Gulf of California.

Bray (1988a) states the Gulf is uniquely characterized by a vertical salinity gradient (salinity decreases with depth) over the top 700 m water column with only occasional exceptions. This condition occurs as a result of the unusual atmospheric forcing over the Gulf, which leads to a net loss of moisture from the ocean surface but a net gain of heat from the atmosphere. She adds that this process is unlike those observed in similar sea basin enclosures such as the Mediterranean and Red seas, where heat is lost to the atmosphere.

The small heat gain (estimated to be $20-50 \text{ W m}^{-2}$) received in the Gulf of California is balanced by an advective flux of colder, fresher Pacific Intermediate Water into the Gulf as warmer, saline Gulf water is transported out (Bray, 1988a). The warm "Gulf Water", as coined by Roden (1964), transported out is a product of water mass formation occurring within the

Gulf. According to Bray (1988b), water mass formation in the Gulf is a result of the following set of complex mechanisms: winter convection; southern transport of newly convected waters via eddylike features; large-scale anticyclonic circulation of northern shelf waters south; and tidal mixing.

Due to restrictions imposed by the Gulf's topography (i.e., transverse ridges or sills) it is assumed that the thermohaline circulation is constrained to depths above 500 m. This corresponds to the controlling sill depth located between the northern and central regions of the Gulf. Observations suggest that the Gulf's thermohaline circulation is a distinctive three-layered system, comprised of: a seasonally driven surface layer; high-saline outflow layer flowing alongshelf the eastern shores of the Baja peninsula; and a deeper, relatively fresh inflow layer entering the central part of the Gulf's mouth (Bray, 1988a).

II. CLIMATOLOGY

The Gulf of California is located between the arid peninsula of Baja California to the west and the equally arid Mexican states of Sonora and Sinaloa to the east. An almost unbroken chain of mountains, 1-3 km high, situated along the Baja peninsula acts to channel seasonal winds along the length of the Gulf. Additionally, these mountains isolate the Gulf from the oceanic climate of the nearby Pacific to the west (Roden, 1964).

There is a large variation of atmospheric temperature over the Gulf between summer and winter periods. Variations are extreme and may exceed 15°C in the northern Gulf region. In the late summer evaporation rates are at a maximum and correlate with increased sea surface temperatures.

Roden (1964) states that precipitation in the region is more prevalent in the south than in the dry,

desert-like northern Gulf, where precipitation is less than 10 cm/yr. In the southern Gulf precipitation can increase to as much as 100 cm/yr, with most of the rain falling during the rainy season months from June to October. The year-to-year variation of precipitation is large. Also, winds in the Gulf of California are extremely variable. The winds blow predominantly out of the northwest from November to May, and out of the southeast during the rest of the year (Roden, 1964). The winter winds are stronger and less humid than the southerly summer winds and are associated with significant upwelling (≈ 3 m/day) along the western shores of the Mexican mainland. The southerly summer winds also induce upwelling along the eastern coast of the Baja peninsula.

Roden (1964) mentions that the Gulf region is noted for its seasonal storms. Northwest gales of two-three days duration are commonly experienced in the northern Gulf between December and February. Their southern counterparts, *chubascos*, violent gales of

short duration, occur in the rainy season from June to October. Also, the Gulf - particularly the extreme southern region - is susceptible to hurricanes during the period between late May and early November.

Isolated from the Pacific Ocean, the Gulf of California is more continental than oceanic in climate. With a related extreme seasonal variation of temperature and wind, the Gulf behaves as the only evaporative basin of the vast Pacific. According to Bray (1988b), the atmosphere over the Gulf influences oceanic circulation through the wind field, which reverses seasonally, through surface heating and cooling, and through evaporation.

III. TOPOGRAPHY

Bray (1988b) explains: the Gulf of California is approximately 1000 km long and 150 km wide, lying between the mountainous Baja California peninsula and the western shores of Mexico. The bathymetry of the Gulf is quite complex, characterized by numerous basins separated by transverse ridges or sills. Most of the basins are deep and in open communication with the Pacific. Progressing northward, the sills become increasingly shallow. Sills located in the southern and central basins are deeper than 1500 m, thus allowing open exchange between the deeper waters of the Pacific and the Gulf waters. South of the region's midriff islands, the San Esteban sill, rising to about 500 m, effectively isolates the northern Gulf from the central region basins (Figure 1).

Bray (1988b) continues, stating the highest salinities found in the Gulf are in the tidal flats of

the north, where evaporation is the greatest and the Gulf is the shallowest. Interestingly, maximum salinities ($\approx 36\%$) are observed at the head of the Gulf in the Colorado River delta. Due to the low fresh water discharge from the river, river runoff has little influence on diluting the salinity of the Gulf waters there.

IV. WATER MASS FORMATION

As defined by Bray (1988b), the term water mass formation refers to processes which convert surface waters of the ocean into deeper waters removed from direct atmospheric forcing. In this context, a water mass is characterized by a temperature versus salinity relationship, T-S, traceable to some observable set of surface conditions.

Evaporation over the Gulf (0.95 m/yr) is comparable to that of the Mediterranean and Red seas, with surface salinities in the northern Gulf 1-2 psu higher than those found along the same latitude in the open Pacific. But the Gulf differs from the aforementioned evaporative basins in that it **gains heat** at an annually estimated average rate of 20-80 W/m² (Bray, 1988b). An accompanying vertical instability condition is possible because temperature and salinity both decrease with depth (Figure 2). This

vertical structure precludes the expected two-layer thermohaline system of warm, fresh subsurface inflow and cold, salty surface outflow. Water mass formation in the Gulf must somehow compensate for the unusual air-sea forcing occurring there. To balance the air-sea heat gain and the evaporative moisture loss, there must be a net upward transport of cold, fresh inflow water and a net downward transport of warm, saline waters, to intermediate depth. Bray (1988b) states that "these constraints force the new water mass to be intermediate (in depth as well as in T-S properties) between the deep, relatively fresh inflow and the surface layer which has been made saline by evaporation." She adds, the following mechanisms are responsible for this process: 1) winter convection, 2) dispersion of convected water in small eddylike features, 3) an anticyclonic circulation in the northern Gulf, and 4) tidal mixing.

An interpretation of Bray's (1988a) detailed explanation of the water mass formation process begins

by stating that evaporation reaches a maximum in the northern Gulf in late summer and early fall following a summer of intense surface heating. This results in a warm, saline surface mass. Localized winter convection transforms some of this saline surface water into a cold, dense, salty bottom water found only in the deep basins of the northern Gulf. Inclusive, there are associated processes relative to winter convection that are key to the entire process. That is, there must be an explanation for the characteristic destabilizing vertical salinity gradient established as a result of less saline Central Gulf Water (CGW) underlying the high-salinity Colorado Delta Water (CDW). Such occurs as a result of cyclonic inflow of CGW at depth into the deep basins of the far north. At depths greater than 100 m, the only conduit for inflow of CGW into the northern Gulf is through the channel connecting Wagner Basin, via depressions to Delfin Basin. Then, as the surface waters of the northern Gulf (CDW) cool in the winter, thus increasing their

density above that of the advected underlying CGW, the CDW sinks below the CGW. If this "penetrative" convection occurs, an identifiable T-S signature of a subsurface salinity minimum (CGW) overlying a deeper salinity maximum (convected CDW) should be observed. Additional properties of this traceable Wagner Basin Water (WBW) are that surface and bottom salinities should be nearly equal, surface temperatures should be warmer than bottom temperatures, and the bottom salinity maximum layer should have higher temperatures than the salinity minimum layer overlying it. Also, density should be nearly uniform with depth in the salinity minimum and maximum layers.

From evidence gathered from hydrographic data, current meter data, and meteorological data (winter '84-'85) it is suspected that at least one mechanism for dispersing Wagner Basin Water is by "Gulfies", or small diameter eddies emanating from the formation region after major cooling events. Thus, the Gulfies are responsible for advecting the newly formed WBW

away from the formation region. These isolated patches of high-salinity water have been discovered several hundred kilometers south of the convection or formation region, and have been traced back in time to specific cooling events, with patches of greater salinity anomaly associated with stronger cooling. Gulfies result from the process of water mass formation itself. Also, as the Gulfies transit south through the sill-strait system of the central-southern Gulf, they can lose much of their T-S signature via tidal mixing with central Gulf water masses.

Another process considered important in the transportation of high-salinity surface waters south from the northern regions of the Gulf is by means of a strong anticyclonic circulation occurring in late winter. Evident in the hydrographic data from March 1985, the gyre centered over the northern Gulf and extending across the width of the Gulf appears responsible for advecting high-salinity surface water from the shelf regions of the north well into the

central Gulf, some 150 km to the south. The water advected is observed as a horizontally isolated salinity maximum, nearly isohaline and extending to approximately 200 m deep in the gyre center (Figure 3). Consequently, the gyre provides a means of transporting high-salinity water away from the northern shelves as well as a mechanism for mixing saline surface waters with deep, fresh inflow water. As a note, the anticyclonic gyre in the northern Gulf does not appear directly related to convection. The gyre is of much larger horizontal scale and is centered far south of the origin of the Wagner Basin Water. A possible driving force for the gyre is the existence of externally imposed density gradients as a circumstance of the cooling of high-salinity surface waters, resulting in denser waters to the north, and consequently anticyclonic circulation.

Inevitably, mixing must be an important factor in water mass formation in the Gulf. Tides provide energy for mixing during water mass formation processes. In

the northern Gulf, tidal mixing is likely induced by bottom friction. Farther south in the island region, particularly near sills, mixing is probably by the breaking of large vertical scale internal waves. Water mass formation in the Gulf is directly affected by these mixing processes. The shallow waters of the northern shelves are vertically mixed during winter, facilitating convection. Likewise, mixing is responsible for reducing the high-salinity signature of northern Gulf waters as they enter the central Gulf.

Bray (1988b) summarizes her explanation of the water mass formation process, contending that water mass formation in the Gulf of California results from a requirement that there be a net upward transport of deep water properties to balance the air-sea heat gain, and a net downward transport of surface water properties to balance evaporative moisture loss. This is accomplished through a series of complex interactions involving atmospheric forcing, tidal

mixing and topographic constraints. The resultant product is a new water mass that is intermediate in depth as well as in its by T-S properties. This intermediate Gulf Water reflects the properties of both the deep, relatively fresh inflow and the salty surface layer formed by evaporation.

V. THERMOHALINE CIRCULATION

As previously discussed, unlike the Mediterranean and Red seas, the Gulf of California actually gains heat from the atmosphere on an annual average. This heat gain is presumably balanced by an advective flux of colder water into the Gulf and warmer water out of the Gulf. This theory correlates with observed vertical gradients of temperature and salinity and with baroclinically determined circulation patterns (Bray, 1988a).

Hydrographic evidence from moored observations and ship measurements suggests that the Gulf's thermohaline circulation is comprised of the following three-layered system: 1) surface layer which is approximately 50 m thick and reverses transport direction with the seasonally reversing large-scale wind field, flowing north in the summer and south in the winter, 2) baroclinic outflow occurring along the

western shores of the Gulf between the surface layer and about 250 m depth, and 3) baroclinic inflow occurring mainly in the central sector of the Gulf between 250 and 500 m depth (Bray, 1988a). There was insufficient data to resolve the circulation at depths deeper than 500 m. To this she adds, "...thermohaline circulation should be constrained to depths above about 500 m, which is the controlling sill depth between the northern and central sections of the Gulf."

The proposed three-layer system has several implications for circulation in the Gulf. In preceding sections of this paper, the formation of an intermediate water mass was discussed. Outflow from the Gulf predominantly consists of this intermediate Gulf Water. Another point of interest is that at the mouth of the Gulf the density of the outflow is such that it forms a near-surface layer. Upon exiting the Gulf, the Gulf Water signature negligibly influences the adjoining Pacific. Also, the Gulf's receipt of

deep, subsurface, nutrient-rich inflow waters from the Pacific gives a sound explanation for the high biological productivity found in the Gulf (Bray, 1988a).

At the mouth of the Gulf, one prominent feature is a thin (10-30 m thick) but pronounced high stability layer sandwiched between the warm surface layer and cooler subsurface layer. This stability layer, depicted in Figure 4, is identified by Väisälä frequencies (where Väisälä freq. $> 0.02 \text{ sec}^{-1}$), and practically extends across the entire southern Gulf. The top of this high stability layer lies at approximately 50 m depth and may be used as an index of the depth of the upper mixed layer. Of particular interest is that breaks in this high-stability layer, clearly evident on the west side of the Gulf, are indicative of strong baroclinic flow (Roden, 1972).

Baroclinic flow across the entrance to the Gulf of California was computed from STD observations (Figure 5). According to Roden (1972), the flow is

referenced to the 1500 dbar surface or the bottom, whichever was encountered first.

Baroclinic outflow, whose origin is traced to the northern Gulf (salinity maximum $> 35.2\%$), flows near the western shores of the southern Gulf, traveling south in a narrow, high-speed velocity core. This core has a characteristic width of about 30 km and deepens to more than 1000 m at the Gulf's entrance. Maximum velocities within the core occur at the surface, reaching 55 cm/sec.

Baroclinic inflow into the Gulf takes place mainly in the central part. Here there are two observable cores of increased velocity entering the Gulf. One core is about 20 km wide and has a maximum velocity of ≈ 26 cm/sec, occurring between 50 and 450 m depth. The other, slightly wider than the first, has a maximum speed of 46 cm/sec and is confined to the upper layer.

VI. SUMMARY

The Gulf of California's hot, arid summer climate makes it the Pacific Ocean's only evaporative sea basin. Surface currents in the Gulf generally follow seasonal variations of the wind, with northwesterlies blowing from November to May and southeasterlies from June to October.

Unlike similar semi-enclosed sea basins (namely, the Mediterranean and Red seas), the Gulf of California is uniquely characterized by a destabilizing vertical salinity gradient (salinity decreases with depth) over the top 700 m water column. This condition occurs as a result of the unusual atmospheric forcing occurring over the Gulf, which results in a net loss of moisture from the ocean surface but a net gain of heat. Given this condition, an intermediate Gulf Water mass is formed. The mechanisms for the formation of this intermediate

water mass include: winter convection in the northern basins; advection of newly convected water via isolated eddies, referred to as Gulfies; transport of water south from the northern shelves by way of a large-scale anticyclonic gyre; and strong tidal mixing.

The thermohaline circulation pattern proposed for the Gulf to balance the net heat and moisture fluxes consists of three layers. There is the surface layer, whose current field is directly influenced by the seasonally varying wind. Baroclinic outflow transports warm and saline Gulf Water of northern origin out of the Gulf along its western boundary. Baroclinic inflow transports relatively fresh, cold Pacific Intermediate Water into the Gulf at the central sector of its entrance.

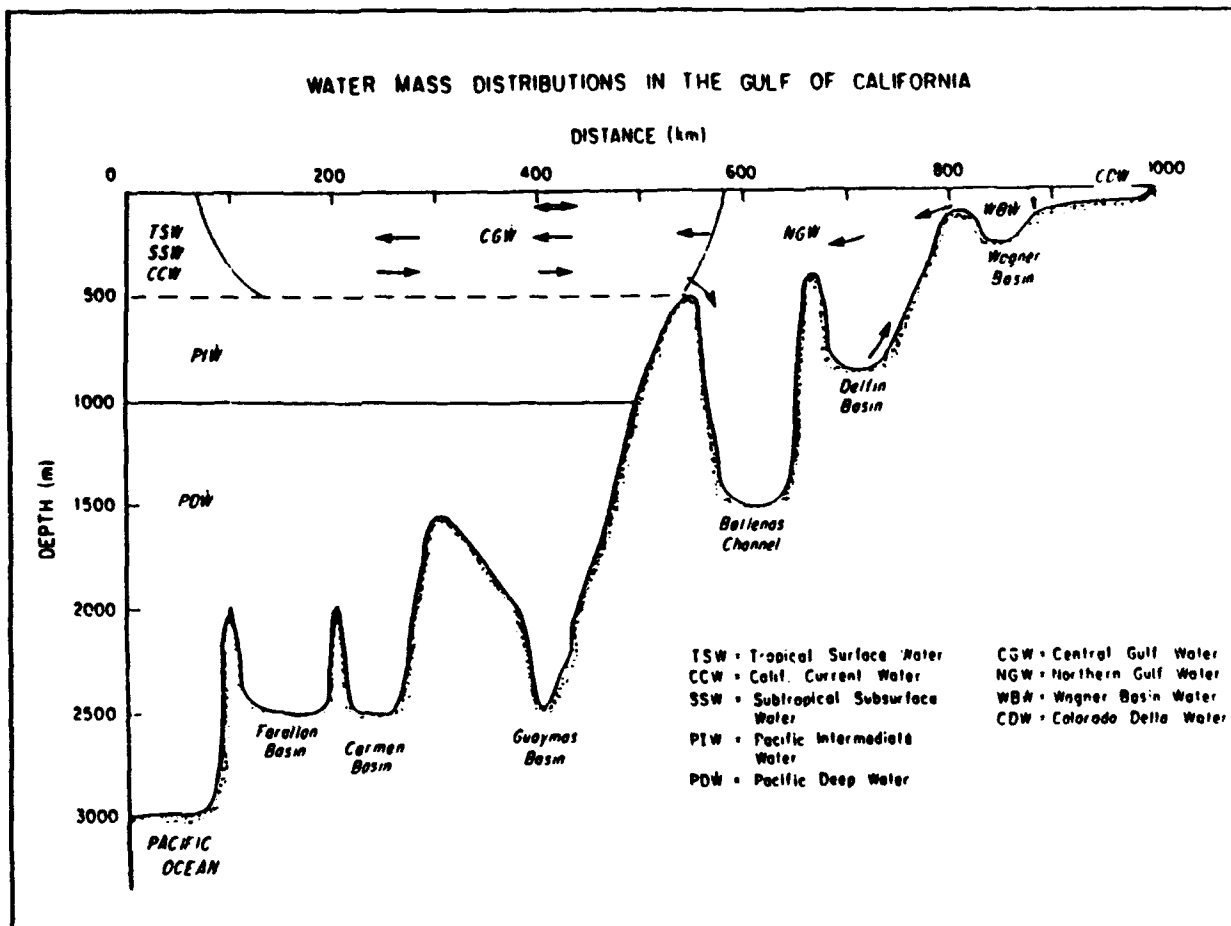


Figure 1. Schematic depicting topography (sills and basins) and water mass distribution in the Gulf of California. Arrows denote hypothesized thermohaline circulation: the open arrow representing the surface wind-driven layer with seasonally reversing transport; solid arrows representing subsurface inflow and outflow; dashed arrow representing deep water formation (Figure 3a., Bray, 1988b).

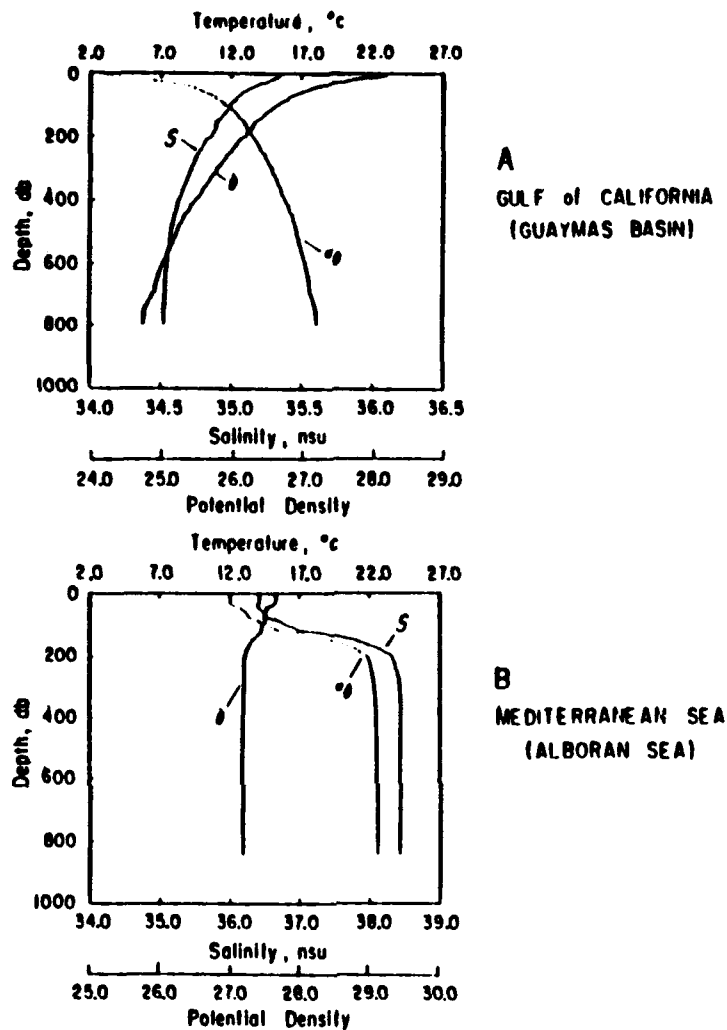


Figure 2. Comparison of the vertical thermohaline structure in the Gulf of California (top graphic, A), and the western Mediterranean Sea (bottom graphic, B). Note that in the case of the Gulf of California, salinity decreases with depth; thus indicating, vertical instability in the water column (Figure 2., Bray, 1988b).

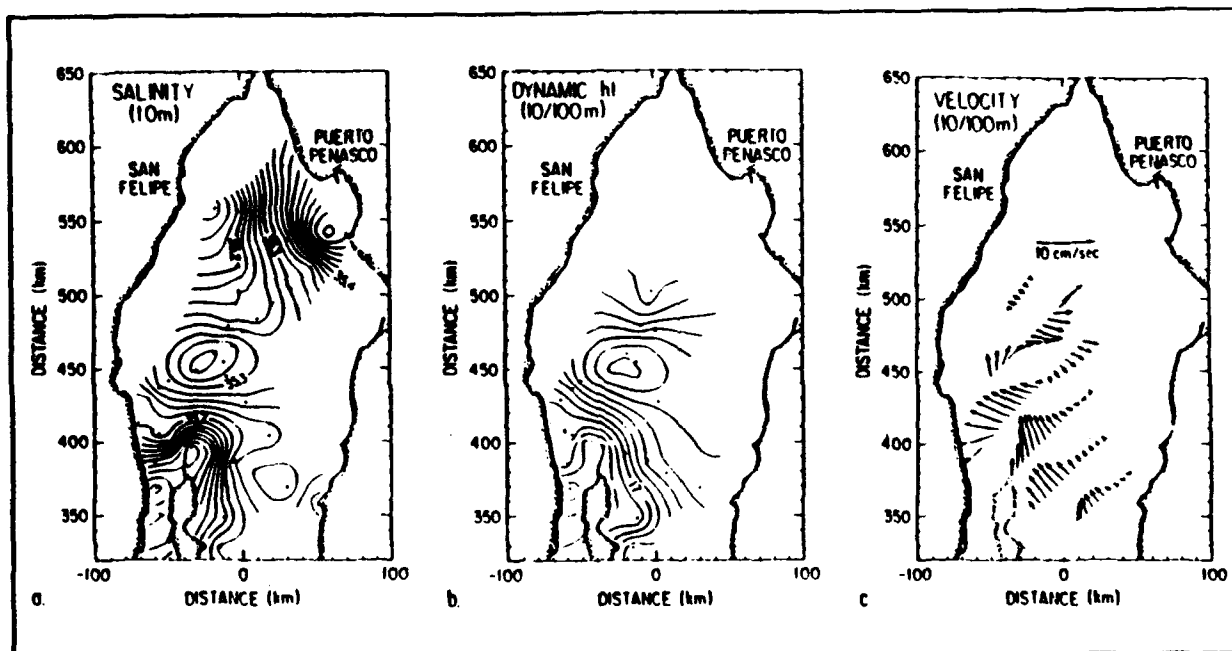


Figure 3. Anticyclonic gyre found in the northern Gulf in March 1985. Plots include: (a) salinity at 10 m, (b) dynamic height at 10 m relative to 100 m, and (c) velocity vectors derived from the dynamic height field. The gyre is presumed to be partially responsible for moving high-salinity waters south from the northern shelf regions. It is also believed to contribute to the mixing processes occurring in the northern Gulf (Figure 15., Bray, 1988b).

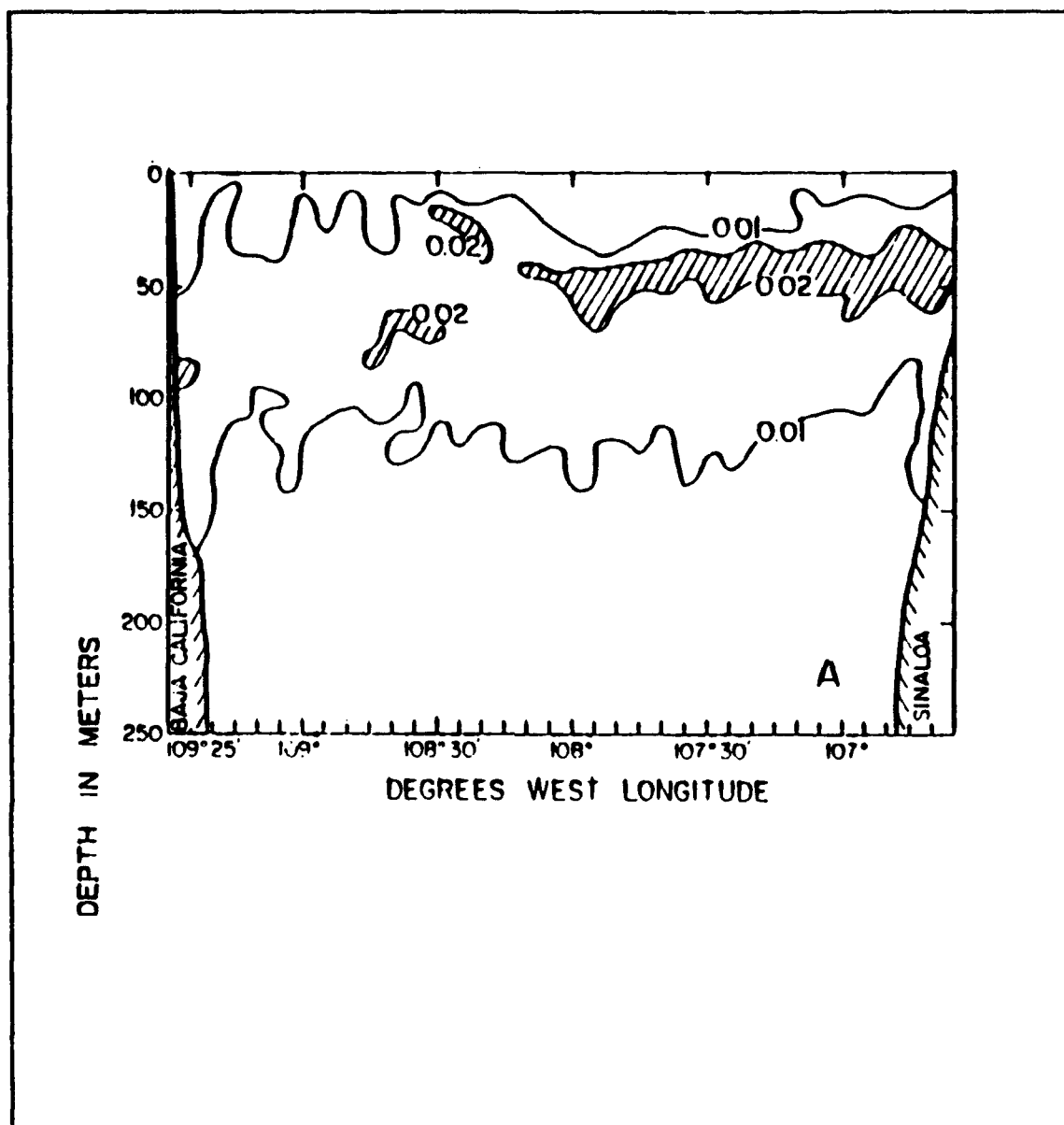


Figure 4. Vertical distribution of Väisälä frequency (sec^{-1}) across the entrance to the Gulf of California. The layer of high stability water is shaded. Breaks in the high stability regions are indicative of baroclinic flow (Figure 2., Roden, 1972).

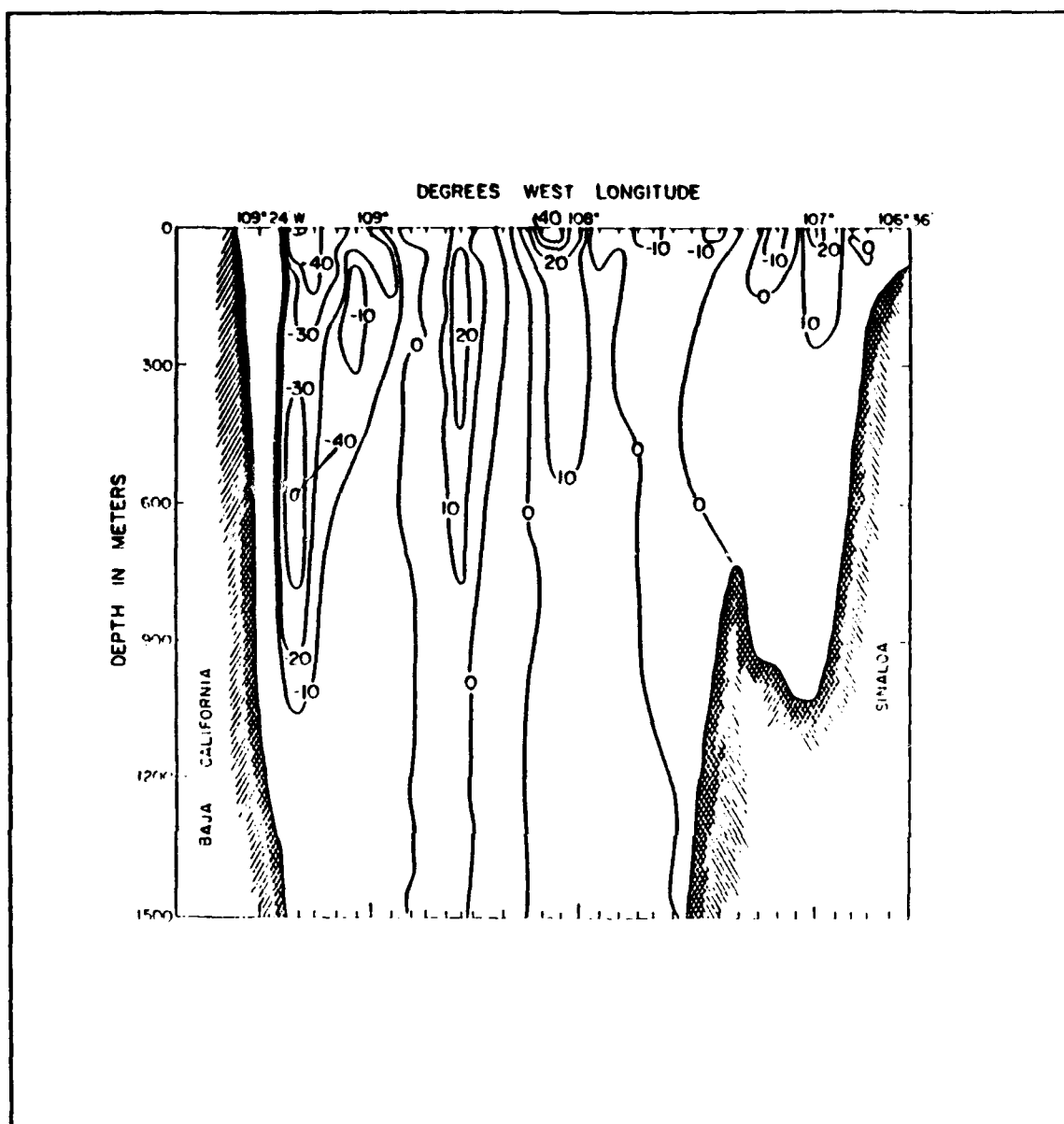


Figure 5. Baroclinic flow (cm/sec) across the entrance to the Gulf of California. The flow is referenced to the 1500 dbar surface. The transection runs from Arroyo de Vinorama, Baja California, to approximately Mazatlán, Sinaloa and was occupied on 5-6 December 1969 (Figure 4., Roden, 1972).

REFERENCES

- Bray, N.A., 1988a: *Thermohaline Circulation in the Gulf of California*, J. Geophys. Res., 93(C5), 4993-5020.
- Bray, N.A., 1988b: *Water Mass Formation in the Gulf of California*, J. Geophys. Res., 93(C8), 9223-9240.
- Roden, G.I., 1964: *Oceanographic Aspects of the Gulf of California*, Marine Geology of the Gulf of California, Amer. Assoc. of Petroleum Geologists, Tulsa, Okla., Memoir No. 3, 30-58.
- Roden, G.I., 1972: *Thermohaline Structure and Baroclinic Flow Across the Gulf of California Entrance and in the Revilla Gigedo Islands Region*, J. Phys. Oceanogr., 2(2), 177-183.

APPENDIX B: SPICINESS (π)

Flament (1986) defined spiciness, π (θ, s), as a state variable which is most sensitive to isopycnal thermohaline variations. He explains that spiciness contributes to examination of double diffusive processes and serves as a tracer for water mass identification. Munk (1981) stated that the largest values of spiciness were indicative of hot and salty water.

γ_θ - π Diagram

The γ_θ - π diagram (Figure B1) shows that spiciness is a monotonic decreasing function of density in this location. Greatest spiciness ($\pi \geq 3.75$) was observed at the surface near the lowest densities, where the effects of insolation are greatest.

The mid-layer regime, where densities range between 24.75 - 26.50 kg/m³, again is a region of variability. From the definition of spiciness, the

variability is associated with contrasts in Gulf, California Current and Tropical Water masses. Because Gulf Water is mostly constrained to and admixed with Tropical Surface Water in the surface layer, this suggests that the variability of the mid-layer is between California Current and Subtropical Subsurface Water masses. One would expect California Current Water, marked by lesser salinity, to coincide with the lesser spiciness in the layer.

The deep-layer regime, where densities are greater than 26.50 kg/m^3 , is uniform, and spiciness decreases more slowly as density increases.

Spiciness (π)

The 500 dbar spiciness transection, shown in Figure B2, supports earlier interpretation of the temperature and salinity structures. Warm, saline surface waters are found across the entire Gulf, with maximum spiciness values ($\pi \geq 3.75$) concentrated at the surface. Depressed curves of spiciness along the Baja banks infer protrusion of warm, saline water down

to 175 m depth there. Positioned east of and fronting this warm, saline water is a ridge centered approximately 55 km offshore. East of the ridge, the spiciness lines exhibit a slight shoaling trend towards the east, indicating cooler and less saline water. Evident within this broad section are two independent cores of cool, fresh water observed via doming features. At 50 to 100 m depth, slight doming occurs 80-100 km offshore from the Baja shore. More pronounced doming of the spiciness curves is observed with the sudden upward protrusion of the 1.5 curve from 150 m depth at 130 km offshore. The doming pushes well into the near-surface layer, with a slight offset east beginning at spiciness curve 3.0. Across the Gulf, the spiciness structure of the upper layer correlates with the locations of the salinity pools previously discussed. In summary, the upper structure shows a frontal ridge centered 55 km offshore from the Baja peninsula separating warm, salty water to the

west from cores of cooler, less saline water to the east.

With depth, spiciness values uniformly decrease (Figure B3). Negative values of spiciness, denoting water of cold and fresher salinity, are not observed until 1000 m depth. Minimum values of spiciness ($\pi \leq -0.1$) are observed at depths greater than 1500 m.

A sense of the along-gulf distribution is accomplished by examining the Leg III transection (Figures B4 and B5). Spiciness curves in the upper layer show similar structuring to the south and up to 32 km north of the transections' intersection (denoted by vertical line on plots). The spiciness contour beyond this northernmost position indicates simultaneous deepening and spreading of the warm, saline surface waters. Such is consistent with Roden's (1964) explanation that Gulf Water, characterized by high salinity and temperature, has its origin in the northern Gulf. In the subsurface layer, the 2.0 and 2.5 spiciness contours shoal at station #59,

suggesting the presence of cooler, less saline water there. Below 200 m the contours tilt downward towards the north, again implying overall warmer and more saline water north of where the transections intersect.

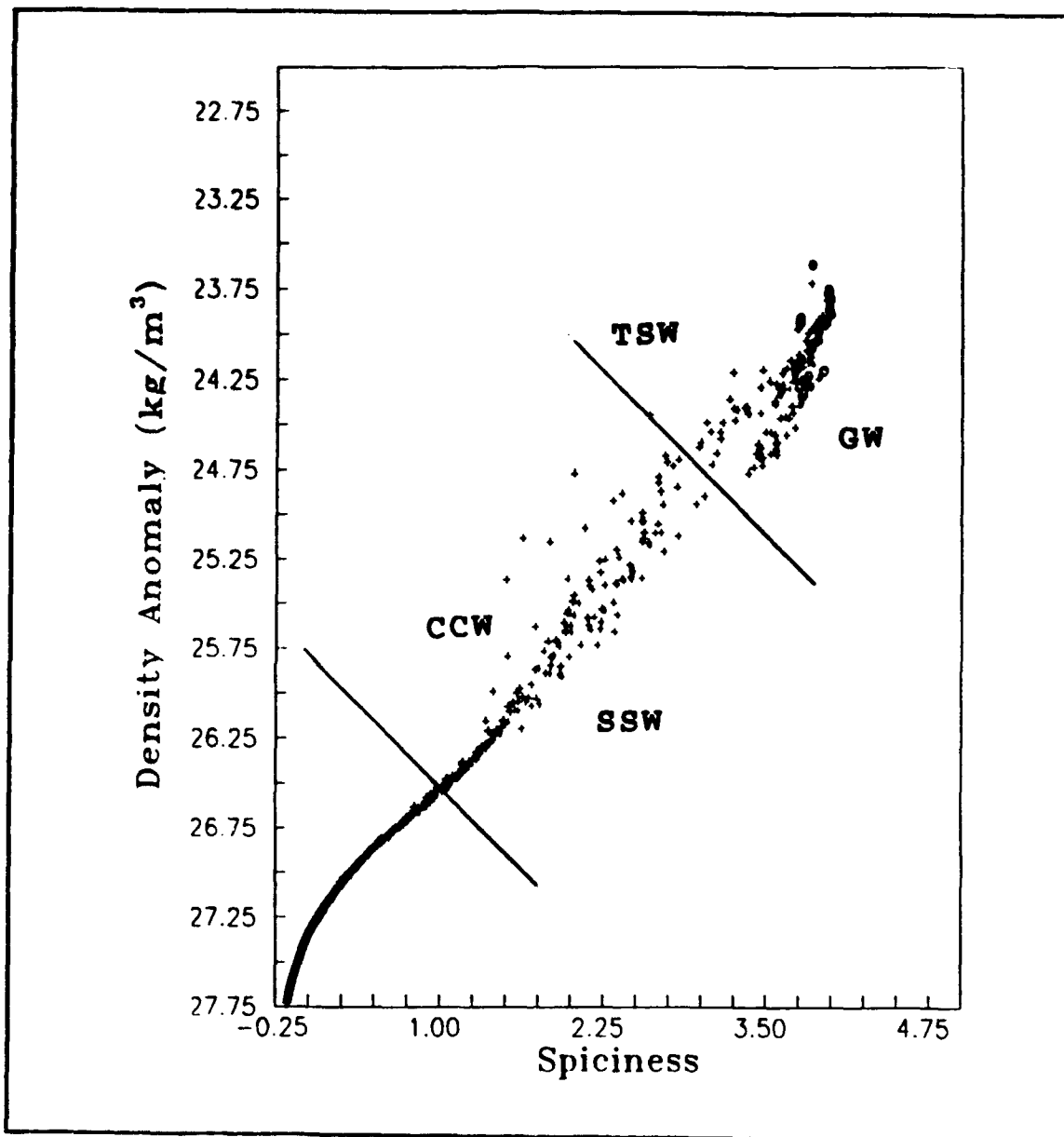


Figure B(1). Full section scatter plot for PESCAR 02 (28 December 1992 - 02 January 1993). Plot is subdivided into sections by water mass: 1) **TSW** denotes Tropical Surface Water, 2) **GW** denotes Gulf Water, 3) **CCW** denotes California Current Water, and 4) **SSW** denotes Subtropical Subsurface Water. The top 10 m section is denoted by circles. Density anomaly - Spiciness ($\gamma_\theta - \pi$) diagram.

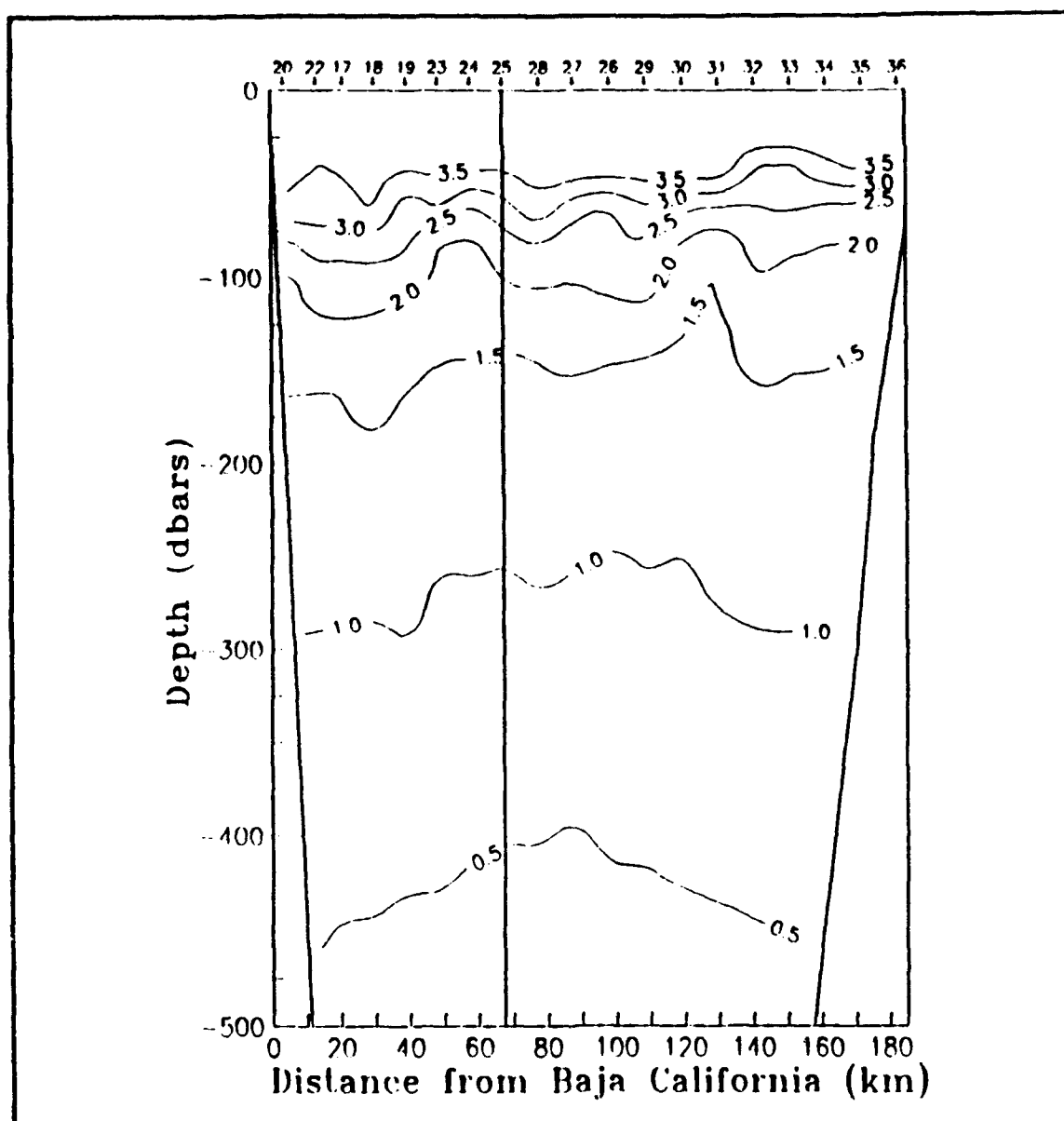


Figure B(2). Spiciness. 500 dbar across-gulf transection for PESCAR 02 (28 December 1992 - 02 January 1993). Cast location and number are given at the top of the figure. Vertical line at cast #25 marks the position of intersection with along-gulf intersection. It also denotes the location of the Alarcon Seamount. Contour spacing is 0.5.

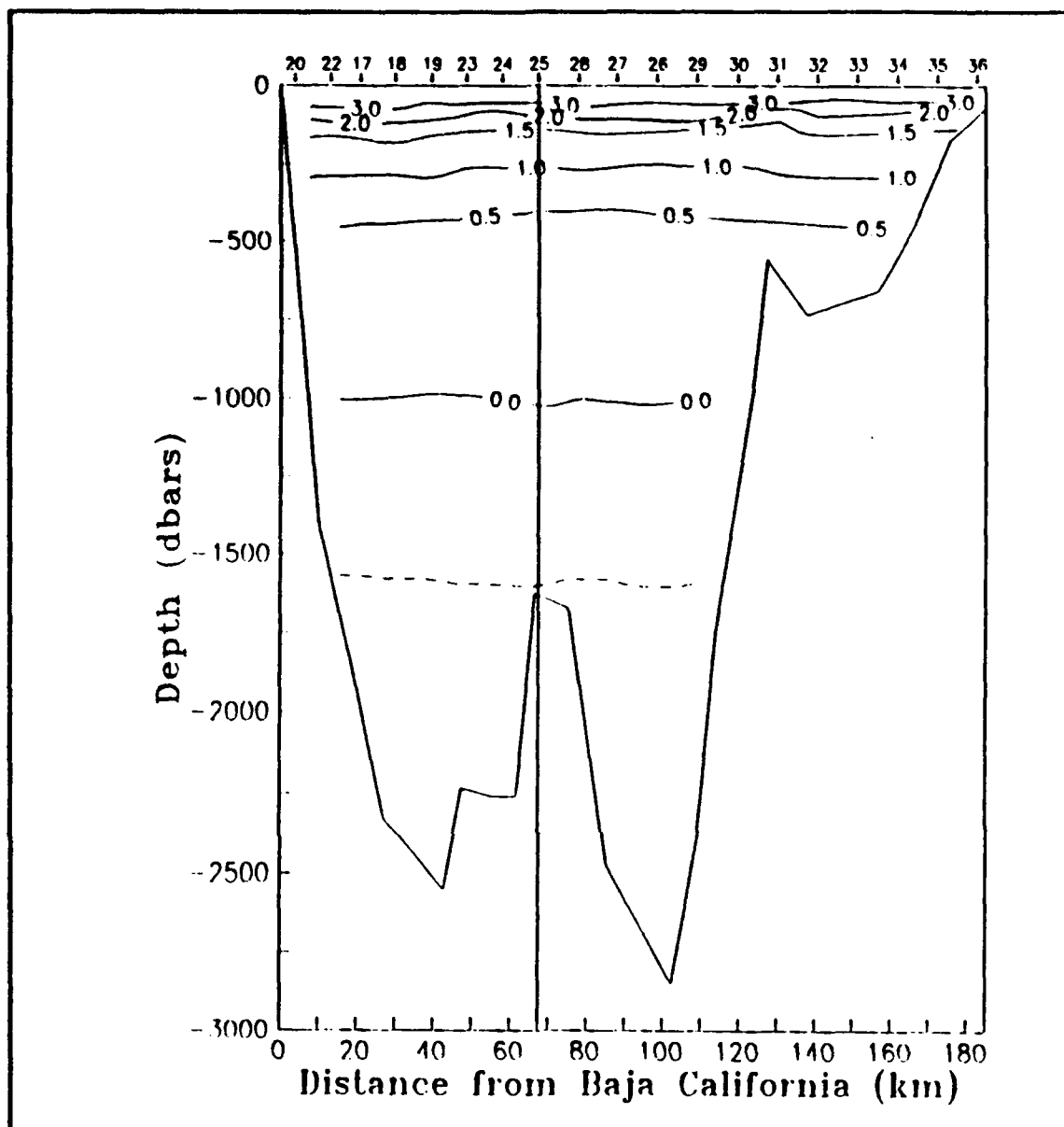


Figure B(3). Spiciness. 3000 dbar across-gulf transection for PESCAR 02 (28 December 1992 - 02 January 1993). Cast location and number are given at the top of the figure. Vertical line at cast #25 marks the position of intersection with along-gulf transection. It also denotes the location of the Alarcon Seamount. Dashed line has spiciness = -0.1.

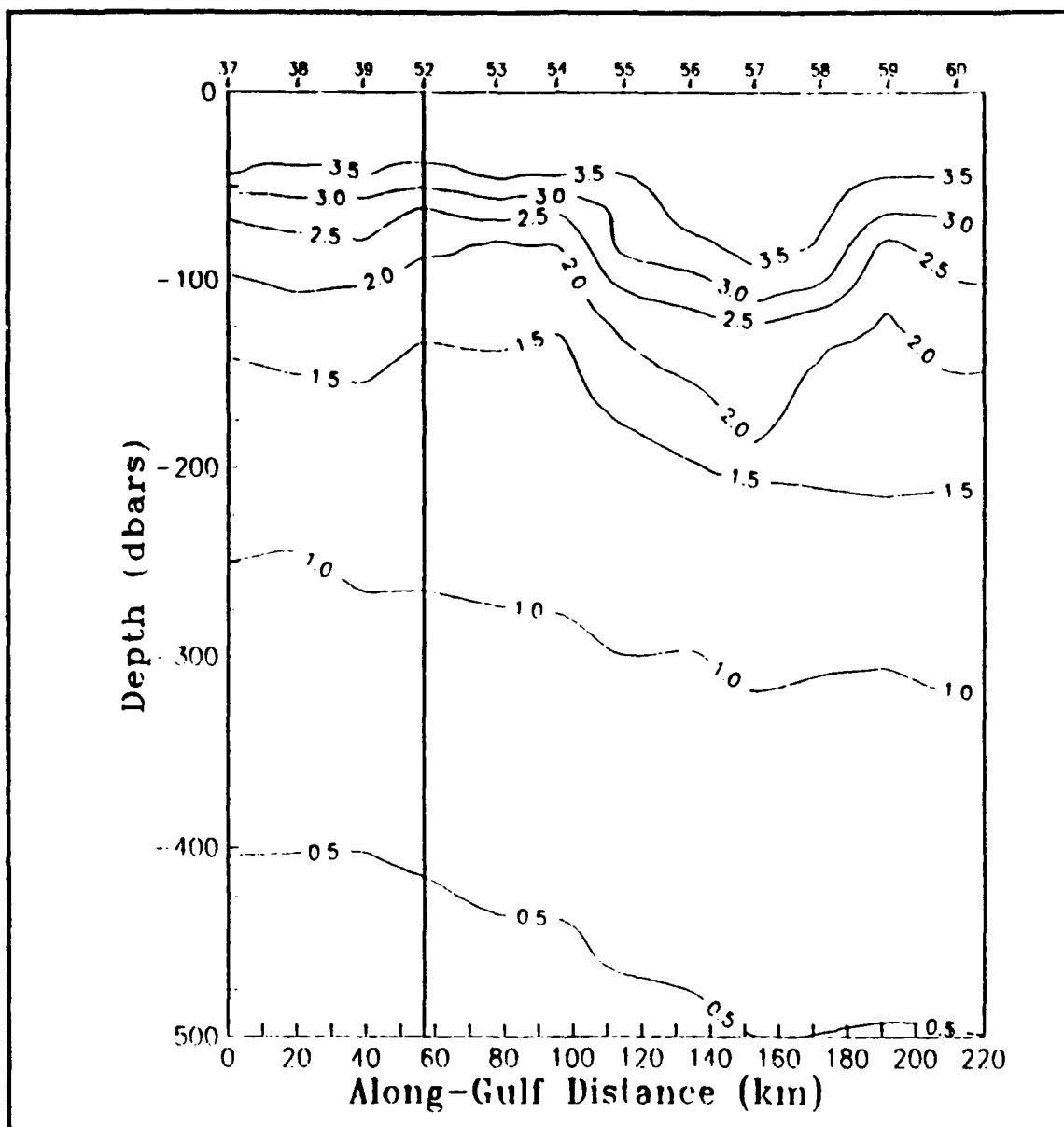


Figure B(4). Spiciness. 500 dbar along-gulf transection for PESCAR 02 (03 - 08 January 1993). Cast location and number are given at the top of the figure. Vertical line at cast #52 marks the position of intersection with the across-gulf transection. It also denotes the location of the Alarcon Seamount. Contour spacing is 0.5.

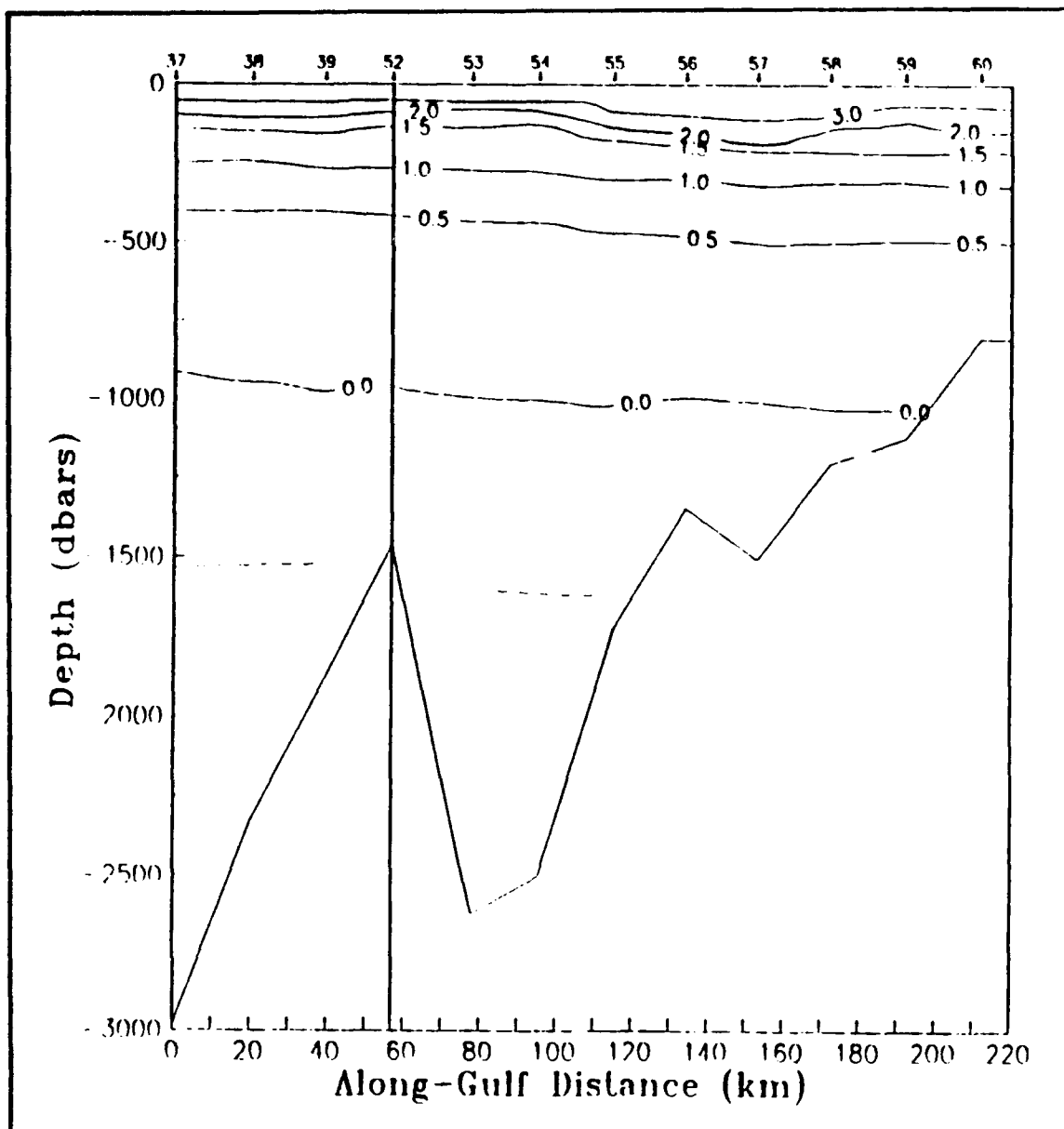


Figure B(5). Spiciness. 3000 dbar along-gulf transection for PESCAR 02 (03 - 08 January 1993). Cast location and number are given at the top of the figure. Vertical line at cast #52 marks the position of intersection with across-gulf transection. It also denotes the location of the Alarcon Seamount. Dashed line has spiciness = -0.1.

APPENDIX C: CTD DATA PROCESSING AND LISTINGS

Tables C1 and C2 summarize dates, locations and bottom depths for across- and along-gulf transections, respectively. In Table C3, hydrographic data are listed for these transections. The specific volume anomaly (δ) is calculated using algorithms found in Volume 4 of the International Oceanographic Tables (UNESCO, 1987). The units for δ are $10^{-8} \text{ m}^3 \text{ kg}^{-1}$. The summation of dynamic height ($\Sigma\Delta D$) is made from the surface, and the units are in dynamic meters ($\text{m}^2 \text{ s}^{-2}$). Spiciness is calculated using an algorithm provided by Flament (1986). Table C4 lists salts used for CTD calibration.

TABLE C1. PESCAR 02 LEG II CTD SOUNDINGS

<u>CTD Cast</u>	<u>Date/Time</u>	<u>Latitude</u>	<u>Longitude</u>	<u>Depth (m)</u>
20	12-29/2218	23-26.8	109-23.6	128
22	12-29/2330	23-27.6	109-18.1	1475
17	12-29/1441	23-29.3	109-13.8	1860
18	12-29/1648	23-30.8	109-08.7	2360
19	12-29/1853	23-32.0	109-03.3	2590
23	12-30/1136	23-33.2	108-58.1	2272
24	12-30/1406	23-34.5	108-52.8	2275
25	12-30/1636	23-35.8	108-47.4	1600
28	12-31/2118	23-38.3	108-41.7	1700
27	12-31/1818	23-41.1	108-36.5	2817
26	12-31/1500	23-43.7	108-30.9	2825
29	01-01/1400	23-46.4	108-25.4	1830
30	01-01/1606	23-49.1	108-19.7	930
31	01-01/1736	23-51.7	108-14.2	922
32	01-01/1853	23-54.4	108-08.7	740
33	01-01/2011	23-57.1	108-03.2	690
34	01-01/2123	23-59.8	107-57.7	445
35	01-01/2230	24-02.4	107-52.2	175
36	01-01/2323	24-05.1	107-46.7	85

TABLE C2. PESCAR 02 LEG III CTD SOUNDINGS

<u>CTD Cast</u>	<u>Date/Time</u>	<u>Latitude</u>	<u>Longitude</u>	<u>Depth (m)</u>
37	01-04/1141	23-11.9	108-25.1	3020
38	01-04/1441	23-20.5	108-32.5	2365
39	01-04/1723	23-27.4	108-40.9	1940
52	01-07/0936	23-35.1	108-47.0	1480
53	01-07/1148	23-43.0	108-55.9	2640
54	01-07/1436	23-49.9	109-03.0	2540
55	01-07/1718	23-57.8	109-10.7	1750
56	01-07/1930	24-05.2	109-18.6	1375
57	01-07/2218	24-12.8	109-26.0	1535
58	01-08/0018	24-20.0	109-34.2	1230
59	01-08/0211	24-27.6	109-42.5	1180
60	01-08-0406	24-35.0	109-51.0	815

TABLE C3. Data listings at selected pressures of temperature ($^{\circ}\text{C}$), salinity (psu), density anomaly (kg m^{-3}), specific volume anomaly (δ), summation of dynamic height ($\Sigma\Delta D$), and spiciness (π) for CTD casts occupied during the PESCAR 02 cruise of 28 December 1992 - 08 January 1993 aboard the R/V Pt. Sur.

CAST 20. DATE: 12/29/92 2218 GMT
 LAT: 23° 26.8' N. LON: 109° 23.6' W.

P(dbar)	T($^{\circ}\text{C}$)	S(psu)	$\gamma_{\theta}(\text{kg m}^{-3})$	δ	$\Sigma\Delta D$	π
1.0	22.182	35.028	24.190	372.02	0.004	3.94
5.0	22.182	35.028	24.190	372.16	0.019	3.94
10.0	22.141	35.028	24.202	371.22	0.037	3.93
15.0	22.076	35.030	24.222	369.54	0.056	3.91
20.0	22.018	35.029	24.238	368.21	0.074	3.89
25.0	21.872	35.025	24.275	364.82	0.093	3.85
30.0	21.663	35.024	24.333	359.53	0.111	3.79
35.0	21.550	35.029	24.368	356.36	0.129	3.76
40.0	21.503	35.031	24.383	355.17	0.146	3.75
45.0	21.336	35.027	24.426	351.24	0.164	3.70
50.0	21.221	35.025	24.457	348.52	0.181	3.67
60.0	20.832	34.988	24.535	341.50	0.216	3.53
70.0	17.827	34.781	25.151	282.96	0.248	2.59
80.0	16.980	34.782	25.356	263.68	0.275	2.39
90.0	16.065	34.785	25.572	243.40	0.301	2.18
100.0	14.738	34.748	25.839	218.15	0.324	1.85
103.0	14.610	34.770	25.883	213.96	0.330	1.84

CAST: 22
LAT: 23° 27.6' N.

DATE: 12/29/92 2330 GMT
LON: 109° 18.1' W.

P(dbar)	T(°C)	S(psu)	$\gamma_0(\text{kg m}^{-3})$	δ	$\Sigma\Delta D$	π
3.0	21.908	34.969	24.222	369.04	0.011	3.82
5.0	21.795	34.969	24.253	366.11	0.018	3.79
10.0	21.801	34.988	24.266	365.07	0.037	3.80
15.0	21.809	35.020	24.289	363.15	0.055	3.83
20.0	21.610	34.997	24.327	359.70	0.073	3.76
25.0	21.181	35.000	24.447	348.43	0.091	3.64
30.0	20.752	34.962	24.535	340.26	0.108	3.49
35.0	20.518	34.968	24.603	334.00	0.125	3.43
40.0	20.513	34.995	24.625	332.10	0.141	3.45
45.0	20.402	34.994	24.654	329.50	0.158	3.42
50.0	20.396	35.026	24.680	327.20	0.174	3.44
60.0	20.220	35.035	24.734	322.44	0.207	3.40
70.0	18.041	34.781	25.098	287.98	0.238	2.65
80.0	17.963	34.892	25.203	278.39	0.266	2.71
90.0	17.300	34.876	25.352	264.48	0.293	2.54
100.0	16.024	34.858	25.637	237.51	0.318	2.22
125.0	14.791	34.842	25.901	213.07	0.375	1.94
150.0	13.843	34.800	26.071	197.47	0.426	1.70
175.0	12.625	34.720	26.256	180.26	0.473	1.39
200.0	12.346	34.709	26.302	176.45	0.518	1.33
225.0	11.798	34.695	26.397	167.94	0.561	1.21
250.0	11.508	34.683	26.442	164.12	0.602	1.15
275.0	11.145	34.651	26.484	160.59	0.643	1.05
300.0	10.720	34.630	26.545	155.21	0.682	0.96
325.0	10.380	34.625	26.601	150.29	0.720	0.90
350.0	9.958	34.610	26.662	144.80	0.757	0.81
375.0	9.671	34.589	26.694	142.08	0.793	0.75
400.0	9.276	34.574	26.747	137.25	0.828	0.67
425.0	8.723	34.544	26.812	131.13	0.862	0.56
450.0	8.469	34.538	26.847	128.08	0.894	0.52
475.0	8.090	34.544	26.910	122.28	0.925	0.46
500.0	7.617	34.510	26.953	118.13	0.955	0.37
550.0	7.278	34.529	27.017	112.61	1.013	0.33
600.0	6.817	34.525	27.078	107.09	1.069	0.27
650.0	6.553	34.519	27.109	104.56	1.121	0.23
700.0	6.291	34.526	27.149	101.11	1.173	0.20
750.0	5.799	34.524	27.210	95.24	1.222	0.13
800.0	5.584	34.524	27.237	93.00	1.269	0.11
850.0	5.339	34.526	27.269	90.18	1.315	0.08
900.0	5.108	34.528	27.297	87.62	1.359	0.05
950.0	4.739	34.532	27.343	83.10	1.402	0.01
1000.0	4.547	34.529	27.362	81.40	1.443	-.01
1100.0	4.207	34.546	27.412	76.87	1.522	-.03
1200.0	3.823	34.562	27.466	71.77	1.597	-.06
1300.0	3.508	34.577	27.509	67.65	1.666	-.08
1400.0	3.336	34.585	27.532	65.70	1.733	-.09

CAST: 17
LAT: 23° 29.3' N.

DATE: 12/29/92 1441 GMT
LON: 109° 13.8' W.

P(dbar)	T(°C)	S(psu)	γ_{θ} (kg m ⁻³)	δ	$\Sigma\Delta D$	π
1.0	21.786	34.957	24.246	366.59	0.004	3.77
5.0	21.672	34.957	24.278	363.72	0.018	3.74
10.0	21.667	35.000	24.313	360.63	0.036	3.77
15.0	21.591	35.016	24.346	357.67	0.054	3.76
20.0	21.100	34.981	24.455	347.50	0.072	3.60
25.0	20.850	35.016	24.549	338.69	0.089	3.56
30.0	20.816	35.056	24.590	335.06	0.106	3.58
35.0	20.717	35.069	24.626	331.77	0.123	3.56
40.0	20.706	35.081	24.639	330.76	0.139	3.57
45.0	20.677	35.100	24.661	328.85	0.156	3.58
50.0	20.359	35.069	24.723	323.10	0.172	3.47
60.0	20.080	35.031	24.768	319.19	0.204	3.36
70.0	19.189	34.891	24.894	307.51	0.236	3.02
80.0	18.357	34.906	25.116	286.68	0.265	2.82
90.0	17.139	34.816	25.344	265.16	0.293	2.45
100.0	16.320	34.813	25.535	247.29	0.318	2.26
125.0	15.152	34.803	25.792	223.50	0.377	1.98
150.0	13.411	34.686	26.072	197.24	0.430	1.52
175.0	12.908	34.736	26.212	184.49	0.478	1.46
200.0	12.466	34.719	26.287	177.93	0.523	1.36
225.0	12.043	34.719	26.369	170.68	0.567	1.28
250.0	11.680	34.694	26.419	166.42	0.609	1.19
300.0	10.582	34.620	26.561	153.60	0.689	0.93
350.0	9.657	34.597	26.702	140.76	0.762	0.75
400.0	8.900	34.555	26.793	132.60	0.830	0.60
450.0	8.239	34.532	26.878	124.96	0.894	0.48
500.0	7.641	34.517	26.955	118.00	0.955	0.38
550.0	7.425	34.519	26.988	115.49	1.013	0.35
600.0	6.774	34.505	27.068	107.96	1.069	0.24
650.0	6.395	34.503	27.117	103.55	1.122	0.19
700.0	5.987	34.505	27.172	98.49	1.173	0.14
750.0	5.711	34.517	27.215	94.59	1.221	0.12
800.0	5.500	34.522	27.246	92.00	1.268	0.09
850.0	5.259	34.525	27.277	89.22	1.313	0.07
900.0	5.005	34.529	27.310	86.19	1.357	0.04
950.0	4.792	34.533	27.338	83.74	1.399	0.02
1000.0	4.522	34.533	27.368	80.79	1.440	-.01
1100.0	4.159	34.544	27.416	76.42	1.519	-.04
1200.0	3.865	34.562	27.461	72.33	1.593	-.06
1300.0	3.528	34.576	27.506	67.93	1.663	-.08
1400.0	3.244	34.590	27.545	64.17	1.729	-.09
1500.0	3.094	34.598	27.566	62.48	1.793	-.10
1600.0	2.875	34.608	27.594	59.72	1.854	-.11
1700.0	2.632	34.620	27.625	56.46	1.912	-.13
1800.0	2.504	34.626	27.641	55.00	1.967	-.13
1825.0	2.466	34.628	27.646	54.51	1.981	-.13

CAST: 18
LAT: 23° 30.8' N.

DATE: 12/29/92 1648 GMT
LON: 109° 8.7' W.

P(dbar)	T(°C)	S(psu)	γ_{θ} (kg m ⁻³)	δ	$\Sigma\Delta D$	π
1.0	22.204	34.878	24.069	383.47	0.004	3.83
5.0	21.974	34.878	24.134	377.46	0.019	3.76
10.0	21.964	34.878	24.137	377.39	0.038	3.76
15.0	21.927	34.879	24.149	376.50	0.057	3.75
20.0	21.886	34.884	24.164	375.24	0.076	3.74
25.0	21.874	34.886	24.169	374.94	0.094	3.74
30.0	21.709	34.919	24.240	368.36	0.113	3.72
35.0	21.381	34.994	24.388	354.45	0.131	3.68
40.0	21.210	35.092	24.510	343.02	0.148	3.71
45.0	21.013	35.074	24.550	339.41	0.165	3.64
50.0	20.788	35.055	24.597	335.15	0.182	3.57
60.0	20.588	35.063	24.658	329.75	0.215	3.52
70.0	20.449	35.038	24.676	328.38	0.248	3.46
80.0	18.985	34.879	24.937	303.81	0.280	2.96
90.0	16.820	34.765	25.381	261.65	0.308	2.33
100.0	16.302	34.794	25.524	248.28	0.334	2.23
150.0	14.020	34.832	26.059	198.67	0.443	1.76
200.0	12.306	34.707	26.308	175.85	0.536	1.31
250.0	11.270	34.674	26.479	160.52	0.619	1.09
300.0	10.490	34.653	26.603	149.58	0.697	0.93
350.0	9.664	34.611	26.712	139.84	0.769	0.76
400.0	8.861	34.559	26.803	131.69	0.837	0.59
450.0	8.257	34.533	26.876	125.17	0.901	0.47
500.0	7.647	34.528	26.963	117.24	0.962	0.38
550.0	7.186	34.515	27.018	112.33	1.020	0.30
600.0	6.745	34.503	27.070	107.71	1.075	0.23
650.0	6.443	34.507	27.114	103.88	1.128	0.20
700.0	6.122	34.507	27.156	100.17	1.179	0.16
750.0	5.800	34.509	27.198	96.37	1.228	0.12
800.0	5.456	34.519	27.248	91.68	1.275	0.08
900.0	4.928	34.521	27.312	85.83	1.363	0.02
1000.0	4.456	34.540	27.380	79.48	1.446	-0.01
1100.0	4.197	34.545	27.413	76.83	1.525	-0.03
1200.0	3.858	34.560	27.460	72.36	1.599	-0.05
1300.0	3.581	34.573	27.499	68.84	1.670	-0.07
1400.0	3.321	34.587	27.536	65.33	1.737	-0.08
1500.0	3.091	34.598	27.566	62.45	1.801	-0.10
1600.0	2.904	34.607	27.590	60.14	1.862	-0.11
1700.0	2.714	34.616	27.615	57.75	1.921	-0.12
1800.0	2.523	34.626	27.640	55.23	1.977	-0.13
1900.0	2.415	34.631	27.653	54.05	2.032	-0.13
2000.0	2.251	34.639	27.674	51.92	2.085	-0.14
2100.0	2.058	34.650	27.698	49.15	2.135	-0.15
2200.0	1.951	34.657	27.713	47.71	2.184	-0.15
2300.0	1.911	34.660	27.719	47.38	2.231	-0.15
2329.0	1.900	34.662	27.721	47.20	2.245	-0.15

CAST: 19
LAT: 23° 32.0' N.

DATE: 12/29/92 1853 GMT
LON: 109° 3.3' W.

P(dbar)	T(°C)	S(psu)	γ_0 (kg m ⁻³)	δ	$\Sigma\Delta D$	π
1.0	22.314	34.878	24.038	386.43	0.004	3.86
5.0	21.929	34.877	24.146	376.33	0.019	3.75
10.0	21.840	34.884	24.176	373.66	0.038	3.73
15.0	21.816	34.889	24.187	372.82	0.056	3.73
20.0	21.792	34.895	24.199	371.95	0.075	3.73
25.0	21.740	34.900	24.217	370.37	0.094	3.72
30.0	21.640	34.910	24.253	367.16	0.112	3.70
35.0	21.531	34.917	24.288	363.98	0.130	3.67
40.0	21.203	34.895	24.362	357.13	0.148	3.56
45.0	20.871	34.864	24.429	350.96	0.166	3.45
50.0	20.436	34.767	24.472	347.03	0.183	3.26
60.0	18.463	34.715	24.942	302.46	0.216	2.70
70.0	18.181	34.763	25.050	292.59	0.246	2.67
80.0	17.815	34.799	25.168	281.65	0.275	2.61
90.0	16.987	34.798	25.367	263.02	0.302	2.40
100.0	15.879	34.786	25.615	239.57	0.327	2.14
150.0	13.203	34.744	26.158	188.96	0.433	1.53
200.0	12.077	34.703	26.350	171.85	0.523	1.27
250.0	11.341	34.662	26.457	162.67	0.607	1.10
300.0	10.727	34.657	26.565	153.35	0.686	0.98
350.0	9.605	34.603	26.715	139.47	0.759	0.75
400.0	8.658	34.548	26.826	129.33	0.826	0.55
450.0	8.131	34.532	26.894	123.37	0.889	0.46
500.0	7.552	34.517	26.968	116.69	0.949	0.36
550.0	7.098	34.503	27.021	111.95	1.006	0.29
600.0	6.640	34.507	27.087	105.95	1.060	0.23
700.0	6.013	34.506	27.169	98.81	1.162	0.15
750.0	5.706	34.509	27.210	95.07	1.211	0.11
800.0	5.426	34.513	27.248	91.69	1.257	0.08
900.0	4.859	34.522	27.321	84.88	1.346	0.02
950.0	4.617	34.530	27.355	81.74	1.387	0.00
1000.0	4.425	34.537	27.381	79.32	1.428	-.02
1100.0	4.105	34.549	27.425	75.38	1.506	-.04
1200.0	3.801	34.564	27.469	71.39	1.579	-.06
1300.0	3.535	34.576	27.505	68.05	1.649	-.08
1400.0	3.308	34.588	27.537	65.14	1.715	-.09
1500.0	3.106	34.597	27.564	62.70	1.779	-.10
1600.0	2.886	34.608	27.593	59.85	1.840	-.11
1700.0	2.700	34.616	27.616	57.58	1.899	-.12
1800.0	2.522	34.626	27.640	55.22	1.955	-.13
1900.0	2.393	34.633	27.657	53.59	2.009	-.14
2000.0	2.254	34.640	27.674	51.88	2.062	-.14
2200.0	2.012	34.654	27.706	48.70	2.162	-.15
2400.0	1.855	34.664	27.727	46.75	2.257	-.16
2500.0	1.831	34.666	27.731	46.65	2.304	-.16
2535.0	1.825	34.666	27.731	46.70	2.321	-.16

CAST: 23
LAT: 23° 33.2' N.

DATE: 12/30/92 1136 GMT
LON: 108° 58.1' W.

P(dbar)	T(°C)	S(psu)	$\gamma_0(\text{kg m}^{-3})$	δ	$\Sigma\Delta D$	π
1.0	22.381	34.892	24.030	387.22	0.004	3.89
5.0	22.381	34.892	24.030	387.37	0.019	3.89
10.0	22.382	34.886	24.026	387.98	0.039	3.89
15.0	22.383	34.873	24.016	389.16	0.058	3.88
20.0	22.363	34.874	24.022	388.75	0.078	3.87
25.0	22.348	34.873	24.026	388.59	0.097	3.87
30.0	22.213	34.899	24.085	383.22	0.116	3.85
35.0	21.871	34.957	24.225	370.09	0.135	3.80
40.0	21.627	34.954	24.290	364.01	0.154	3.73
45.0	21.619	35.004	24.331	360.36	0.172	3.76
50.0	20.712	34.809	24.431	351.00	0.190	3.36
60.0	19.827	34.791	24.652	330.22	0.223	3.11
70.0	17.793	34.739	25.127	285.19	0.255	2.55
80.0	15.997	34.606	25.449	254.73	0.282	2.02
90.0	14.981	34.644	25.706	230.50	0.306	1.83
100.0	14.891	34.800	25.846	217.52	0.329	1.93
150.0	12.848	34.747	26.232	181.90	0.428	1.46
200.0	12.077	34.714	26.358	171.03	0.515	1.28
250.0	10.890	34.668	26.543	154.27	0.596	1.02
300.0	10.328	34.648	26.627	147.19	0.672	0.91
350.0	9.517	34.600	26.728	138.25	0.743	0.73
400.0	8.669	34.552	26.827	129.25	0.810	0.56
450.0	7.989	34.534	26.917	121.04	0.873	0.44
500.0	7.386	34.519	26.993	114.13	0.932	0.34
550.0	6.853	34.507	27.058	108.15	0.987	0.26
600.0	6.427	34.509	27.117	102.86	1.040	0.20
700.0	5.796	34.513	27.201	95.39	1.139	0.12
750.0	5.574	34.515	27.231	92.90	1.186	0.10
800.0	5.322	34.518	27.264	89.98	1.231	0.07
850.0	4.928	34.524	27.315	85.04	1.275	0.03
900.0	4.703	34.530	27.345	82.32	1.317	0.01
950.0	4.547	34.536	27.367	80.39	1.358	0.00
1000.0	4.395	34.543	27.389	78.50	1.398	-.01
1100.0	4.081	34.554	27.432	74.72	1.474	-.04
1200.0	3.769	34.569	27.476	70.64	1.547	-.06
1300.0	3.490	34.582	27.514	67.06	1.616	-.08
1400.0	3.291	34.592	27.542	64.64	1.682	-.09
1500.0	3.090	34.602	27.569	62.13	1.745	-.10
1600.0	2.878	34.612	27.597	59.46	1.806	-.11
1700.0	2.725	34.619	27.616	57.66	1.865	-.12
1800.0	2.568	34.626	27.636	55.75	1.922	-.13
1900.0	2.433	34.631	27.652	54.28	1.977	-.13
2000.0	2.267	34.640	27.674	52.01	2.030	-.14
2100.0	2.104	34.651	27.695	49.66	2.081	-.15
2200.0	2.005	34.656	27.708	48.43	2.130	-.15
2235.0	1.997	34.657	27.709	48.43	2.147	-.15

CAST: 24
LAT: 23° 34.5' N.

DATE: 12/30/92 1406 GMT
LON: 108° 52.8' W.

P(dbar)	T(°C)	S(psu)	γ_t (kg m ⁻³)	δ	$\Sigma\Delta D$	π
1.0	22.309	34.731	23.928	396.94	0.004	3.74
5.0	22.309	34.731	23.928	397.09	0.020	3.74
10.0	22.310	34.736	23.932	396.93	0.040	3.75
15.0	22.310	34.741	23.936	396.75	0.060	3.75
20.0	22.311	34.747	23.941	396.53	0.079	3.76
25.0	22.313	34.750	23.943	396.55	0.099	3.76
30.0	22.226	34.747	23.966	394.58	0.119	3.73
35.0	21.903	34.865	24.146	377.60	0.138	3.73
40.0	21.470	34.871	24.270	365.90	0.157	3.61
45.0	21.336	34.896	24.327	360.73	0.175	3.60
50.0	20.684	34.802	24.433	350.80	0.193	3.35
60.0	17.966	34.470	24.878	308.51	0.226	2.39
70.0	17.134	34.827	25.354	263.58	0.254	2.46
80.0	15.722	34.635	25.533	246.65	0.280	1.98
90.0	15.137	34.700	25.715	229.68	0.304	1.90
100.0	14.402	34.689	25.866	215.51	0.326	1.73
150.0	12.924	34.742	26.213	183.68	0.424	1.46
200.0	11.835	34.705	26.397	167.29	0.511	1.22
250.0	10.942	34.676	26.540	154.61	0.591	1.03
300.0	10.090	34.630	26.654	144.46	0.666	0.85
350.0	9.322	34.587	26.750	136.01	0.736	0.69
400.0	8.470	34.548	26.854	126.47	0.802	0.52
450.0	7.777	34.531	26.945	118.15	0.863	0.40
500.0	7.146	34.513	27.022	111.10	0.920	0.30
550.0	6.740	34.509	27.075	106.43	0.975	0.24
600.0	6.359	34.506	27.123	102.16	1.027	0.19
650.0	6.068	34.509	27.164	98.64	1.077	0.15
700.0	5.905	34.508	27.184	97.17	1.126	0.13
750.0	5.666	34.510	27.215	94.51	1.174	0.10
800.0	5.396	34.514	27.252	91.23	1.220	0.07
850.0	5.162	34.518	27.283	88.48	1.265	0.05
900.0	5.000	34.521	27.305	86.71	1.309	0.03
1000.0	4.542	34.532	27.365	81.16	1.392	-0.00
1100.0	4.108	34.550	27.426	75.35	1.470	-0.03
1200.0	3.807	34.565	27.469	71.39	1.544	-0.05
1300.0	3.643	34.572	27.492	69.66	1.615	-0.07
1400.0	3.339	34.587	27.534	65.55	1.682	-0.08
1500.0	3.159	34.597	27.559	63.34	1.746	-0.09
1600.0	2.849	34.611	27.599	59.17	1.807	-0.11
1700.0	2.692	34.618	27.619	57.30	1.866	-0.12
1800.0	2.571	34.625	27.635	55.89	1.922	-0.12
1900.0	2.376	34.635	27.660	53.24	1.977	-0.13
2000.0	2.253	34.641	27.675	51.76	2.030	-0.14
2100.0	2.080	34.650	27.697	49.39	2.080	-0.14
2200.0	1.995	34.656	27.708	48.34	2.129	-0.15
2257.0	1.972	34.658	27.712	48.13	2.157	-0.15

CAST: 25

DATE: 12/30/92

1636 GMT

LAT: 23° 35.8' N.

LON: 108° 47.4' W.

P(dbar)	T(°C)	S(psu)	γ_t (kg m ⁻³)	δ	ΣAD	π
1.0	23.033	34.587	23.613	427.05	0.004	3.85
5.0	23.033	34.587	23.613	427.20	0.021	3.85
10.0	23.036	34.587	23.612	427.47	0.043	3.85
15.0	23.032	34.589	23.615	427.40	0.064	3.85
20.0	22.850	34.651	23.715	418.11	0.085	3.84
25.0	22.329	34.813	23.986	392.42	0.106	3.82
30.0	22.147	34.869	24.080	383.65	0.125	3.81
35.0	21.926	34.907	24.171	375.17	0.144	3.77
40.0	21.371	34.889	24.311	361.99	0.162	3.61
45.0	20.576	34.736	24.411	352.66	0.180	3.27
50.0	20.046	34.763	24.573	337.43	0.197	3.15
60.0	18.881	34.724	24.844	311.84	0.230	2.82
70.0	17.878	34.725	25.095	288.23	0.260	2.56
80.0	16.625	34.721	25.392	260.18	0.287	2.26
90.0	15.947	34.754	25.575	243.07	0.312	2.13
100.0	15.499	34.819	25.726	228.95	0.336	2.08
125.0	13.556	34.697	26.049	198.65	0.389	1.56
150.0	12.737	34.707	26.223	182.72	0.436	1.40
175.0	12.109	34.705	26.344	171.71	0.481	1.28
200.0	11.643	34.687	26.419	165.09	0.523	1.18
225.0	11.283	34.679	26.480	159.84	0.563	1.10
250.0	10.909	34.650	26.526	155.92	0.603	1.01
275.0	10.534	34.635	26.581	151.12	0.641	0.93
300.0	10.047	34.614	26.649	144.91	0.678	0.83
325.0	9.532	34.586	26.714	139.03	0.713	0.72
350.0	9.151	34.566	26.761	134.86	0.748	0.65
375.0	8.703	34.555	26.823	129.09	0.781	0.57
400.0	8.355	34.534	26.861	125.74	0.813	0.50
450.0	7.775	34.518	26.936	119.05	0.874	0.40
500.0	7.267	34.506	27.000	113.35	0.932	0.31
550.0	6.830	34.496	27.052	108.68	0.988	0.25
600.0	6.461	34.508	27.112	103.40	1.041	0.21
650.0	6.045	34.507	27.165	98.51	1.091	0.15
700.0	5.743	34.508	27.204	95.02	1.140	0.11
750.0	5.480	34.512	27.240	91.88	1.186	0.09
800.0	5.361	34.514	27.256	90.82	1.232	0.07
850.0	5.210	34.516	27.275	89.28	1.277	0.06
900.0	5.021	34.519	27.301	87.13	1.321	0.04
950.0	4.883	34.523	27.319	85.64	1.364	0.02
1000.0	4.673	34.529	27.348	83.03	1.406	0.00
1100.0	4.113	34.549	27.425	75.49	1.486	-0.04
1200.0	3.848	34.562	27.463	72.12	1.559	-0.06
1300.0	3.611	34.573	27.496	69.16	1.630	-0.07
1400.0	3.370	34.585	27.529	66.12	1.698	-0.09
1500.0	3.212	34.595	27.552	64.14	1.763	-0.09
1589.0	2.949	34.606	27.586	60.69	1.818	-0.11

CAST: 28
LAT: 23° 38.3' N.

DATE: 12/31/92 2118 GMT
LON: 108° 41.7' W.

P(dbar)	T(°C)	S(psu)	γ_θ (kg m ⁻³)	δ	$\Sigma\Delta D$	π
1.0	22.378	34.721	23.901	399.52	0.004	3.76
5.0	22.361	34.721	23.906	399.21	0.020	3.76
10.0	22.360	34.721	23.907	399.38	0.040	3.76
15.0	22.357	34.722	23.909	399.40	0.060	3.76
20.0	22.354	34.724	23.911	399.35	0.080	3.76
25.0	22.354	34.726	23.913	399.39	0.100	3.76
30.0	22.350	34.732	23.919	399.01	0.120	3.76
35.0	22.347	34.739	23.925	398.62	0.140	3.76
40.0	22.311	34.745	23.940	397.41	0.160	3.76
45.0	22.254	34.746	23.958	395.98	0.179	3.74
50.0	22.230	34.831	24.029	389.37	0.199	3.80
60.0	21.148	34.771	24.284	365.42	0.237	3.45
70.0	18.999	34.580	24.705	325.52	0.271	2.73
80.0	17.731	34.744	25.146	283.71	0.302	2.54
90.0	16.834	34.776	25.386	261.16	0.329	2.35
100.0	15.858	34.815	25.642	237.04	0.354	2.15
125.0	13.858	34.678	25.972	206.04	0.409	1.61
150.0	13.114	34.710	26.150	189.72	0.458	1.48
175.0	12.684	34.736	26.256	180.21	0.504	1.42
200.0	12.056	34.721	26.368	170.14	0.548	1.28
225.0	11.498	34.688	26.447	163.02	0.589	1.15
250.0	11.061	34.670	26.514	157.14	0.629	1.06
275.0	10.660	34.646	26.567	152.47	0.668	0.96
300.0	10.321	34.633	26.617	148.13	0.706	0.89
325.0	9.729	34.599	26.691	141.29	0.742	0.77
350.0	9.218	34.574	26.756	135.30	0.777	0.66
400.0	8.351	34.531	26.859	125.90	0.842	0.49
450.0	8.020	34.528	26.907	121.98	0.904	0.44
500.0	7.424	34.518	26.987	114.76	0.963	0.35
550.0	6.829	34.507	27.061	107.86	1.018	0.25
600.0	6.475	34.504	27.107	103.85	1.071	0.20
650.0	6.104	34.504	27.155	99.53	1.122	0.16
700.0	5.815	34.507	27.195	96.04	1.171	0.12
750.0	5.614	34.509	27.221	93.90	1.218	0.10
800.0	5.389	34.513	27.252	91.22	1.265	0.07
850.0	5.106	34.514	27.286	88.05	1.310	0.04
900.0	4.882	34.522	27.318	85.17	1.353	0.02
950.0	4.696	34.527	27.343	82.97	1.395	0.01
1000.0	4.486	34.535	27.373	80.23	1.436	-0.01
1100.0	4.196	34.543	27.412	76.92	1.515	-0.04
1200.0	3.879	34.560	27.458	72.65	1.589	-0.06
1300.0	3.643	34.570	27.490	69.81	1.660	-0.07
1400.0	3.428	34.582	27.521	67.05	1.729	-0.08
1500.0	3.108	34.598	27.564	62.65	1.794	-0.10
1600.0	2.852	34.609	27.597	59.32	1.855	-0.11
1671.0	2.671	34.620	27.622	56.77	1.896	-0.11

CAST: 27
LAT: 23° 41.1' N.

DATE: 12/31/92 1818 GMT
LON: 108° 36.5' W.

P(dbar)	T(°C)	S(psu)	γ_t (kg m ⁻³)	δ	$\Sigma\Delta D$	π
1.0	22.607	34.852	23.936	396.24	0.004	3.93
5.0	22.607	34.853	23.937	396.31	0.020	3.93
10.0	22.607	34.852	23.936	396.57	0.040	3.93
15.0	22.601	34.852	23.938	396.59	0.059	3.92
20.0	22.602	34.820	23.914	399.09	0.079	3.90
25.0	22.596	34.828	23.922	398.56	0.099	3.90
30.0	22.578	34.833	23.931	397.85	0.119	3.90
35.0	22.448	34.850	23.981	393.32	0.139	3.88
40.0	22.140	34.917	24.120	380.32	0.158	3.84
45.0	22.097	34.954	24.160	376.70	0.177	3.86
50.0	21.862	34.886	24.174	375.53	0.196	3.74
60.0	20.567	34.659	24.353	358.72	0.233	3.21
70.0	17.452	34.162	24.768	319.34	0.266	2.03
80.0	16.248	34.289	25.148	283.37	0.296	1.84
90.0	16.556	34.827	25.491	251.18	0.323	2.32
100.0	15.488	34.726	25.657	235.55	0.347	2.00
150.0	13.112	34.734	26.169	187.89	0.452	1.50
200.0	11.894	34.694	26.377	169.14	0.541	1.23
250.0	10.935	34.665	26.533	155.27	0.622	1.03
300.0	10.078	34.617	26.646	145.25	0.697	0.84
350.0	9.152	34.574	26.767	134.25	0.767	0.65
400.0	8.231	34.529	26.876	124.19	0.831	0.47
450.0	7.732	34.521	26.944	118.19	0.892	0.39
500.0	7.149	34.511	27.020	111.29	0.949	0.30
550.0	6.874	34.515	27.061	107.89	1.003	0.27
600.0	6.503	34.513	27.110	103.61	1.056	0.21
700.0	5.910	34.513	27.187	96.87	1.156	0.14
750.0	5.556	34.509	27.228	93.10	1.204	0.09
800.0	5.275	34.513	27.265	89.78	1.250	0.06
900.0	4.827	34.527	27.329	84.07	1.337	0.02
1000.0	4.515	34.536	27.371	80.51	1.420	-.01
1100.0	4.104	34.551	27.427	75.22	1.498	-.04
1200.0	3.803	34.565	27.470	71.35	1.571	-.06
1300.0	3.581	34.575	27.500	68.65	1.641	-.07
1400.0	3.358	34.586	27.531	65.85	1.708	-.09
1500.0	3.110	34.599	27.565	62.60	1.772	-.10
1600.0	2.854	34.610	27.597	59.31	1.833	-.11
1700.0	2.643	34.620	27.624	56.59	1.891	-.12
1800.0	2.473	34.629	27.646	54.40	1.946	-.13
1900.0	2.349	34.636	27.663	52.87	2.000	-.14
2000.0	2.216	34.643	27.680	51.16	2.052	-.14
2100.0	2.079	34.651	27.697	49.34	2.102	-.15
2200.0	1.968	34.658	27.712	47.85	2.150	-.15
2300.0	1.905	34.661	27.720	47.24	2.198	-.15
2400.0	1.887	34.661	27.722	47.34	2.245	-.16
2473.0	1.864	34.664	27.727	47.13	2.280	-.16

CAST: 26
LAT: 23° 43.7' N.

DATE: 12/31/92 1500 GMT
LON: 108° 30.9' W.

P(dbar)	T(°C)	S(psu)	γ_{θ} (kg m ⁻³)	δ	$\Sigma \Delta D$	π
1.0	22.463	34.828	23.958	394.07	0.004	3.87
5.0	22.464	34.828	23.958	394.24	0.020	3.87
10.0	22.468	34.829	23.958	394.46	0.039	3.87
20.0	22.472	34.825	23.955	395.21	0.079	3.87
30.0	22.460	34.822	23.956	395.50	0.118	3.86
35.0	22.467	34.819	23.952	396.08	0.138	3.86
40.0	22.451	34.823	23.960	395.55	0.158	3.86
60.0	19.244	34.314	24.439	350.48	0.232	2.59
80.0	17.248	34.809	25.313	267.83	0.294	2.48
100.0	15.779	34.903	25.728	228.84	0.343	2.20
125.0	13.898	34.755	26.024	201.20	0.396	1.68
150.0	12.910	34.725	26.203	184.69	0.445	1.45
175.0	12.212	34.716	26.333	172.81	0.489	1.31
200.0	11.682	34.694	26.417	165.28	0.532	1.19
225.0	11.259	34.680	26.485	159.34	0.572	1.10
250.0	10.694	34.642	26.558	152.78	0.611	0.97
275.0	10.236	34.634	26.632	146.12	0.648	0.88
300.0	9.763	34.600	26.686	141.27	0.684	0.77
350.0	9.352	34.590	26.747	136.31	0.754	0.70
400.0	8.501	34.541	26.844	127.46	0.820	0.52
450.0	7.832	34.526	26.934	119.30	0.881	0.41
500.0	7.215	34.505	27.006	112.71	0.939	0.31
550.0	6.796	34.508	27.066	107.32	0.994	0.25
600.0	6.444	34.505	27.111	103.39	1.047	0.20
650.0	6.186	34.509	27.149	100.23	1.098	0.17
700.0	5.934	34.515	27.186	97.08	1.147	0.14
750.0	5.628	34.518	27.226	93.42	1.195	0.11
800.0	5.382	34.520	27.258	90.65	1.241	0.08
850.0	5.170	34.520	27.284	88.43	1.285	0.05
900.0	4.941	34.524	27.313	85.77	1.329	0.03
1000.0	4.573	34.536	27.365	81.21	1.412	0.00
1100.0	4.140	34.551	27.424	75.64	1.490	-.04
1200.0	3.806	34.567	27.471	71.23	1.564	-.06
1300.0	3.531	34.579	27.509	67.74	1.633	-.07
1400.0	3.308	34.591	27.540	64.92	1.699	-.09
1500.0	3.152	34.598	27.561	63.15	1.763	-.10
1600.0	2.915	34.609	27.591	60.13	1.825	-.11
1700.0	2.731	34.619	27.616	57.74	1.884	-.12
1800.0	2.510	34.630	27.644	54.78	1.940	-.13
1900.0	2.432	34.635	27.655	53.97	1.994	-.13
2000.0	2.249	34.643	27.677	51.60	2.047	-.14
2200.0	2.028	34.656	27.706	48.75	2.147	-.15
2400.0	1.895	34.664	27.724	47.26	2.242	-.15
2600.0	1.858	34.668	27.731	47.23	2.337	-.15
2800.0	1.854	34.669	27.734	47.83	2.432	-.15
2805.0	1.853	34.669	27.734	47.83	2.434	-.15

CAST: 29
LAT: 23° 46.4' N.

DATE: 1/ 1/93 1400 GMT
LON: 108° 25.4' W.

P(dbar)	T(°C)	S(psu)	γ_θ (kg m ⁻³)	δ	$\Sigma \Delta \eta$	π
1.0	22.674	34.868	23.929	396.90	0.004	3.96
5.0	22.622	34.868	23.944	395.63	0.020	3.94
10.0	22.623	34.869	23.944	395.77	0.040	3.94
15.0	22.625	34.869	23.944	396.01	0.059	3.94
20.0	22.624	34.869	23.945	396.18	0.079	3.94
25.0	22.621	34.870	23.947	396.20	0.099	3.94
30.0	22.502	34.876	23.985	392.73	0.119	3.91
35.0	22.241	34.895	24.074	384.48	0.138	3.85
40.0	22.049	34.918	24.146	377.82	0.157	3.82
45.0	21.326	34.796	24.253	367.72	0.176	3.52
50.0	20.697	34.762	24.399	354.03	0.194	3.32
60.0	19.650	34.816	24.717	324.05	0.228	3.09
70.0	18.131	34.805	25.095	288.31	0.259	2.69
80.0	17.269	34.770	25.278	271.15	0.287	2.45
90.0	16.483	34.895	25.559	244.63	0.312	2.36
100.0	16.233	34.942	25.654	235.97	0.336	2.34
125.0	14.031	34.795	26.027	200.94	0.391	1.74
150.0	12.980	34.727	26.190	185.86	0.439	1.47
175.0	12.436	34.708	26.283	177.58	0.484	1.34
200.0	11.924	34.717	26.389	168.04	0.527	1.25
225.0	11.382	34.684	26.465	161.24	0.568	1.13
250.0	10.944	34.653	26.521	156.35	0.608	1.02
275.0	10.613	34.646	26.575	151.66	0.646	0.96
300.0	10.221	34.621	26.625	147.32	0.684	0.87
325.0	9.924	34.609	26.666	143.78	0.720	0.81
350.0	9.426	34.584	26.730	137.91	0.756	0.70
400.0	8.618	34.546	26.830	128.90	0.822	0.55
450.0	8.007	34.521	26.904	122.31	0.885	0.43
500.0	7.415	34.512	26.983	115.07	0.944	0.34
550.0	6.976	34.509	27.043	109.77	1.000	0.28
600.0	6.534	34.506	27.100	104.55	1.054	0.21
650.0	6.155	34.506	27.151	100.02	1.105	0.16
700.0	5.840	34.506	27.191	96.46	1.154	0.12
750.0	5.563	34.510	27.228	93.12	1.201	0.09
800.0	5.363	34.511	27.253	91.03	1.247	0.07
900.0	5.052	34.521	27.298	87.43	1.336	0.04
1000.0	4.489	34.535	27.373	80.23	1.421	-0.01
1100.0	4.137	34.548	27.421	75.85	1.499	-0.04
1200.0	3.846	34.561	27.462	72.17	1.572	-0.06
1300.0	3.616	34.572	27.495	69.30	1.643	-0.07
1400.0	3.464	34.580	27.516	67.64	1.712	-0.08
1500.0	3.094	34.597	27.565	62.52	1.777	-0.10
1600.0	2.903	34.606	27.590	60.16	1.838	-0.11
1700.0	2.738	34.615	27.612	58.12	1.897	-0.12
1800.0	2.541	34.625	27.637	55.52	1.955	-0.13
1819.0	2.504	34.626	27.641	55.09	1.965	-0.13

CAST: 30
LAT: 23° 49.1' N.

DATE: 1/ 1/93 1606 GMT
LON: 108° 19.7' W.

P(dbar)	T(°C)	S(psu)	$\gamma_\theta(\text{kg m}^{-3})$	δ	$\Sigma\Delta D$	π
1.0	22.824	34.836	23.861	403.31	0.004	3.98
5.0	22.824	34.836	23.862	403.45	0.020	3.98
10.0	22.825	34.838	23.863	403.54	0.040	3.98
15.0	22.827	34.838	23.863	403.76	0.061	3.98
20.0	22.827	34.839	23.864	403.89	0.081	3.98
25.0	22.829	34.840	23.864	404.04	0.101	3.98
30.0	22.829	34.845	23.868	403.88	0.121	3.98
35.0	22.645	34.881	23.949	396.42	0.141	3.96
40.0	22.156	34.887	24.092	382.95	0.161	3.82
45.0	21.403	34.871	24.289	364.30	0.179	3.60
50.0	21.176	34.905	24.378	356.04	0.197	3.56
60.0	19.046	34.545	24.666	328.84	0.232	2.72
70.0	16.987	34.415	25.072	290.34	0.263	2.11
80.0	16.088	34.514	25.357	263.45	0.291	1.97
90.0	15.558	34.698	25.619	238.86	0.316	2.00
100.0	14.777	34.659	25.761	225.49	0.339	1.79
125.0	13.766	34.681	25.994	203.99	0.392	1.59
150.0	12.697	34.673	26.204	184.46	0.441	1.37
175.0	12.179	34.694	26.322	173.82	0.485	1.28
200.0	11.709	34.672	26.395	167.42	0.528	1.18
225.0	11.192	34.669	26.488	158.96	0.569	1.08
250.0	10.808	34.647	26.541	154.38	0.608	0.99
275.0	10.474	34.619	26.579	151.27	0.646	0.91
300.0	10.046	34.587	26.628	146.92	0.683	0.81
325.0	9.955	34.610	26.662	144.23	0.720	0.81
350.0	9.606	34.590	26.705	140.41	0.755	0.74
375.0	9.068	34.564	26.773	134.16	0.790	0.63
400.0	8.620	34.536	26.822	129.66	0.823	0.54
425.0	8.377	34.539	26.862	126.15	0.855	0.50
450.0	8.033	34.526	26.904	122.30	0.886	0.44
475.0	7.722	34.518	26.944	118.71	0.916	0.39
500.0	7.540	34.521	26.973	116.22	0.945	0.36
550.0	6.895	34.509	27.054	108.64	1.001	0.26
600.0	6.493	34.509	27.108	103.77	1.054	0.21
650.0	6.215	34.512	27.148	100.39	1.105	0.18
700.0	5.891	34.511	27.188	96.80	1.155	0.13
750.0	5.610	34.511	27.223	93.70	1.202	0.10
800.0	5.497	34.512	27.238	92.74	1.249	0.09
850.0	5.299	34.514	27.264	90.58	1.295	0.06
900.0	5.173	34.516	27.280	89.35	1.340	0.05
915.0	5.081	34.517	27.292	88.25	1.353	0.04

CAST: 31
LAT: 23° 51.7' N.

DATE: 1/ 1/93 1736 GMT
LON: 108° 14.2' W.

P(dbar)	T(°C)	S(psu)	$\gamma_0(\text{kg m}^{-3})$	δ	$\Sigma\Delta D$	π
1.0	22.857	34.827	23.845	404.86	0.004	3.98
5.0	22.857	34.827	23.845	405.01	0.020	3.98
10.0	22.859	34.827	23.845	405.23	0.041	3.98
15.0	22.861	34.829	23.846	405.34	0.061	3.98
20.0	22.860	34.829	23.847	405.51	0.081	3.98
25.0	22.861	34.830	23.848	405.64	0.101	3.98
30.0	22.861	34.830	23.848	405.83	0.122	3.98
35.0	22.858	34.830	23.849	405.93	0.142	3.98
40.0	22.565	34.836	23.937	397.71	0.162	3.90
45.0	21.759	34.862	24.184	374.35	0.181	3.69
50.0	21.446	34.891	24.293	364.18	0.200	3.62
60.0	19.048	34.625	24.726	323.15	0.234	2.78
70.0	15.836	34.147	25.132	284.45	0.264	1.63
80.0	15.041	34.214	25.361	262.95	0.292	1.50
90.0	14.941	34.530	25.627	238.00	0.317	1.72
100.0	14.069	34.500	25.790	222.61	0.340	1.51
125.0	13.332	34.559	25.988	204.39	0.393	1.40
150.0	12.780	34.625	26.151	189.52	0.442	1.34
175.0	12.346	34.698	26.293	176.63	0.487	1.31
200.0	11.754	34.664	26.380	168.79	0.530	1.17
225.0	11.488	34.694	26.454	162.40	0.572	1.15
250.0	11.211	34.673	26.489	159.54	0.612	1.08
275.0	10.899	34.658	26.534	155.75	0.651	1.01
300.0	10.399	34.626	26.598	149.97	0.690	0.90
325.0	10.031	34.616	26.654	145.05	0.727	0.83
350.0	9.567	34.589	26.711	139.88	0.762	0.73
375.0	9.159	34.568	26.761	135.32	0.797	0.64
400.0	8.860	34.554	26.798	132.08	0.830	0.58
425.0	8.487	34.542	26.847	127.61	0.863	0.52
450.0	8.198	34.530	26.882	124.53	0.894	0.46
475.0	7.858	34.527	26.931	120.06	0.925	0.41
500.0	7.609	34.517	26.960	117.50	0.954	0.37
525.0	7.104	34.512	27.027	110.99	0.983	0.29
550.0	6.789	34.506	27.066	107.34	1.010	0.24
557.0	6.779	34.507	27.068	107.26	1.018	0.24

CAST: 32
LAT: 23° 54.4' N.

DATE: 1/ 1/93 1853 GMT
LON: 108° 8.7' W.

P(dbar)	T(°C)	S(psu)	$\gamma_\theta(\text{kg m}^{-3})$	δ	$\Sigma\Delta D$	π
1.0	22.961	34.803	23.797	409.45	0.004	3.99
5.0	22.961	34.803	23.797	409.59	0.020	3.99
10.0	22.959	34.805	23.800	409.59	0.041	3.99
15.0	22.947	34.807	23.805	409.29	0.061	3.99
20.0	22.943	34.811	23.809	409.09	0.082	3.99
25.0	22.927	34.815	23.817	408.53	0.102	3.99
30.0	22.675	34.820	23.894	401.44	0.123	3.92
35.0	21.829	34.825	24.136	378.53	0.142	3.68
40.0	19.964	34.684	24.533	340.80	0.160	3.07
45.0	18.635	34.611	24.819	313.64	0.176	2.67
50.0	18.582	34.656	24.867	309.27	0.192	2.69
60.0	18.060	34.639	24.984	298.44	0.222	2.54
70.0	17.238	34.650	25.193	278.87	0.251	2.35
80.0	16.709	34.653	25.321	266.99	0.278	2.23
90.0	16.369	34.674	25.416	258.20	0.305	2.16
100.0	15.673	34.640	25.549	245.77	0.330	1.98
125.0	14.478	34.699	25.858	217.06	0.387	1.76
150.0	13.483	34.733	26.093	195.20	0.438	1.57
175.0	12.601	34.725	26.264	179.44	0.484	1.39
200.0	12.059	34.715	26.362	170.66	0.528	1.28
225.0	11.710	34.709	26.424	165.31	0.570	1.21
250.0	11.361	34.698	26.481	160.42	0.611	1.13
275.0	11.023	34.680	26.529	156.30	0.650	1.06
300.0	10.547	34.646	26.588	151.04	0.689	0.94
325.0	10.097	34.616	26.642	146.16	0.726	0.84
350.0	9.701	34.587	26.687	142.23	0.762	0.75
375.0	9.288	34.580	26.750	136.50	0.797	0.68
400.0	8.995	34.576	26.794	132.60	0.831	0.63
425.0	8.615	34.556	26.839	128.56	0.863	0.55
450.0	8.210	34.533	26.883	124.49	0.895	0.47
475.0	7.976	34.535	26.920	121.23	0.926	0.44
500.0	7.592	34.518	26.963	117.21	0.955	0.37
550.0	7.073	34.507	27.028	111.30	1.012	0.29
600.0	6.672	34.503	27.080	106.65	1.067	0.23
650.0	6.326	34.508	27.130	102.24	1.119	0.19
700.0	6.055	34.506	27.163	99.37	1.169	0.15
735.0	5.861	34.507	27.189	97.13	1.203	0.13

CAST: 33
LAT: 23° 57.1' N.

DATE: 1/ 1/93 2011 GMT
LON: 108° 3.2' W.

P(dbar)	T(°C)	S(psu)	$\gamma_0(\text{kg m}^{-3})$	δ	$\Sigma\Delta D$	π
1.0	22.963	34.789	23.786	410.51	0.004	3.98
5.0	22.963	34.789	23.786	410.66	0.021	3.98
10.0	22.957	34.788	23.788	410.73	0.041	3.97
15.0	22.953	34.789	23.790	410.76	0.062	3.97
20.0	22.951	34.790	23.791	410.82	0.082	3.97
25.0	22.949	34.791	23.793	410.87	0.103	3.97
30.0	22.946	34.793	23.796	410.81	0.123	3.97
35.0	21.699	34.834	24.179	374.43	0.143	3.65
40.0	19.632	34.683	24.619	332.56	0.161	2.97
45.0	19.195	34.628	24.690	325.96	0.177	2.82
50.0	18.718	34.594	24.786	317.00	0.193	2.67
60.0	17.998	34.678	25.029	294.14	0.224	2.55
70.0	17.185	34.689	25.235	274.84	0.253	2.36
80.0	16.420	34.620	25.363	262.96	0.280	2.13
90.0	15.423	34.696	25.648	236.07	0.304	1.96
100.0	14.897	34.719	25.782	223.53	0.327	1.86
125.0	13.665	34.718	26.043	199.27	0.380	1.60
150.0	13.145	34.712	26.145	190.18	0.428	1.48
175.0	12.781	34.723	26.227	183.01	0.475	1.42
200.0	12.412	34.725	26.302	176.48	0.520	1.35
225.0	11.744	34.690	26.403	167.32	0.563	1.19
250.0	11.397	34.693	26.470	161.43	0.604	1.13
275.0	11.080	34.682	26.520	157.16	0.644	1.06
300.0	10.636	34.654	26.578	152.03	0.683	0.96
325.0	10.333	34.639	26.620	148.46	0.721	0.90
350.0	9.895	34.615	26.677	143.34	0.757	0.80
375.0	9.451	34.591	26.732	138.33	0.792	0.71
400.0	8.970	34.567	26.791	132.86	0.826	0.61
425.0	8.671	34.557	26.831	129.36	0.859	0.56
450.0	8.402	34.549	26.867	126.20	0.891	0.51
475.0	7.960	34.533	26.921	121.14	0.922	0.43
500.0	7.702	34.528	26.955	118.05	0.952	0.39
525.0	7.474	34.525	26.985	115.36	0.981	0.35
550.0	7.180	34.512	27.017	112.46	1.009	0.30
575.0	7.028	34.510	27.037	110.81	1.037	0.28
600.0	6.760	34.507	27.071	107.59	1.065	0.24
625.0	6.573	34.507	27.096	105.37	1.091	0.21
650.0	6.414	34.507	27.118	103.49	1.117	0.19
659.0	6.358	34.506	27.124	102.94	1.127	0.18

CAST: 34
LAT: 23° 59.8' N.

DATE: 1/ 1/93 2123 GMT
LON: 107° 57.7' W.

P(dbar)	T(°C)	S(psu)	$\gamma_0(\text{kg m}^{-3})$	δ	$\Sigma\Delta D$	π
1.0	22.997	34.767	23.759	413.04	0.004	3.98
5.0	22.997	34.767	23.760	413.19	0.021	3.97
10.0	22.998	34.767	23.760	413.40	0.041	3.97
15.0	22.983	34.765	23.763	413.32	0.062	3.97
20.0	22.973	34.765	23.766	413.21	0.083	3.97
25.0	22.961	34.766	23.770	413.01	0.103	3.96
30.0	22.943	34.766	23.776	412.67	0.124	3.96
35.0	22.892	34.789	23.808	409.83	0.145	3.96
40.0	21.344	34.722	24.192	373.37	0.164	3.47
45.0	20.245	34.714	24.482	345.83	0.182	3.16
50.0	19.716	34.676	24.593	335.49	0.199	3.00
60.0	17.806	34.618	25.031	293.98	0.230	2.47
70.0	16.937	34.629	25.248	273.57	0.259	2.26
80.0	15.901	34.621	25.483	251.49	0.285	2.01
90.0	15.492	34.656	25.602	240.42	0.310	1.95
100.0	15.128	34.677	25.699	231.49	0.333	1.88
125.0	13.801	34.721	26.017	201.75	0.388	1.63
150.0	13.112	34.732	26.167	188.08	0.437	1.50
175.0	12.559	34.725	26.272	178.65	0.482	1.38
200.0	12.183	34.718	26.341	172.74	0.526	1.30
225.0	11.678	34.700	26.423	165.39	0.568	1.19
250.0	11.472	34.700	26.462	162.22	0.609	1.15
275.0	10.982	34.679	26.535	155.66	0.649	1.05
300.0	10.642	34.659	26.581	151.72	0.687	0.97
325.0	10.278	34.640	26.630	147.45	0.724	0.89
350.0	9.856	34.611	26.680	142.98	0.761	0.80
375.0	9.530	34.597	26.724	139.18	0.796	0.73
400.0	9.417	34.594	26.741	138.02	0.831	0.71
425.0	9.010	34.574	26.791	133.45	0.865	0.63
429.0	8.965	34.572	26.796	132.96	0.870	0.62

CAST: 35
LAT: 24° 2.4' N.

DATE: 1/ 1/93 2230 GMT
LON: 107° 52.2' W.

P(dbar)	T(°C)	S(psu)	$\gamma_\theta(\text{kg m}^{-3})$	δ	ΣAD	π
1.0	23.012	34.762	23.751	413.81	0.004	3.97
5.0	23.011	34.762	23.752	413.93	0.021	3.97
10.0	23.011	34.762	23.752	414.12	0.041	3.97
15.0	23.010	34.763	23.753	414.20	0.062	3.97
20.0	23.003	34.765	23.757	414.07	0.083	3.97
25.0	22.998	34.768	23.761	413.88	0.104	3.97
30.0	22.992	34.769	23.764	413.80	0.124	3.97
35.0	22.958	34.780	23.782	412.29	0.145	3.97
40.0	21.592	34.830	24.205	372.10	0.165	3.62
45.0	20.740	34.771	24.394	354.32	0.183	3.34
50.0	20.099	34.733	24.536	340.93	0.200	3.14
60.0	17.955	34.668	25.032	293.92	0.232	2.54
70.0	16.370	34.645	25.393	259.76	0.259	2.14
80.0	15.383	34.696	25.657	234.88	0.284	1.95
90.0	15.107	34.719	25.735	227.69	0.307	1.91
100.0	14.824	34.716	25.796	222.24	0.330	1.84
125.0	13.383	34.714	26.098	194.01	0.382	1.53
150.0	12.868	34.712	26.201	184.81	0.429	1.43
169.0	12.439	34.714	26.287	177.05	0.464	1.35

CAST: 36
LAT: 24° 5.1' N.

DATE: 1/ 1/93 2323 GMT
LON: 107° 46.7' W.

P(dbar)	T(°C)	S(psu)	γ_θ (kg m ⁻³)	δ	ΣAD	π
1.0	22.814	34.863	23.885	401.08	0.004	4.00
5.0	22.812	34.863	23.886	401.17	0.020	3.99
10.0	22.814	34.862	23.885	401.45	0.040	3.99
15.0	22.812	34.863	23.886	401.54	0.060	3.99
20.0	22.799	34.862	23.889	401.45	0.080	3.99
25.0	22.774	34.863	23.898	400.87	0.100	3.98
30.0	22.674	34.880	23.940	397.07	0.120	3.97
35.0	22.120	34.914	24.122	379.85	0.140	3.83
40.0	21.395	34.836	24.264	366.49	0.159	3.57
45.0	20.538	34.713	24.404	353.36	0.176	3.24
50.0	20.006	34.631	24.482	346.03	0.194	3.04
60.0	16.829	34.605	25.255	272.61	0.224	2.22
70.0	15.986	34.659	25.492	250.27	0.250	2.06
79.0	15.752	34.679	25.561	244.04	0.273	2.03

CAST: 37
LAT: 23° 11.9' N.

DATE: 1/ 4/93 1141 GMT
LON: 108° 25.1' W.

P(dbar)	T(°C)	S(psu)	γ_θ (kg m ⁻³)	δ	$\Sigma\Delta D$	π
1.0	22.214	34.710	23.939	395.91	0.004	3.71
5.0	22.213	34.711	23.940	395.95	0.020	3.71
10.0	22.203	34.749	23.972	393.13	0.040	3.73
15.0	22.178	34.758	23.986	391.97	0.059	3.73
20.0	22.043	34.767	24.031	387.90	0.079	3.70
25.0	22.007	34.779	24.051	386.24	0.098	3.70
30.0	21.921	34.806	24.095	382.18	0.117	3.70
35.0	21.567	34.856	24.232	369.35	0.136	3.63
40.0	21.474	34.865	24.265	366.40	0.154	3.62
45.0	20.854	34.800	24.385	355.16	0.173	3.40
50.0	19.917	34.729	24.580	336.68	0.190	3.09
60.0	18.464	34.658	24.899	306.60	0.222	2.66
70.0	17.605	34.680	25.128	285.13	0.251	2.46
80.0	16.508	34.677	25.386	260.79	0.279	2.20
90.0	15.789	34.774	25.626	238.22	0.304	2.11
100.0	15.046	34.758	25.779	223.84	0.327	1.93
150.0	12.810	34.710	26.211	183.85	0.428	1.42
200.0	11.720	34.673	26.393	167.55	0.516	1.18
250.0	10.806	34.650	26.544	154.12	0.596	0.99
300.0	10.000	34.611	26.655	144.36	0.671	0.82
350.0	9.200	34.570	26.756	135.36	0.741	0.66
400.0	8.402	34.534	26.854	126.46	0.806	0.50
450.0	7.872	34.519	26.922	120.41	0.868	0.41
500.0	7.347	34.507	26.989	114.42	0.926	0.33
550.0	6.899	34.508	27.052	108.77	0.982	0.26
600.0	6.415	34.509	27.119	102.66	1.035	0.20
650.0	5.964	34.506	27.174	97.50	1.085	0.14
700.0	5.674	34.507	27.211	94.22	1.133	0.10
800.0	5.023	34.512	27.293	86.63	1.223	0.03
900.0	4.605	34.528	27.354	81.24	1.307	0.00
1000.0	4.266	34.542	27.403	76.95	1.386	-.03
1100.0	3.928	34.558	27.451	72.52	1.461	-.05
1200.0	3.686	34.568	27.484	69.67	1.532	-.07
1300.0	3.456	34.580	27.517	66.76	1.600	-.08
1400.0	3.237	34.591	27.547	64.01	1.666	-.09
1500.0	3.050	34.601	27.572	61.73	1.728	-.10
1600.0	2.831	34.611	27.600	58.96	1.789	-.12
1700.0	2.664	34.620	27.622	56.85	1.847	-.12
1800.0	2.528	34.626	27.640	55.25	1.903	-.13
1900.0	2.399	34.634	27.657	53.63	1.957	-.14
2000.0	2.284	34.639	27.671	52.32	2.010	-.14
2200.0	2.028	34.654	27.704	48.90	2.111	-.15
2400.0	1.886	34.663	27.724	47.23	2.207	-.15
2600.0	1.842	34.667	27.731	47.09	2.301	-.16
2800.0	1.808	34.669	27.737	47.20	2.395	-.16
2981.0	1.792	34.671	27.741	47.46	2.481	-.16

CAST: 38
LAT: 23° 20.5' N.

DATE: 1/ 4/93 1441 GMT
LON: 108° 32.5' W.

P(dbar)	T(°C)	S(psu)	γ_0 (kg m ⁻³)	δ	$\Sigma \Delta D$	π
1.0	22.351	34.799	23.968	393.15	0.004	3.81
5.0	22.351	34.799	23.968	393.29	0.020	3.81
10.0	22.346	34.800	23.970	393.28	0.039	3.81
15.0	22.347	34.801	23.971	393.41	0.059	3.81
20.0	22.336	34.802	23.976	393.22	0.079	3.81
25.0	22.270	34.806	23.997	391.33	0.098	3.79
30.0	22.024	34.794	24.058	385.75	0.118	3.71
35.0	21.551	34.859	24.239	368.71	0.137	3.63
40.0	21.203	34.865	24.339	359.31	0.155	3.54
45.0	20.591	34.751	24.418	351.95	0.173	3.28
50.0	19.894	34.633	24.514	343.03	0.190	3.00
60.0	19.180	34.651	24.712	324.42	0.223	2.83
70.0	18.293	34.679	24.958	301.31	0.255	2.63
80.0	16.866	34.716	25.332	265.97	0.283	2.31
90.0	16.308	34.797	25.525	247.89	0.309	2.24
100.0	15.639	34.798	25.679	233.49	0.333	2.09
150.0	13.117	34.763	26.191	185.89	0.435	1.52
200.0	11.622	34.698	26.431	163.90	0.522	1.18
250.0	10.649	34.648	26.570	151.55	0.601	0.96
300.0	9.804	34.600	26.679	141.92	0.674	0.78
350.0	8.991	34.559	26.781	132.80	0.743	0.61
400.0	8.351	34.538	26.865	125.38	0.807	0.49
450.0	7.684	34.519	26.949	117.67	0.868	0.38
500.0	7.205	34.512	27.013	112.05	0.925	0.30
550.0	6.757	34.504	27.068	107.07	0.980	0.24
600.0	6.302	34.504	27.129	101.52	1.032	0.18
650.0	5.938	34.505	27.177	97.23	1.082	0.13
700.0	5.559	34.504	27.223	92.95	1.129	0.08
750.0	5.307	34.508	27.257	89.99	1.175	0.06
800.0	5.107	34.508	27.281	87.99	1.219	0.03
900.0	4.724	34.521	27.335	83.25	1.305	0.00
1000.0	4.306	34.538	27.395	77.77	1.385	-0.02
1100.0	4.029	34.549	27.433	74.46	1.461	-0.04
1200.0	3.731	34.563	27.475	70.58	1.533	-0.06
1300.0	3.445	34.578	27.516	66.77	1.602	-0.08
1400.0	3.227	34.589	27.545	64.08	1.667	-0.09
1500.0	3.022	34.599	27.573	61.50	1.730	-0.10
1600.0	2.798	34.610	27.602	58.64	1.790	-0.11
1700.0	2.634	34.619	27.624	56.56	1.847	-0.12
1800.0	2.546	34.623	27.635	55.74	1.903	-0.13
1900.0	2.444	34.628	27.649	54.59	1.958	-0.13
2000.0	2.336	34.634	27.663	53.34	2.012	-0.14
2100.0	2.149	34.644	27.687	50.69	2.065	-0.14
2200.0	2.011	34.652	27.704	48.80	2.115	-0.15
2300.0	1.951	34.658	27.714	48.03	2.163	-0.15
2335.0	1.919	34.660	27.718	47.61	2.180	-0.15

CAST: 39
LAT: 23° 27.4' N.

DATE: 1/ 4/93 1723 GMT
LON: 108° 40.9' W.

P(dbar)	T(°C)	S(psu)	$\gamma_t(\text{kg m}^{-3})$	δ	$\Sigma\Delta D$	π
1.0	22.703	34.666	23.767	412.31	0.004	3.81
5.0	22.703	34.666	23.767	412.46	0.021	3.81
10.0	22.701	34.666	23.768	412.59	0.041	3.81
15.0	22.697	34.666	23.770	412.66	0.062	3.81
20.0	22.690	34.670	23.775	412.33	0.082	3.81
25.0	22.669	34.676	23.786	411.54	0.103	3.81
30.0	22.610	34.694	23.816	408.83	0.124	3.81
35.0	22.511	34.738	23.878	403.13	0.144	3.81
40.0	21.890	34.832	24.124	379.85	0.164	3.71
45.0	20.566	34.642	24.342	359.22	0.182	3.20
50.0	19.699	34.536	24.490	345.24	0.200	2.88
60.0	19.094	34.661	24.742	321.61	0.233	2.82
70.0	17.727	34.676	25.095	288.24	0.264	2.49
80.0	17.274	34.787	25.290	270.01	0.292	2.46
90.0	16.443	34.840	25.527	247.72	0.317	2.31
100.0	15.298	34.817	25.770	224.82	0.341	2.03
125.0	14.122	34.749	25.972	206.14	0.395	1.72
150.0	13.318	34.721	26.118	192.85	0.445	1.53
175.0	12.610	34.716	26.256	180.27	0.491	1.38
200.0	11.941	34.702	26.375	169.42	0.535	1.24
250.0	11.085	34.668	26.508	157.72	0.616	1.06
300.0	10.243	34.623	26.622	147.58	0.692	0.87
325.0	9.700	34.593	26.691	141.26	0.729	0.76
350.0	9.330	34.574	26.738	137.11	0.763	0.68
400.0	8.323	34.536	26.868	125.07	0.829	0.49
450.0	7.795	34.519	26.933	119.31	0.890	0.40
500.0	7.197	34.506	27.010	112.34	0.948	0.30
550.0	6.653	34.505	27.084	105.52	1.003	0.23
600.0	6.247	34.500	27.133	101.04	1.054	0.17
650.0	5.973	34.499	27.168	98.14	1.104	0.14
700.0	5.701	34.502	27.204	94.95	1.152	0.10
750.0	5.407	34.504	27.242	91.57	1.199	0.07
800.0	5.195	34.508	27.270	89.12	1.244	0.05
850.0	4.967	34.513	27.301	86.34	1.288	0.03
900.0	4.828	34.520	27.323	84.60	1.331	0.02
950.0	4.592	34.525	27.353	81.81	1.372	-.01
1000.0	4.453	34.533	27.375	79.96	1.413	-.02
1100.0	4.075	34.546	27.426	75.24	1.490	-.05
1200.0	3.842	34.558	27.460	72.34	1.563	-.06
1300.0	3.613	34.570	27.493	69.41	1.634	-.07
1400.0	3.398	34.580	27.523	66.78	1.703	-.09
1500.0	3.007	34.600	27.575	61.28	1.767	-.11
1600.0	2.725	34.613	27.611	57.50	1.826	-.12
1700.0	2.522	34.622	27.636	54.95	1.882	-.13
1800.0	2.416	34.628	27.651	53.74	1.936	-.14
1883.0	2.316	34.633	27.663	52.60	1.980	-.14

CAST: 52
LAT: 23° 35.1' N.

DATE: 1/ 7/93
LON: 108° 47.0' W.

0936 GMT

P(dbar)	T(°C)	S(psu)	$\gamma_{\theta}(\text{kg m}^{-3})$	δ	$\Sigma\Delta D$	π
1.0	22.580	34.721	23.844	404.99	0.004	3.82
5.0	22.580	34.720	23.843	405.21	0.020	3.82
10.0	22.580	34.723	23.846	405.14	0.041	3.82
15.0	22.583	34.727	23.848	405.15	0.061	3.82
20.0	22.513	34.741	23.879	402.38	0.081	3.81
25.0	22.309	34.779	23.966	394.34	0.101	3.79
30.0	22.277	34.795	23.988	392.47	0.121	3.79
35.0	21.909	34.833	24.120	380.08	0.140	3.71
40.0	21.155	34.847	24.338	359.40	0.158	3.51
45.0	19.882	34.730	24.590	335.54	0.176	3.08
50.0	19.092	34.712	24.781	317.51	0.192	2.86
60.0	17.813	34.687	25.082	289.13	0.222	2.52
70.0	17.147	34.625	25.196	278.60	0.251	2.31
80.0	16.178	34.648	25.440	255.60	0.277	2.10
90.0	15.345	34.678	25.652	235.68	0.302	1.93
100.0	14.623	34.695	25.823	219.62	0.325	1.79
125.0	13.488	34.724	26.084	195.33	0.377	1.57
150.0	12.654	34.707	26.239	181.15	0.424	1.39
175.0	12.028	34.686	26.345	171.62	0.468	1.25
200.0	11.607	34.691	26.429	164.15	0.510	1.17
225.0	11.190	34.657	26.479	159.81	0.550	1.07
250.0	10.964	34.661	26.524	156.07	0.590	1.03
275.0	10.636	34.653	26.577	151.55	0.628	0.97
300.0	10.223	34.628	26.630	146.84	0.665	0.87
325.0	9.747	34.603	26.691	141.30	0.701	0.77
350.0	9.483	34.589	26.725	138.51	0.736	0.72
375.0	9.047	34.561	26.774	134.05	0.770	0.62
400.0	8.610	34.543	26.829	128.95	0.803	0.54
425.0	8.219	34.527	26.876	124.63	0.835	0.47
450.0	7.848	34.520	26.926	120.01	0.865	0.41
500.0	7.360	34.506	26.986	114.72	0.924	0.33
550.0	6.896	34.498	27.045	109.43	0.980	0.26
600.0	6.655	34.498	27.078	106.79	1.034	0.22
650.0	6.331	34.505	27.127	102.49	1.086	0.19
700.0	5.960	34.499	27.170	98.58	1.137	0.13
750.0	5.663	34.505	27.212	94.81	1.185	0.10
800.0	5.296	34.499	27.252	91.04	1.231	0.05
850.0	5.082	34.506	27.283	88.33	1.276	0.03
900.0	4.768	34.514	27.325	84.32	1.319	0.00
950.0	4.596	34.522	27.350	82.08	1.361	-.01
1000.0	4.466	34.528	27.370	80.50	1.401	-.02
1100.0	4.162	34.541	27.413	76.68	1.479	-.04
1200.0	3.851	34.557	27.459	72.49	1.554	-.06
1300.0	3.679	34.565	27.483	70.63	1.625	-.07
1400.0	3.433	34.577	27.517	67.43	1.694	-.09
1467.0	3.224	34.588	27.546	64.57	1.738	-.10

CAST: 53 DATE: 1/ 7/93 1148 GMT
LAT: 23° 43.0' N. LON: 108° 55.9' W.

P(dbar)	T(°C)	S(psu)	γ_θ (kg m ⁻³)	δ	$\Sigma\Delta D$	π
1.0	22.681	34.671	23.777	411.35	0.004	3.81
5.0	22.681	34.671	23.777	411.50	0.021	3.81
10.0	22.684	34.672	23.778	411.65	0.041	3.81
15.0	22.682	34.674	23.780	411.67	0.062	3.81
20.0	22.624	34.673	23.796	410.32	0.082	3.79
25.0	22.616	34.700	23.819	408.36	0.103	3.81
30.0	22.709	34.769	23.845	406.09	0.123	3.89
35.0	22.758	34.818	23.869	404.06	0.143	3.94
40.0	22.246	34.818	24.014	390.34	0.163	3.79
45.0	21.379	34.880	24.303	363.02	0.182	3.60
50.0	19.855	34.595	24.495	344.81	0.200	2.97
60.0	18.978	34.667	24.776	318.35	0.233	2.79
70.0	18.157	34.745	25.042	293.33	0.264	2.64
80.0	15.614	34.358	25.345	264.54	0.292	1.74
90.0	15.744	34.706	25.584	242.19	0.317	2.04
100.0	15.351	34.813	25.754	226.28	0.341	2.03
150.0	12.701	34.713	26.235	181.56	0.441	1.40
200.0	11.775	34.694	26.400	166.97	0.527	1.20
250.0	11.053	34.666	26.512	157.27	0.608	1.05
300.0	10.317	34.625	26.612	148.65	0.685	0.88
350.0	9.627	34.587	26.699	141.01	0.757	0.73
400.0	8.844	34.545	26.794	132.47	0.825	0.58
450.0	8.122	34.526	26.890	123.67	0.890	0.45
500.0	7.628	34.514	26.954	118.04	0.950	0.37
550.0	7.189	34.503	27.009	113.25	1.008	0.29
600.0	6.740	34.501	27.069	107.74	1.063	0.23
650.0	6.404	34.502	27.115	103.71	1.116	0.19
700.0	5.963	34.498	27.169	98.73	1.167	0.13
800.0	5.386	34.502	27.243	92.03	1.262	0.06
850.0	5.218	34.510	27.270	89.79	1.308	0.05
900.0	5.012	34.517	27.300	87.21	1.352	0.03
1000.0	4.517	34.529	27.365	81.03	1.436	-.01
1100.0	4.147	34.542	27.416	76.39	1.515	-.04
1200.0	3.845	34.557	27.459	72.45	1.589	-.06
1300.0	3.627	34.569	27.491	69.66	1.660	-.07
1400.0	3.359	34.581	27.527	66.28	1.728	-.09
1500.0	3.138	34.592	27.557	63.46	1.793	-.10
1600.0	2.942	34.602	27.583	60.97	1.855	-.11
1700.0	2.751	34.611	27.608	58.57	1.915	-.12
1800.0	2.597	34.619	27.628	56.65	1.972	-.13
1900.0	2.450	34.626	27.646	54.85	2.028	-.13
2000.0	2.367	34.630	27.657	54.02	2.083	-.14
2200.0	2.055	34.647	27.697	49.75	2.186	-.15
2400.0	1.920	34.656	27.716	48.14	2.284	-.15
2600.0	1.871	34.660	27.724	47.95	2.380	-.15
2633.0	1.862	34.661	27.725	47.91	2.396	-.15

CAST: 54 DATE: 1/ 7/93 1436 GMT
LAT: 23° 49.9' N. LON: 109° 3.0' W.

P(dbar)	T(°C)	S(psu)	γ_{θ} (kg m ⁻³)	δ	ΣAD	π
1.0	22.540	34.824	23.933	396.45	0.004	3.89
5.0	22.540	34.824	23.934	396.59	0.020	3.89
10.0	22.544	34.824	23.933	396.90	0.040	3.89
15.0	22.546	34.824	23.932	397.12	0.060	3.89
20.0	22.544	34.824	23.933	397.25	0.079	3.89
25.0	22.515	34.825	23.943	396.58	0.099	3.88
30.0	22.420	34.827	23.972	394.02	0.119	3.85
35.0	22.312	34.826	24.001	391.38	0.139	3.82
40.0	21.977	34.825	24.095	382.63	0.158	3.73
45.0	20.648	34.725	24.383	355.30	0.176	3.28
50.0	19.459	34.683	24.665	328.59	0.194	2.93
60.0	18.274	34.619	24.916	304.92	0.225	2.58
70.0	17.684	34.608	25.053	292.24	0.255	2.43
80.0	16.624	34.519	25.238	274.89	0.283	2.10
90.0	15.317	34.421	25.459	253.93	0.310	1.73
100.0	14.835	34.516	25.639	237.13	0.334	1.69
150.0	13.012	34.641	26.117	192.83	0.440	1.41
200.0	12.118	34.694	26.334	173.30	0.531	1.27
250.0	11.134	34.677	26.506	157.88	0.614	1.07
300.0	10.336	34.626	26.609	148.91	0.690	0.89
350.0	9.669	34.597	26.700	140.96	0.763	0.75
400.0	8.845	34.560	26.806	131.37	0.831	0.59
450.0	8.092	34.536	26.903	122.44	0.894	0.46
500.0	7.524	34.518	26.973	116.18	0.954	0.36
550.0	7.118	34.531	27.040	110.17	1.010	0.31
600.0	6.556	34.502	27.094	105.15	1.064	0.21
650.0	6.132	34.501	27.149	100.12	1.116	0.16
700.0	5.832	34.503	27.189	96.60	1.165	0.12
750.0	5.610	34.503	27.217	94.26	1.213	0.09
800.0	5.355	34.508	27.252	91.18	1.259	0.07
850.0	5.147	34.512	27.280	88.73	1.304	0.05
900.0	4.957	34.516	27.305	86.57	1.348	0.03
1000.0	4.542	34.529	27.362	81.37	1.432	-.01
1100.0	4.189	34.541	27.411	76.98	1.511	-.04
1200.0	3.922	34.555	27.450	73.55	1.586	-.06
1300.0	3.656	34.568	27.487	70.12	1.657	-.07
1400.0	3.436	34.579	27.518	67.36	1.726	-.09
1500.0	3.204	34.589	27.548	64.48	1.792	-.10
1600.0	3.010	34.599	27.575	62.02	1.855	-.11
1700.0	2.807	34.608	27.600	59.48	1.916	-.12
1800.0	2.654	34.616	27.621	57.57	1.975	-.13
1900.0	2.459	34.625	27.645	54.99	2.031	-.14
2000.0	2.332	34.632	27.662	53.40	2.085	-.14
2200.0	2.057	34.648	27.698	49.67	2.188	-.15
2400.0	1.904	34.658	27.718	47.82	2.285	-.16
2507.0	1.873	34.661	27.724	47.59	2.336	-.16

CAST: 55
LAT: 23° 57.8' N.

DATE: 1/ 7/93 1718 GMT
LON: 109° 10.7' W.

P(dbar)	T(°C)	S(psu)	γ_0 (kg m ⁻³)	δ	$\Sigma\Delta D$	π
1.0	21.737	34.867	24.192	371.82	0.004	3.69
5.0	21.737	34.867	24.192	371.96	0.019	3.69
10.0	21.705	34.897	24.224	369.10	0.037	3.70
15.0	21.715	34.907	24.229	368.84	0.056	3.71
20.0	21.684	34.920	24.248	367.24	0.074	3.71
25.0	21.592	34.936	24.286	363.85	0.092	3.70
30.0	21.418	34.969	24.359	357.06	0.110	3.68
35.0	21.303	34.967	24.389	354.37	0.128	3.64
40.0	20.907	34.993	24.518	342.32	0.145	3.55
45.0	20.850	35.028	24.560	338.52	0.162	3.56
50.0	20.106	34.834	24.611	333.75	0.179	3.22
60.0	19.637	34.823	24.726	323.20	0.212	3.08
70.0	19.648	34.930	24.805	316.05	0.244	3.17
80.0	19.381	35.044	24.962	301.48	0.275	3.18
90.0	18.721	34.993	25.092	289.40	0.304	2.98
100.0	17.668	34.963	25.331	266.92	0.332	2.69
150.0	13.999	34.778	26.021	202.22	0.448	1.71
200.0	12.370	34.722	26.308	175.91	0.542	1.34
250.0	11.467	34.693	26.458	162.64	0.626	1.14
300.0	10.761	34.665	26.564	153.38	0.705	0.99
350.0	9.922	34.627	26.682	142.90	0.779	0.82
400.0	9.211	34.598	26.777	134.42	0.849	0.67
450.0	8.461	34.555	26.862	126.70	0.914	0.52
500.0	7.582	34.516	26.963	117.17	0.975	0.36
550.0	6.899	34.502	27.048	109.18	1.032	0.25
600.0	6.440	34.500	27.108	103.70	1.085	0.19
650.0	6.175	34.501	27.144	100.70	1.136	0.16
700.0	5.872	34.502	27.183	97.21	1.186	0.12
750.0	5.567	34.506	27.224	93.51	1.234	0.09
800.0	5.361	34.509	27.252	91.14	1.280	0.06
850.0	5.194	34.513	27.275	89.30	1.325	0.05
900.0	5.019	34.517	27.299	87.30	1.369	0.03
950.0	4.789	34.523	27.330	84.43	1.412	0.01
1000.0	4.575	34.530	27.360	81.72	1.453	-0.00
1100.0	4.246	34.546	27.408	77.36	1.533	-0.02
1200.0	3.931	34.557	27.450	73.52	1.608	-0.05
1300.0	3.617	34.571	27.493	69.43	1.680	-0.07
1400.0	3.335	34.586	27.533	65.58	1.747	-0.08
1500.0	3.143	34.596	27.560	63.19	1.812	-0.09
1600.0	3.031	34.602	27.575	62.06	1.875	-0.10
1700.0	2.836	34.610	27.600	59.69	1.935	-0.11
1721.0	2.787	34.613	27.606	58.99	1.947	-0.11

CAST: 56
LAT: 24° 5.2' N.

DATE: 1/ 7/93 1930 GMT
LON: 109° 18.6' W.

P(dbar)	T(°C)	S(psu)	$\gamma_0(\text{kg m}^{-3})$	δ	$\Sigma\Delta D$	π
1.0	22.032	35.003	24.213	369.81	0.004	3.88
5.0	22.032	35.003	24.213	369.96	0.018	3.88
10.0	21.967	35.006	24.234	368.19	0.037	3.86
15.0	21.940	35.006	24.241	367.65	0.055	3.85
20.0	21.930	35.009	24.247	367.31	0.074	3.85
25.0	21.915	35.017	24.257	366.55	0.092	3.86
30.0	21.880	35.028	24.276	365.02	0.110	3.85
35.0	21.854	35.034	24.288	364.06	0.129	3.85
40.0	21.837	35.041	24.299	363.24	0.147	3.85
45.0	21.770	35.046	24.321	361.32	0.165	3.84
50.0	21.474	35.065	24.417	352.31	0.183	3.77
60.0	21.307	35.120	24.506	344.28	0.217	3.76
70.0	20.890	35.067	24.580	337.62	0.252	3.61
80.0	20.302	34.976	24.669	329.46	0.285	3.38
90.0	19.831	34.924	24.754	321.70	0.318	3.21
100.0	19.038	34.872	24.919	306.22	0.349	2.97
125.0	16.237	34.835	25.572	244.61	0.417	2.26
150.0	15.192	34.877	25.841	219.63	0.474	2.05
175.0	13.687	34.745	26.061	199.06	0.527	1.62
200.0	12.727	34.697	26.218	184.52	0.575	1.39
225.0	12.130	34.680	26.322	175.15	0.620	1.26
250.0	11.770	34.686	26.395	168.69	0.663	1.20
275.0	11.206	34.635	26.461	162.85	0.704	1.05
300.0	10.775	34.621	26.528	156.87	0.744	0.96
325.0	10.480	34.615	26.576	152.74	0.783	0.91
350.0	10.165	34.608	26.625	148.43	0.821	0.85
375.0	9.763	34.594	26.683	143.24	0.857	0.77
400.0	9.395	34.574	26.729	139.14	0.892	0.69
425.0	8.988	34.562	26.785	133.98	0.927	0.62
450.0	8.580	34.543	26.835	129.40	0.960	0.54
475.0	8.355	34.532	26.861	127.21	0.992	0.49
500.0	8.056	34.525	26.901	123.57	1.023	0.44
550.0	7.346	34.507	26.990	115.23	1.082	0.32
600.0	6.878	34.500	27.050	109.77	1.139	0.25
650.0	6.454	34.500	27.107	104.56	1.192	0.20
700.0	6.168	34.502	27.146	101.20	1.244	0.16
750.0	5.822	34.507	27.194	96.76	1.293	0.12
800.0	5.585	34.509	27.225	94.09	1.341	0.09
850.0	5.234	34.511	27.269	89.96	1.387	0.05
900.0	4.985	34.518	27.303	86.78	1.431	0.03
950.0	4.763	34.524	27.334	84.03	1.474	0.01
1000.0	4.489	34.532	27.371	80.45	1.514	-.01
1100.0	4.132	34.546	27.420	75.95	1.592	-.04
1200.0	3.808	34.562	27.467	71.63	1.666	-.06
1300.0	3.457	34.578	27.514	66.95	1.734	-.08
1347.0	3.441	34.579	27.517	67.03	1.766	-.08

CAST: 57
LAT: 24° 12.8' N.

DATE: 1/ 7/93 2218 GMT
LON: 109° 26.0' W.

P(dbar)	T(°C)	S(psu)	$\gamma_t(\text{kg m}^{-3})$	δ	$\Sigma\Delta D$	π
1.0	22.167	35.007	24.178	373.14	0.004	3.92
5.0	22.167	35.007	24.178	373.28	0.019	3.92
10.0	22.039	35.008	24.215	369.98	0.037	3.88
15.0	22.003	35.010	24.227	369.04	0.056	3.87
20.0	21.992	35.016	24.235	368.49	0.074	3.87
25.0	21.982	35.020	24.241	368.12	0.093	3.87
30.0	21.980	35.028	24.248	367.68	0.111	3.88
35.0	21.978	35.036	24.255	367.22	0.129	3.88
40.0	21.974	35.047	24.265	366.46	0.148	3.89
45.0	21.938	35.057	24.282	365.00	0.166	3.89
50.0	21.824	35.064	24.320	361.60	0.184	3.86
60.0	21.365	35.074	24.455	349.15	0.220	3.74
70.0	21.134	35.089	24.530	342.34	0.254	3.69
80.0	20.992	35.083	24.565	339.42	0.288	3.64
90.0	20.907	35.077	24.584	338.04	0.322	3.61
100.0	20.734	35.061	24.619	335.05	0.356	3.55
150.0	16.240	34.958	25.667	236.43	0.487	2.35
200.0	13.556	34.722	26.071	198.81	0.598	1.57
250.0	12.021	34.756	26.403	168.13	0.688	1.30
300.0	10.879	34.700	26.571	152.86	0.768	1.04
350.0	10.093	34.662	26.680	143.20	0.842	0.87
400.0	9.345	34.623	26.775	134.75	0.911	0.72
450.0	8.648	34.600	26.869	126.26	0.976	0.59
500.0	8.104	34.579	26.936	120.34	1.038	0.49
550.0	7.529	34.558	27.004	114.09	1.097	0.39
600.0	7.172	34.552	27.051	110.13	1.153	0.33
650.0	6.695	34.529	27.098	105.77	1.207	0.25
700.0	6.225	34.517	27.150	100.86	1.259	0.18
750.0	5.835	34.513	27.197	96.50	1.308	0.12
800.0	5.598	34.520	27.232	93.45	1.356	0.10
850.0	5.355	34.520	27.262	90.87	1.402	0.07
900.0	4.865	34.520	27.319	85.10	1.446	0.01
950.0	4.720	34.524	27.338	83.49	1.488	0.00
1000.0	4.520	34.536	27.370	80.58	1.529	-.00
1100.0	4.120	34.549	27.424	75.58	1.607	-.03
1200.0	3.830	34.564	27.466	71.72	1.681	-.05
1300.0	3.547	34.576	27.505	68.16	1.750	-.07
1400.0	3.332	34.587	27.534	65.50	1.817	-.08
1507.0	3.095	34.597	27.565	62.61	1.886	-.10

CAST: 58
LAT: 24° 20.0' N.

DATE: 1/ 8/93 0018 GMT
LON: 109° 34.2' W.

P(dbar)	T(°C)	S(psu)	$\gamma_0(\text{kg m}^{-3})$	δ	$\Sigma\Delta D$	π
1.0	22.326	35.017	24.141	376.69	0.004	3.97
5.0	22.326	35.017	24.141	376.83	0.019	3.97
10.0	22.157	35.020	24.191	372.27	0.038	3.93
15.0	21.913	34.921	24.184	373.08	0.056	3.78
20.0	21.888	34.782	24.086	382.68	0.075	3.67
25.0	21.874	34.846	24.139	377.84	0.094	3.71
30.0	21.798	34.863	24.173	374.75	0.113	3.71
35.0	21.508	34.893	24.277	365.11	0.132	3.65
40.0	21.340	34.927	24.349	358.41	0.150	3.63
45.0	21.340	34.925	24.348	358.74	0.168	3.62
50.0	21.330	34.929	24.354	358.33	0.186	3.62
60.0	21.266	34.932	24.374	356.79	0.221	3.61
70.0	21.149	34.994	24.454	349.60	0.257	3.62
80.0	21.042	34.992	24.482	347.31	0.292	3.59
90.0	19.511	34.757	24.710	325.84	0.325	3.00
100.0	19.469	35.015	24.918	306.42	0.357	3.19
125.0	15.523	34.777	25.689	233.30	0.425	2.05
150.0	14.816	34.846	25.899	213.97	0.481	1.94
175.0	13.548	34.837	26.161	189.56	0.532	1.67
200.0	12.955	34.807	26.258	180.83	0.578	1.52
225.0	12.707	34.775	26.284	179.05	0.623	1.45
250.0	11.872	34.743	26.420	166.38	0.666	1.26
275.0	11.245	34.706	26.509	158.32	0.706	1.12
300.0	10.773	34.677	26.572	152.70	0.745	1.01
325.0	10.434	34.663	26.621	148.42	0.783	0.94
350.0	10.093	34.647	26.668	144.30	0.819	0.87
375.0	9.645	34.628	26.729	138.78	0.854	0.77
400.0	9.330	34.615	26.771	135.06	0.889	0.71
425.0	9.057	34.604	26.807	131.99	0.922	0.66
450.0	8.480	34.597	26.892	123.86	0.954	0.56
475.0	8.253	34.593	26.924	121.14	0.985	0.53
500.0	8.042	34.585	26.950	118.97	1.015	0.49
550.0	7.611	34.568	27.000	114.57	1.073	0.41
600.0	7.396	34.553	27.020	113.35	1.130	0.37
650.0	6.800	34.513	27.071	108.47	1.185	0.25
700.0	6.532	34.536	27.126	103.67	1.238	0.24
750.0	5.892	34.518	27.194	96.90	1.288	0.14
800.0	5.506	34.523	27.246	92.04	1.335	0.10
850.0	5.253	34.523	27.276	89.32	1.380	0.07
900.0	5.027	34.526	27.305	86.73	1.424	0.04
950.0	4.777	34.530	27.337	83.77	1.467	0.02
1000.0	4.672	34.533	27.352	82.69	1.508	0.01
1100.0	4.243	34.544	27.408	77.43	1.587	-0.03
1200.0	4.082	34.552	27.431	75.73	1.664	-0.04
1211.0	3.975	34.558	27.447	74.07	1.672	-0.05

CAST: 59
LAT: 24° 27.6' N.

DATE: 1/ 8/93 0211 GMT
LON: 109° 42.5' W.

P(dbar)	T(°C)	S(psu)	γ_0 (kg m ⁻³)	δ	ΣAD	π
1.0	21.871	34.971	24.233	367.84	0.004	3.80
5.0	21.871	34.971	24.234	367.98	0.018	3.80
10.0	21.663	34.997	24.312	360.74	0.037	3.77
15.0	21.637	35.009	24.328	359.39	0.055	3.77
20.0	21.580	35.021	24.353	357.17	0.073	3.76
25.0	21.446	35.029	24.397	353.27	0.090	3.73
30.0	21.341	35.034	24.430	350.29	0.108	3.70
35.0	21.215	35.019	24.453	348.30	0.125	3.66
40.0	20.982	35.000	24.502	343.79	0.143	3.58
45.0	20.705	35.007	24.583	336.31	0.160	3.51
50.0	20.553	35.029	24.641	330.96	0.176	3.48
60.0	19.486	34.947	24.860	310.42	0.209	3.14
70.0	18.115	34.827	25.115	286.37	0.239	2.70
80.0	16.730	34.801	25.429	256.67	0.266	2.34
90.0	15.895	34.806	25.626	238.18	0.290	2.15
100.0	15.315	34.840	25.783	223.54	0.313	2.05
125.0	14.842	34.870	25.911	212.08	0.367	1.96
150.0	14.326	34.876	26.028	201.68	0.419	1.86
175.0	13.782	34.851	26.123	193.19	0.468	1.72
200.0	13.047	34.809	26.242	182.46	0.516	1.54
225.0	12.577	34.791	26.321	175.40	0.561	1.43
250.0	12.118	34.764	26.390	169.37	0.604	1.32
275.0	11.385	34.721	26.495	159.73	0.645	1.15
300.0	10.747	34.681	26.580	151.92	0.684	1.00
325.0	10.456	34.667	26.620	148.50	0.721	0.94
350.0	9.904	34.634	26.690	142.13	0.758	0.82
375.0	9.376	34.611	26.760	135.64	0.792	0.71
400.0	9.153	34.605	26.792	132.94	0.826	0.67
425.0	8.986	34.596	26.812	131.45	0.859	0.64
450.0	8.813	34.593	26.838	129.36	0.892	0.61
475.0	8.471	34.588	26.887	124.87	0.923	0.55
500.0	7.980	34.565	26.943	119.51	0.954	0.46
525.0	7.882	34.569	26.961	118.15	0.983	0.45
550.0	7.742	34.568	26.981	116.55	1.013	0.42
575.0	7.661	34.568	26.993	115.75	1.042	0.41
600.0	7.499	34.560	27.011	114.34	1.071	0.38
650.0	7.208	34.555	27.049	111.19	1.127	0.34
700.0	6.680	34.521	27.094	106.89	1.181	0.24
750.0	6.089	34.509	27.162	100.23	1.233	0.15
800.0	5.748	34.519	27.213	95.51	1.282	0.12
850.0	5.435	34.514	27.248	92.33	1.329	0.08
900.0	5.143	34.524	27.290	88.37	1.374	0.05
950.0	4.906	34.526	27.319	85.71	1.418	0.02
1000.0	4.670	34.532	27.351	82.74	1.460	0.00
1100.0	4.194	34.547	27.415	76.60	1.539	-0.03
1131.0	4.063	34.554	27.434	74.77	1.563	-0.04

CAST: 60
LAT: 24° 35.0' N.

DATE: 1/ 8/93 0406 GMT
LON: 109° 51.0' W.

P(dbar)	T(°C)	S(psu)	$\gamma_0(\text{kg m}^{-3})$	δ	$\Sigma\Delta D$	π
1.0	21.442	35.000	24.374	354.40	0.004	3.71
5.0	21.442	35.000	24.375	354.54	0.018	3.71
10.0	21.424	35.012	24.389	353.34	0.035	3.72
15.0	21.401	35.015	24.398	352.74	0.053	3.71
20.0	21.295	35.011	24.424	350.41	0.071	3.68
25.0	21.044	35.018	24.498	343.56	0.088	3.61
30.0	20.967	35.016	24.518	341.90	0.105	3.59
35.0	20.957	35.016	24.521	341.81	0.122	3.59
40.0	20.896	35.014	24.537	340.51	0.139	3.57
45.0	20.827	35.016	24.557	338.80	0.156	3.55
50.0	20.664	35.010	24.596	335.22	0.173	3.50
60.0	19.068	34.956	24.974	299.52	0.205	3.04
70.0	18.781	34.927	25.026	294.96	0.235	2.95
80.0	18.544	34.931	25.089	289.31	0.264	2.89
90.0	18.140	35.025	25.262	273.17	0.292	2.86
100.0	16.944	34.993	25.527	248.12	0.318	2.54
125.0	15.376	34.919	25.831	219.78	0.375	2.12
150.0	14.896	34.918	25.938	210.38	0.429	2.02
175.0	13.837	34.887	26.140	191.66	0.479	1.77
200.0	13.184	34.847	26.244	182.31	0.526	1.60
225.0	12.498	34.803	26.346	173.02	0.570	1.43
250.0	11.964	34.760	26.417	166.78	0.612	1.29
275.0	11.607	34.760	26.484	160.87	0.653	1.22
300.0	10.982	34.712	26.562	153.80	0.693	1.07
325.0	10.465	34.684	26.632	147.41	0.731	0.96
350.0	9.999	34.665	26.698	141.40	0.767	0.86
375.0	9.521	34.624	26.746	137.04	0.802	0.75
400.0	8.995	34.590	26.805	131.53	0.835	0.64
425.0	8.799	34.596	26.841	128.49	0.867	0.61
450.0	8.474	34.589	26.887	124.40	0.899	0.56
475.0	8.227	34.583	26.920	121.48	0.930	0.51
500.0	8.097	34.577	26.935	120.35	0.960	0.49
550.0	7.676	34.567	26.990	115.64	1.019	0.42
600.0	7.331	34.559	27.033	111.95	1.076	0.36
650.0	6.841	34.550	27.095	106.28	1.130	0.29
700.0	6.249	34.534	27.161	99.90	1.182	0.20
750.0	6.120	34.532	27.176	98.99	1.232	0.18
800.0	5.745	34.530	27.222	94.69	1.280	0.13
807.0	5.740	34.530	27.223	94.71	1.287	0.13

TABLE C4: SALINITY CORRECTION

Cast Number	Pressure (dbar)	Salinity (psu)		
		CTD (Uncorrected)	Bottle	Difference
18	1.4	34.9518	34.897	0.0548
	503.4	34.5866	34.538	0.0486
	1009.3	34.5892	34.538	0.0512
	2328.7	34.7109	34.658	0.0529
19	1.2	34.9628	34.912	0.0508
	95.8	34.8903	34.825	0.0653
	575.2	34.5595	34.506	0.0535
	1016.1	34.5886	34.535	0.0536
	2532.9	34.7163	34.662	0.0543
21	24.6	35.1102	35.061	0.0492
22	1.8	35.0343	34.981	0.0533
	1009.4	34.581	34.531	0.05
	1418.2	34.6358	34.585	0.0508
23	3	34.9013	34.844	0.0573
	87.5	34.6232	34.584	0.0392
	620.8	34.5595	34.51	0.0495
24	1517.3	34.6483	34.594	0.0543
25	1010.1	34.5793	34.528	0.0513
	1588	34.6566	34.605	0.0516
26	2.2	34.8635	34.809	0.0545
	72.4	34.2954	34.234	0.0614
	598.8	34.5648	34.511	0.0538
	1008.4	34.5844	34.53	0.0544
	2806.9	34.7184	34.671	0.0474
	1008.8	34.5865	34.533	0.0535
28	100.7	34.8576	34.805	0.0526
29	2.2	34.9357	34.882	0.0537
	1820.7	34.6753	34.623	0.0523
	202.5	34.7727	34.717	0.0557
35	171.1	34.7633	34.716	0.0473
36	13.8	34.9139	34.86	0.0539
38	1.9	34.8718	34.823	0.0488
	97.2	34.8717	34.821	0.0507
	525.9	34.5558	34.51	0.0458
	96.9	34.8503	34.817	0.0333
39	625.8	34.5521	34.502	0.0501
	1884.5	34.6831	34.63	0.0531
	303.8	34.7003	34.651	0.0493
45	330.5	34.6803	34.635	0.0453
47	312.4	34.6129	34.567	0.0459
48	84.2	34.2959	34.251	0.0449
	305.7	34.687	34.639	0.048

Cast Number	Pressure (dbar)	Salinity (psu)		
		CTD (Uncorrected)	Bottle	Difference
52	604.5	34.5446	34.499	0.0456
	1468.7	34.6373	34.586	0.0513
53	45.3	34.8518	34.782	0.0698
	2636.4	34.7108	34.659	0.0518
55	1722.8	34.6613	34.608	0.0533
56	606	34.5515	34.501	0.0505
57	1502.6	34.6465	34.595	0.0515
58	117.7	34.8682	34.816	0.0522
	1009.1	34.5836	34.536	0.0476
	1211.8	34.6075	34.555	0.0525
59	1.9	35.05	34.998	0.052
	90.1	34.8894	34.837	0.0524
	1008.9	34.5851	34.535	0.0501
60	2.4	35.0441	34.995	0.0491
	98.6	35.0423	34.984	0.0583
	799.2	34.5802	34.53	0.0502

REFERENCES

- Alvarez-Borrego, S., Gulf of California, in *Estuaries and Enclosed Seas*, edited by B.H. Ketchum, Chapter 17, Elsevier, New York, 1983.
- Bray, N.A., 1988a: *Thermohaline Circulation in the Gulf of California*, J. Geophys. Res., 93(C5), 4993-5020.
- Bray, N.A., 1988b: *Water Mass Formation in the Gulf of California*, J. Geophys. Res., 93(C8), 9223-9240.
- EG & G Ocean Products, 1989: *Oceansoft Post Processing Software Manual*, P/N MANUL 10241: 110 pp.
- Flament, P., 1986: *A Note on Seawater Spiciness and Diffusive Stability*, submitted to *Deep-Sea Res.*, Scripps Institution of Oceanography, La Jolla, CA., 9 pp.
- Golden Software, Inc., 1989: *Surfer*, 4, Golden, Co., 384 pp.
- Griffiths, R.C., 1968: *Physical, Chemical, and Biological Oceanography of the Entrance to the Gulf of California, Spring of 1960*, U.S. Fish Wildl. Serv. Spec. Sci. Rep. Fish., 573, 1-47.
- Merrifield, M.A., and C.D. Winant, 1989: *Shelf Circulation in the Gulf of California: A Description of the Variability*, J. Geophys. Res., 94, 18, 133-18, 160.
- Munk, W., 1981: *Internal Waves and Small-Scale Processes, Evolution of Physical Oceanography*, ed. by Warren and C. Wunsch, MIT Press, Cambridge, MA., 264-292.
- Pickard, G.L., and W.J. Emery, *Descriptive Physical Oceanography*, Pergamon Press, Oxford, 1990.

- Rago, T., R. Mitchell, L.F. Navarro-Olache, N. Garfield, and C.A. Collins, 1992: Hydrographic Data from the Pegasus in the Sea of Cortes Area Cruise (PESCAR-01) 21 April-08 May 1992, Data Report (NPS-OC-92-009), Naval Postgraduate School, Monterey, CA., 51 pp.
- Reid, J.L., 1965: Intermediate Waters of the Pacific Ocean, Baltimore, The Johns Hopkins Press, 86 pp.
- Reid, J.L., and A.W. Mantyla, 1976: The Effect of the Geostrophic Flow Upon Coastal Elevations in the Northern North Pacific Ocean, J. Geophys. Res., 81, 3100-3110.
- Robles, J.M., and S.G. Marinone, 1987: Seasonal and Interannual Thermohaline Variability on the Guaymas Basin in the Gulf of California, Cont. Shelf Res., 715-733.
- Roden, G.I., 1964: Oceanographic Aspects of the Gulf of California, Marine Geology of the Gulf of California, Amer. Assoc. of Petroleum Geologists, Tulsa, OK., Memoir No. 3, 30-58.
- Roden, G.I., 1972: Thermohaline Structure and Baroclinic Flow Across the Gulf of California Entrance and in the Revilla Gigedo Islands Region, J. Phys. Oceanogr., 2(2), 177-183.
- Roden, G.I., and G.W. Groves, 1959: Recent Oceanographic Investigations in the Gulf of California, J. Mar. Res., 18, 10-35.
- Stevenson, M.R., 1970: On the Physical and Biological Oceanography near the Entrance of the Gulf of California, October 1966-August 1967, Inter-Am. Trop. Tuna Comm. Bull., 4(3), 389-504.

- Sverdrup, H.U., 1941: *The Gulf of California: Preliminary Discussion on the Cruise of the E.W. Scripps in February and March 1939*, 6th Pac. Sci. Congr. Proc., 3, 161-166.
- Warsh, C.E., K.L. Warsh, and R.C. Stanley, 1973: *Nutrients and Water Masses at the Mouth of the Gulf of California*, Deep Sea Res., 20, 561-570.
- Wyrтки, K., 1967: *Circulation and Water Masses in the Eastern Equatorial Pacific Ocean*, Int. J. Oceanol. Limnol., 1(2), 117-147.
- Unesco, 1987: *International Oceanographic Tables, Vol. 4, Properties Derived from the International Equation of State of Seawater*, 1980, Unesco Tech. Pap. Mar. Sci., 40, 195 pp.
- Unesco, 1991: *Processing of Oceanographic Station Data*, Unesco Tech. Pap. Mar. Sci., 138 pp.

INITIAL DISTRIBUTION LIST

	No. Copies
1. Defense Technical Information Center Cameron Station Alexandria, VA 22304-6145	2
2. Librarian Code 52 Naval Postgraduate School 411 Dyer RD RM 104 Monterey, CA 93943-5002	2
3. Oceanography Department Code OC/CO Naval Postgraduate School 833 Dyer RD RM 331 Monterey, CA 93943-5112	1
4. Dr. Newell Garfield (Code OC/GF) Oceanography Department Naval Postgraduate School 833 Dyer RD RM 331 Monterey, CA 93943-5112	1
5. LT Monty G. Spearman FLENUMOCEANCEN 7 Grace Hopper Ave Stop 4 Monterey, CA 93943-0001-0120	1

- | | | |
|-----|---|----|
| 6. | Tarry Rago (Code OC/RG)
Oceanography Department
Naval Postgraduate School
833 Dyer RD RM 331
Monterey, CA 93943-5112 | 10 |
| 7. | Paul Jessen (Code OC/JE)
Oceanography Department
Naval Postgraduate School
833 Dyer RD RM 331
Monterey, CA 93943-5112 | 1 |
| 8. | Director Naval Oceanography Division
Naval Observatory
34th and Massachusetts Ave. NW
Washington, D.C. 20390 | 1 |
| 9. | Commander
Naval Oceanography Command
Stennis Space Center
MS 39529-5000 | 1 |
| 10. | Commanding Officer
Naval Oceanographic Office
Stennis Space Center
MS 39522-5001 | 1 |
| 11. | Library
Scripps Institution of Oceanography
P.O. Box 2367
La Jolla, CA 92307 | 1 |
| 12. | Library
Moss Landing Marine Lab
California State Colleges
Sandholdt Road
Moss Landing, CA 95039 | 1 |

- | | | |
|-----|--|---|
| 13. | Library | 1 |
| | Hopkins Marine Station | |
| | Stanford University | |
| | Pacific Grove, CA 93950 | |
| 14. | Prof. N.A. Bray | 1 |
| | Scripps Institution of Oceanography | |
| | La Jolla, CA 92093 | |
| 15. | Prof. J.L. Reid | 1 |
| | Scripps Institution of Oceanography | |
| | La Jolla, CA 92093 | |
| 16. | Dr. Affonso da Silveira Mascarenhas, Jr. | 2 |
| | Universidad Autonoma de Baja California | |
| | Apartado Postal 453 | |
| | Ensenada, Baja California, Mexico CP22800 | |
| 17. | Dr. Antonio Sanchez-Devora | 2 |
| | Secretaria de Marina Estacion Oceanologica | |
| | Vincente Guerrero No. 133 | |
| | Altos Fracc. Bahia | |
| | Ensenada, Baja California, Mexico CP22880 | |